LA-7851-T
Thesis

UC-34a
Issued: May 1979

The Study of Elastic Pion Scattering from ^{9}Be, ^{28}Si, ^{58}Ni, and ^{208}Pb at 162 MeV

Michael John Devereux*

---

*Visiting Staff Member. Laboritorium fur Hochenergiephysik, ETH-Z, c/o SIN, 5234 Villigen, SWITZERLAND.

TABLE OF CONTENTS

TABLE OF CONTENTS (continued)

LIST OF TABLES

LIST OF FIGURES

Page

Page

THE STUDY OF ELASTIC PION SCATTERING FROM ^{9}Be, ^{28}Si, ^{58}Ni, AND ^{208}Pb AT 162 MeV

by

Michael John Devereux

ABSTRACT

Elastic pion scattering from ^{9}Be, ^{28}Si, ^{58}Ni, and ^{208}Pb at 162 MeV is analyzed and compared with an optical model theory which incorporates a pion-nucleon range. Excellent fits to the data are obtained in all but one case. The fitted values of the pion-nucleon range, as well as other fitted values are listed.

I. INTRODUCTION

It may be wondered why one spends the large quantities of time, money, and effort which are a prerequisite for the successful investigation of complex scientific questions. Part of the answer surely is the instinct of natural curiosity.

Aristotle speculated gratis that all matter is composed of indivisible entities called atoms, and in terms of the scientific criteria which now are used to evaluate nature, there was surely more than a grain of truth in his speculation. It is now known that the chemical properties of matter which so wonderfully diversify the physical world are functions of the microscopic atoms, the atomic, and the molecular bonds which construct our macroscopic environment.

But it has been found that atoms are not indivisible. Indeed, every single atom is composed of a small central nucleus and a spatially dispersed cloud of electrons surrounding the nucleus. One yearns to understand the integrity of a single nucleus, the individual particles that compose a nucleus, the forces that bind parts of a nucleus together, and the organization that mediates different nuclear properties for different types of nuclei. To satisty one's curiosity about the continued divisibility and the coherent complexity of matter, the price is often that of extremely expensive machinery and the outlay of prodigious quantities of time and effort by highly skilled people.

The orderly arrangement of different atoms into elements of the periodic table was elucidated by Dalton at the beginning of the nineteenth century.[1] However, the divisibility of the atom into constituent parts was not decisively shown until the conclusion of that century. J. J. Thompson discovered the electron[2] in 1897 and measured some of its properties. The fact that electrons are emitted from various oxide cathodes of a cathode ray tube implies the inclusion of electrons in many different atoms. But atoms were known to be neutral in charge. However, a singly ionized atom has a charge equal and opposite to the electron's charge. Thompson was thus led to propose a model[3] of the atom which specified a uniform distribution of electrons imbedded in a sphere of positive charge whose magnitude was equal, but opposite to the charge held by the electrons.

Thompson's atomic model contrasted with that of Nagaoka's 1904 model[4] in which a positive core was surrounded by electron rings as in a planetary system. Experiments performed by Geiger and Marsden[5,6] indicated the impossibility of atoms as Thompson conceived them. Alpha particles from natural radiation were directed on target nuclei and the distribution of scattered alpha particles was detected by the scintillation light produced when the scattered alpha hit a small piece of the crystalline compound ZnS. The percentage of alphas scattered to large angles in the experiments was incompatible with the predictions of the Thompson atomic model. Rutherford proposed a model in 1911[7] similar to Nagaoka's which correctly accounted for the amount of large-angle alpha scattering. This model, hypothesized to have nonradiative electron orbits by Bohr[8] was in concurrence with Plank's quantum hypothesis.[9] The model was modified by Sommerfeld[10] to have elliptical orbits and again modified to have dispersed, quantum-mechanical clouds of electron location probability.[11,12]

Rutherford was first to discover one of the constituent parts of the nucleus as a consequence of experiments which included the first transmutation of one atom into an entirely different atom. The transmutation experiment changed atoms of nitrogen into atoms of oxygen by bombardment, with naturally occurring alpha particles yielding protons as an end product. Symbolically,

$$^{14}N + {}^{4}He \rightarrow {}^{17}O + {}^{1}H \ .$$

It was first assumed by scientists of the time that protons, the nuclei of hydrogen atoms, combined with electrons in varying ratios to form the nuclei of all atoms. Later quantum mechanical arguments, however, threw doubt on the notion that nuclei are composed of electrons and protons. Chadwick, in 1932, discovered a neutral particle[13] to be called the neutron and it is the neutron which combines with protons to compose all the various nuclei of atoms. Iwanenko[14] and Heisenberg[15] take credit for the model of nuclei composed of protons and neutrons but not electrons, a model not substantially refuted by any subsequent evidence.

It is for investigations of today, in particular this experiment, to accumulate information about the internal structure of atomic nuclei. The problem of completely describing nuclei from first physical principles has so far proved unsolvable, and one must resort instead to mathematical models of nuclei. Several models of nuclear excitation have been developed, including the shell model and liquid drop model.[16] There are also many mathematical models which describe the interaction of various elementary particles with nuclei. One such model is the optical potential model which is based on the assumption that particles impinging on nuclei may be treated as waves encountering a medium described by an index of refraction. The optical model, described in detail in chapter IV of this thesis, is one tool that will be used to investigate nuclear structure.

The Pi Meson

The pion is the least massive, strongly interacting, elementary particle and is the nuclear probe of this experiment. The construction of pi meson factories[17,18] around the world and the increase in experiments examining the pion-nucleus interaction hinge on the felicitous properties[19] of this spin zero, negative parity particle which carries nature's strong (nuclear) force.

The pi meson was predicted in 1935 by the Japanese physicist H. Yukawa,[20] some twelve years before its experimental discovery in nuclear emulsions.[21] Yukawa's insightful paper postulates the pion as the quantum of the hadronic force. It was known by 1934 that this force had a range of approximately two fermi and Yukawa argued correctly that an unobserved, virtual particle transmitting this force must exist and have a mass near 100 MeV/c^2.

Suppose the interaction between two hadrons is mediated by the exchange of pions. According to the Pauli uncertainty principle, the creation of a pion, and this consequent energy imbalance, can survive only for the short time

$$t \leq \hbar/\Delta E,$$

where ΔE is the energy imbalance and $\hbar$ is Planck's constant divided by 2π. Assuming the virtual pion to have the velocity of light, c, then its range must be approximately given by

$$R = ct = c\hbar/\Delta E.$$

The energy imbalance must be at least as large as the rest energy of the pion, so that

$$E \geq m_\pi c^2 \ .$$

Therefore the pion rest mass is

$$m_\pi > \hbar/cR = 99 \text{ MeV}/c^2.$$

The actual mass of the pion is about 140 MeV/c^2. It is now known that other heavier mesons also transmit the strong force over distances that are, however, much shorter than the range of the force carried by the pi meson.

The pion has isospin I=1. It therefore comprises an isospin triplet,[22] with isospin projections $I_3 = (-1,0,1)$ and three charge states. Electromagnetic effects may give the two charged pions a slightly higher mass than the neutral pion

$$m_{\pi^+},\ m_{\pi^-} = 139.576\ \mathrm{MeV}/c^2$$

$$m_{\pi^0} = 134.972\ \mathrm{MeV}/c^2.$$ [23,24]

The fact that the pion is about one seventh the mass of the lightest nucleus is significant. The pion-nucleus interaction imparts little of the incident pion momentum to the nucleus, thus simplifying nuclear experiments using pions. More importantly, one may formulate approximations to the description of pion-nucleus physics in terms of expansions in powers of pion mass divided by nucleon mass. For example, one may approximate radiative energy losses in pion-nucleus scattering by just such an expansion.

Because the charged pion is a relatively long-lived meson, a beam of these particles can be transported through extended apparatus designed to define the phase space of the beam. This allows for the necessary careful control of the parameters of pion-nucleus experiments. Charged pions have a mean life of $\tau = 2.60 \times 10^{-8}$ sec.,[25] so their mean decay length is

$$L_0 = \frac{P}{m_\pi} c\tau = 5.57\ P\ \mathrm{cm}\ ,$$

where the pion momentum P is given in MeV/c. Thirty-seven percent of the charged pions in a beam of momentum 300 MeV/c would therefore survive a distance of 6.7 meters. Unfortunately, neutral pions have a mean life of only 0.89×10^{-16} sec.[25] and survive only short distances after their creation, making it difficult to work with these particles. Even charged pions do not live long enough to be used in conventional particle accelerators and must be produced by the collision of energetic particles with a production target. The fact that the pion is a particle with three-charge states makes it especially useful as a nuclear probe. One may examine charge exchange reactions of the sort (π^+,π^o) and (π^-,π^o), or even double-charge exchange such as (π^+,π^-).[26,27] Such reactions permit the production of otherwise inaccessible nuclei. Additionally, it may be possible to distinguish proton from neutron distributions in nuclei due to the different way in which the two species of charged pions interact with neutrons and protons,[28,29,30] and, by using incident pions of opposite sign, the separation of electromagnetic effects in pion-nucleus collisions is feasible.

Because of the pion zero spin, pion-nucleus interactions are simplified. There are, for example, no spin-orbit complications introduced by the pion, and while the nucleus wave function must be antisymmetric because its nucleons are fermions, antisymmetrization of wave functions with respect to an incident pion is not necessary since nucleons and pions are not identical particles. Since the pion is a boson, it can be created or destroyed singly, and pion absorption and creation in nuclei are phenomena with the potential of yielding a deeper understanding of nuclear structure.[31]

The interaction of a pion with an individual nucleon at intermediate energies (approximately 50 to 500 MeV), such as are available at the Los Alamos Meson Physics Facility (LAMPF) where this experiment was performed, shows a large variation with energy. There is, in fact, a resonance at about 180 MeV kinetic energy. Below this resonance, called the (3,3) resonance because the significant partial wave exhibits the quantum numbers J=I=3/2,[32] in the energy range of about 50 to 150 MeV, the pion wavelength is much larger than the nucleon diameter and the pion-nucleon cross section is at least an order of magnitude smaller than the nucleon-nucleon cross section. Near the (3,3) resonance the pion-nucleon cross section grows very large. Above the resonance, the pion wavelength is about the size of the nucleon diameter.

The pion-nucleon cross section, though smaller than at resonance, now is about the same size as the steadily decreasing nucleon-nucleon cross section. One may thus use the pion-nucleon interaction at intermediate energies to probe both nuclear surface and deeper-lying effects and to examine the (3,3) resonance.

Motivation

This experiment, whose spokesman was Ben Zeidman of Argonne National Laboratory, is a survey of pion-nucleus scattering at intermediate energies. It studies the elastic scattering of both positive and negative pions from four nuclei at incident energy 162 MeV. The nuclei chosen for this experiment were ^{9}Be, ^{28}Si,

^{58}Ni, and ^{208}Pb, selected primarily for their wide range of mass, because the first excited state in each nucleus is at least 1 MeV above the ground state, providing sufficient separation of this excited level, and because each of them has interesting nuclear structure. The experiment is not a measurement of the values of the energy levels of nuclear inelastic states. Other nuclear probes are more adept at measuring these values and evaluating the suitability of particular models of nuclear excitation. The goal of this experiment is to generate a body of the best possible pion scattering data which may be applied to the verification of existing models or perhaps the formulation of new models of the pion-nucleus interaction with nuclei. If such a model aptly describes pion-nucleus interaction, then the ultimate goal of understanding the structure of the nucleus is facilitated. The experimental data that will be presented later in this thesis will be compared with the predictions of a rudimentary optical model of the pion-nucleus interaction. Nuclear structure information generated by the experimental data, particularly proton and neutron distributions in nuclei, will be investigated in the light of the validity of these models.

Prior to this experiment, other intermediate energy pion-nucleus scattering data existed, much of it the result of recent investigations at the Swiss meson factory, Schweizerisches Institut Fur Nuklearforschung, (SIN) Zurich, Switzerland. The first high-quality data appeared about eleven years ago, consisting of elastic and inelastic negative pion-scattering differential cross sections for ^{12}C.[33] The usefulness of this data, particularly the scattering to inelastic states, was limited by low statistics due to low-incident beam intensity. Such low intensity also hampered other experiments[34,35,36,37] done before the completion of meson factories. More recently published data, benefiting from smaller statistical uncertainty, include elastic and inelastic pion-scattering cross sections for ^{18}O at 230 MeV[38] and elastic pion-scattering cross sections for ^{40}Ca and ^{48}Ca at 130 MeV.[39] These data may have their primary usefulness in determining neutron and proton densities and nuclear shapes in both the ground and excited states.

Low-energy pion-scattering information, the 50 MeV elastic and inelastic differential cross sections for ^{12}C,[40] indicates that a rudimentary optical interaction model may need major revisions if it is to describe scattering at 50 MeV, well below the (3,3) resonance. Recent data which will complement the information gleaned from this experiment are the pion differential cross sections of ^{12}C at 148, 162, and 226 MeV.[41] Total cross-sectional pion-scattering data has also been published. Some total cross sections were measured by Jakobsen[42] and Wilkin[43] as well as others. Recent work, with as yet unpublished results, has been the pion scattering from ^{9}Li, ^{14}N, ^{16}O, and ^{18}O at SIN and scattering from ^{12}C, ^{16}O, and ^{18}O at LAMPF. Additionally, elastic and inelastic pion differential scattering on ^{28}Si at 130 MeV and on ^{208}Pb at 116 MeV has been carried out at SIN.

Pion scattering at 50 MeV from ^{208}Pb was done at LAMPF. These unpublished results have been presented in preliminary form at conferences.[44]

Scattering energy and target nuclei examined by this dissertation experiment were chosen to complement pion-nucleus data already available. In particular, ^{58}Ni is a target of intermediate mass, and scattering data from this nucleus fills a void in previous results. The elastic differential cross sections obtained for each nucleus will be compared with the description of pion-nucleus elastic scattering given by the first-order optical model.[45,46,47] Pion-nucleus potential parameters derived from fits to the elastic data can be used in an evaluation of the differential cross sections of certain inelastic nuclear states given by a distorted wave impulse approximation.[48] Proton and neutron distributions obtained will be compared with results gathered from electron and proton scattering and from total cross-sectional measurements.

More detailed reviews of pion-nucleus scattering are given by Huffner,[49] Sternheim and Silbar,[50] Tabakin,[51] and in the lectures from the LAMPF summer school.[52] Earlier reviews are by Tanner[53] and Wilkin.[54] Brown[55] discusses nuclear models in a concise but readable way. Intermediate energy nuclear physics is described rather comprehensively by Lock and Measday.[56] Experimental aspects of pion-nucleus scattering are reviewed by Stroot[57] and Binon.[58] Koltun[59] reviews the more general field of pion-nucleus interactions.

II. THE ENERGETIC PION CHANNEL AND SPECTROMETER

A pi meson is somewhat smaller than a basketball, in the approximate ratio of 10^{-14} to 1, and thus its position and velocity are not so easily measured as one might measure these properties for the basketball. A scattering experiment, such as pion scattering by nuclei, depends on the momentum measurement of every pion scattered into a specified solid angle. Pions that scatter from atomic nuclei sometimes lose energy by inducing nuclear excited levels, so one must have an accurate measurement of each scattered pion's momentum if he is to decipher the nuclear interaction. It is of primary importance to determine the percentage of nuclear probes that interact with a nucleus, relative to the total number of such probes incident on the nucleus, and the percentage of each particular kind of nuclear interaction. This is so because the total information gleaned from the scattering of a single pion on a nucleus is the existence of an interaction, but no description whatsoever of the nature of that interaction. One wishes to determine precisely the pion-nucleus interaction mechanism, and therefore an instrument capable of measuring the momentum of great numbers of pions before and after a nuclear collision is a necessity. This tool must determine the number, trajectories, and velocities of pions, one-hundred-thousandth as large as an atom, traveling at nearly the velocity of light. At LAMPF such an instrument exists. It is called the Energetic Pion Channel and Spectrometer (EPICS), and is capable of analyzing 10^8 pions per second incident on a scattering target.

This chapter describes the EPICS system.[60] The pion channel is detailed first, then the spectrometer, and finally other instrumentation including the on-line computer and its software.

The EPICS Channel

The Los Alamos Meson Physics Facility (see Figure 1) is built around an 800 MeV linear proton accelerator.[18] The accelerator incorporates three different types of accelerator technology. Normally two 750 KeV Cockcroft-Walton generators alternately inject protons and H^- ions into the accelerator beam line at precise intervals, timed to coincide with the rf field at the entry end of an Alverez-type drift-tube linear accelerator. The LAMPF machine is also equipped with a third Cockcroft-Walton injector which supplies polarized ions. A beam transport system makes it possible to feed these polarized ions, in place of the H^- ions, to the linear accelerator.

The drift-tube accelerator, fed by electrical fields oscillating at a 201.25 MHz rate, boosts the injected particles to 100 MeV in a length of 202.5 feet. The final beam energy of 800 MeV is accomplished by feeding the 100 MeV beam particles into a sidecoupled resonant-cavity linear accelerator operated at 805 MHz.

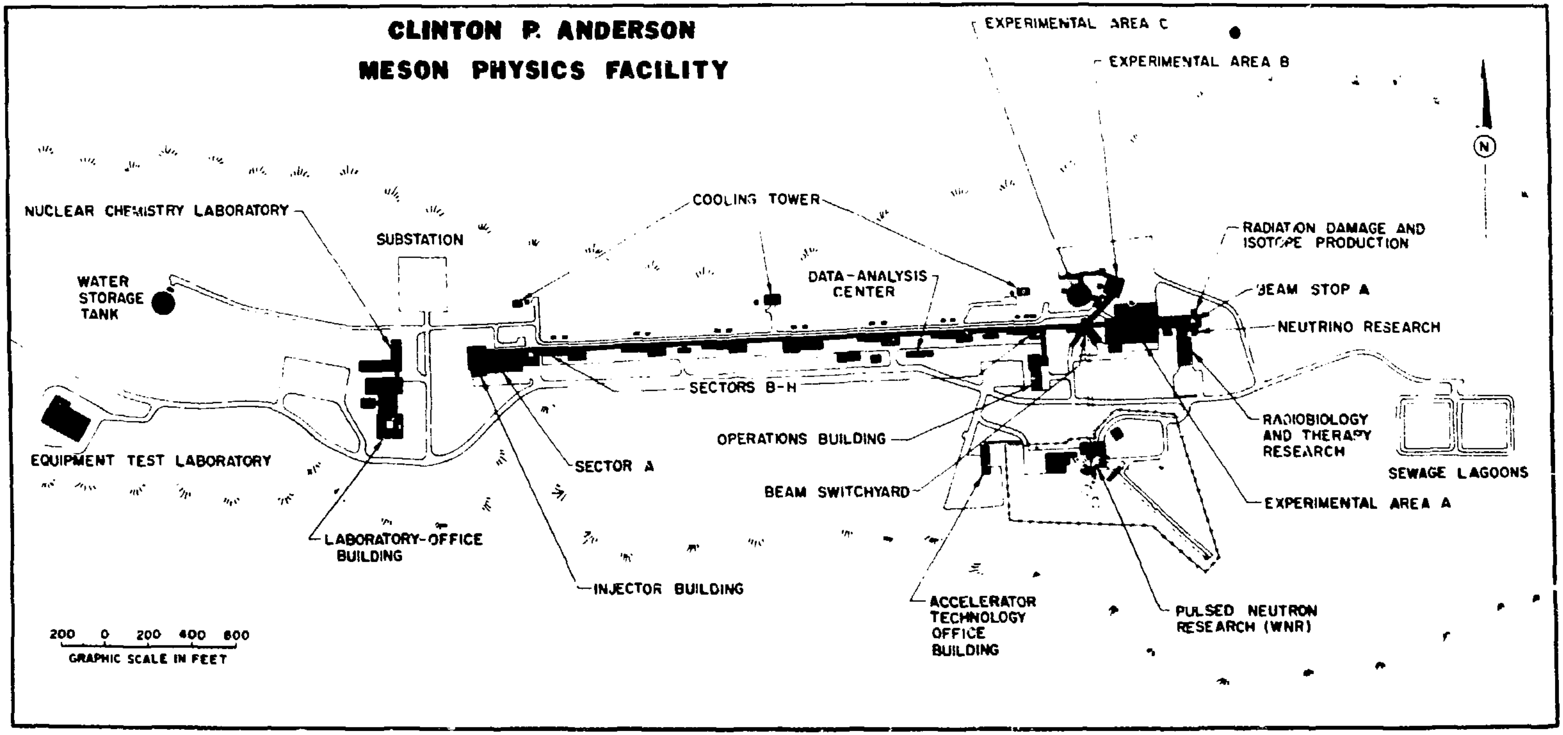

Fig. 1. Clinton P. Anderson Meson Physics Facility.

This portion of the accelerator is about half a mile long. The LAMPF beam is designed to have an average current of 1 mA of protons, with a peak current of 17 mA at 6% duty factor. During this experiment the average proton current was 300 μA at a 6% duty factor. The gross beam structure showed a proton beam of 520 μsec duration at 120 Hz.

Eight hundred MeV protons from the accelerator are separated from the energetic negative ions of the beam and guided into the experimental area, beam area A (see Figure 2). Pi mesons, as well as other elementary particles, of varying energies, are created by directing the proton beam into a rotating carbon target, called the A-1 target, in Figure 3. Pions from the target are collimated, transported, and defined by the EPICS pion channel, 15.24 m long. The channel can deliver pions in the 50- to 300-MeV kinetic energy range.

The EPICS channel is basically composed of four large dipole magnets, which define the charge sign and momentum of particles directed onto a scattering target. It is this target that contains nuclei of interest for nuclear structure studies. A pion channel can well define the momenta of exiting pions by severely limiting the momentum spread of particles which may traverse the channel. Suppose a pion channel allows a momentum bite of 0.01% of central momentum, then obviously the momenta of pions striking the scattering target is known to one part in 10^4. Such a channel has a debilitating drawback. It severely limits the intensity of its pion

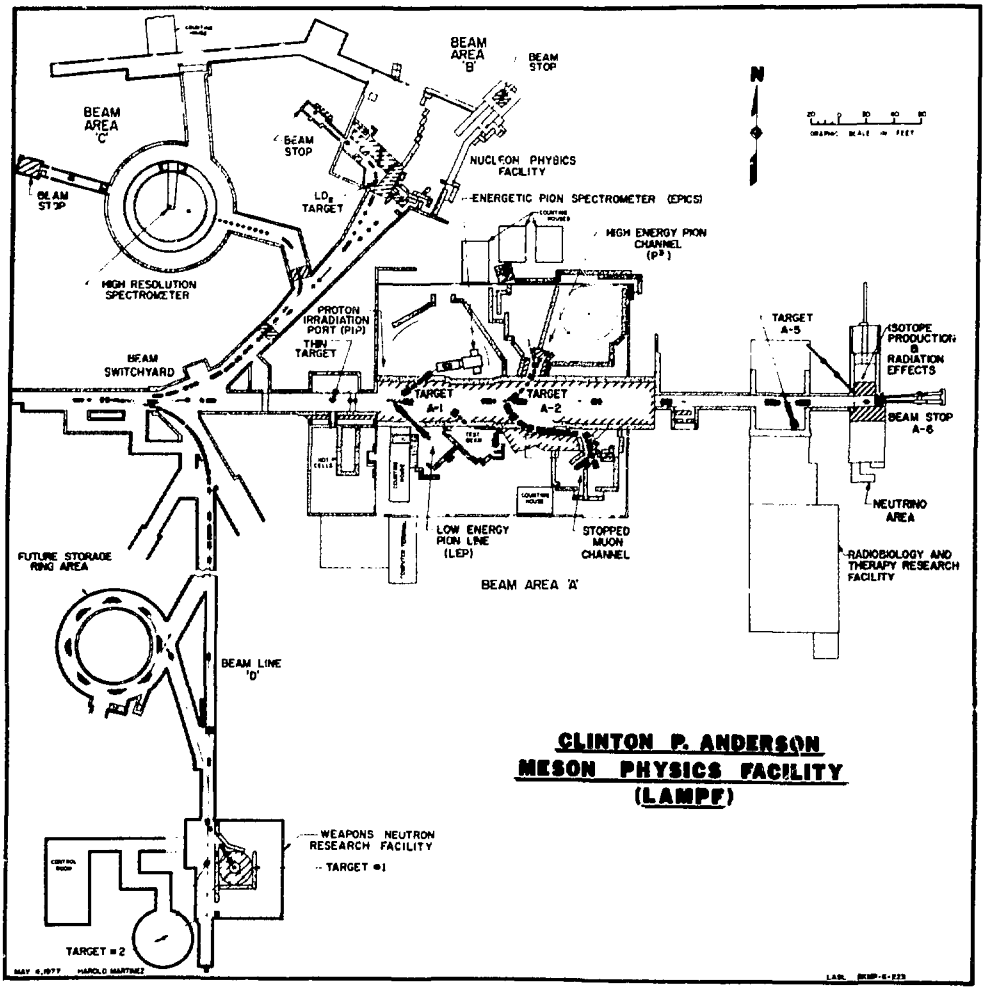

Fig. 2. The pion experimental area at LAMPF.

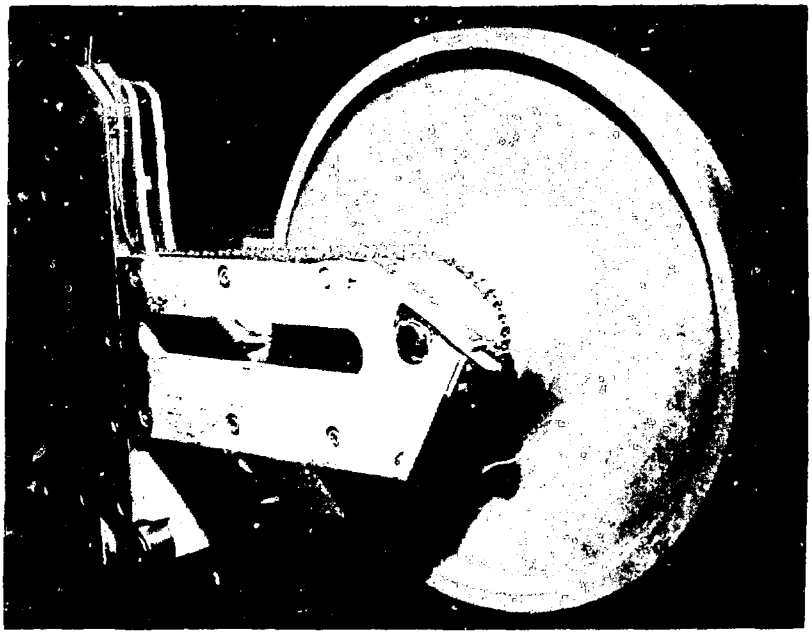

Fig. 3. The A-1 production target rotates in the proton beam. It creates pions for the EPICS system.

beam. The EPICS channel overcomes this problem by accepting a moderate momentum bite of pions, and vertically dispersing pions of different momenta at the scattering target. A careful correlation of pion momentum with vertical position at the scattering target permits the EPICS channel to have an excellent momentum resolution and high intensity.

As shown in Figure 4, the four large dipoles, labeled BM01-BM04, are arranged in a symmetric fashion, and those charged particles with proper momenta traverse the channel from the position labeled S, the location of target A-1, to the focal plane, FP in the figure, where the scattering target is mounted. The first bending magnet, BM01, directs upward a given sign of charged particles passing through the aperture of the fixed collimator located near target A-1. Oppositely charged particles are bent downward and are absorbed by equipment and blocks of radiation shielding which surround the pion channel. The magnetic field in each bending magnet is separately adjustable from zero to 18 kG and defines the range of momenta of those particles which will pass through the entire channel and hit the scattering target. A probe, operating on the principle of nuclear magnetic resonance,[61] may be inserted into each dipole magnet to precisely measure the field. These probes are labeled NMR1-NMR4 in the figure. Notice that particles with larger momenta than that of the channel are not sufficiently bent by the dipole magnets to allow them to arrive at the focal plane. They are absorbed by material surrounding

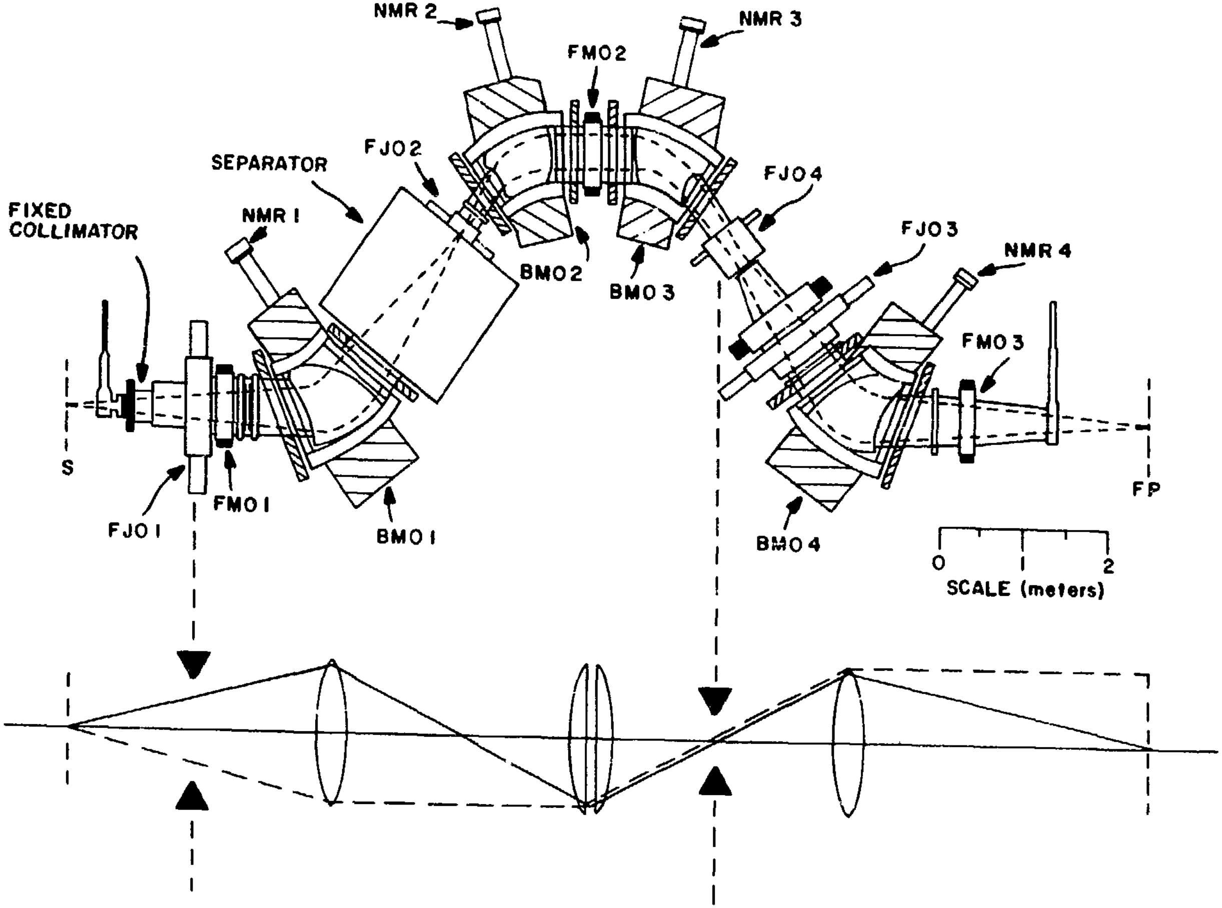

Fig. 4. The EPICS channel. Pion energy is defined by the channel. Optics in the vertical plane (solid line) is point-to-point. Optics in the horizontal plane (dotted line) is point-to-parallel.

the channel. In like fashion, particles with too small momenta are bent too much to traverse the pion channel.

There are also three small magnets in the EPICS pion channel. These magnets generate quadrupole and sextupole fields. The three small magnets, FM01-FM03, fine tune the magnetic-optic properties of the channel, such as focusing at the focal plane.

Particles other than pions are created in the A-1 production target and it is possible for some of these particles to follow the EPICS channel through to the scattering target. In fact, when the channel is optimized for 200 MeV positive pion transport, there can be 20 times more protons than pions arriving at the focal plane of the channel. Thus is the justification for including a stationary-field separator in the channel. A strong magnetic and a strong electrostatic field aligned orthogonally are maintained in the separator shown in Figure 4. The separator should deflect out of the pion channel all particles not having the same charge to mass ratio as pions. However, at a pion kinetic energy of 151 MeV the particle beam at the focal plane is not exclusively pions. The separator does a good job of removing protons but has more difficulty with muons and electrons. Table I shows the beam content at 151 MeV.

Shown in Figure 4, below the channel drawing, is a schematic diagram of the magnetic optics of the channel. The solid line represents a ray in the horizontal plane. From production target to scattering target the optics configuration is point-to-point in the

Table 1. The composition of the EPICS beam at the scattering target is shown.[a]

Particle	P (MeV/c)	T_π	π (Percent)	μ (Percent) and e (Percent)	p (Percent)
π^+	255	151	76 ± 3	22 ± 3	2.2 ± 0.2
π^-	255	151	69 ± 2	31 ± 2	
π^+	310	200	77 ± 5	19 ± 5	3.8 ± 1.0
π^-	310	200	82 ± 5	18 ± 5	

[a] H. A. Thiessen et al., "EPICS Pion Channel Performance," Los Alamos Scientific Laboratory Report (LA-6663-MS, 1977).[62]

vertical plane, but is point-to-parallel in the horizontal plane.

Four jaws, labeled FJ01-FJ04 in Figure 4, act as adjustable apertures and may be opened or closed remotely to control the pion flux through the channel. Jaw 1, FJ01 in the drawing, regulates the intensity of the pion beam. It also controls the vertical angular divergence of the beam at the focal plane. Jaw 4, labeled FJ04, has a more subtle function. It determines the momentum spread of pions that will pass through the channel. Jaw 4 contains two sliding obstructions, one above and one below the beam line, which may be used to narrow vertical acceptance. Since the dipole magnets bend charged particles in the vertical plane, pions of varying momenta are dispersed vertically, so that restricting the vertical opening of the channel at FJ04 produces a more nearly monoenergetic, although less intense, pion beam at the focal plane. Restricting the vertical size at FJ04 also trims the vertical size of the pion beam incident on the scattering target. Jaw 4 contains another set of two movable blocks which limit the horizontal opening of the beam line at FJ04. This horizontal slit size regulates both the width of the pion beam at the focal plane and the horizontal angular divergence of the beam there. Jaws FJ02 and FJ03 are essentially redundant, though FJ03 can be used to eliminate pions scattered from the edges of beam apertures farther upstream.

The entire EPICS channel from production target to a point downstream of FM03, is maintained at high vacuum. This minimizes pion scattering from gaseous particles. There is a single vacuum window, made of steel, 0.005 in thick, downstream of the production target. Measured properties of the EPICS channel were detailed in a laboratory report in 1977.[62] Several characteristics of the channel are noteworthy. With all jaws wide open, the beam spot at the focal plane containing 95% of all pions, measured 20.4 cm vertically and 6.4 cm horizontally. Angular divergence was ±77.5 mrad in the vertical plane and ±15 mrad in the horizontal plane. Figure 5 illustrates the beam disposition at the focal plane. The channel accepts a momentum bite of ±1.0%. Pion momentum at the focal plane is correlated with vertical position such that

$$\delta_B = |x|/D_B \ , \qquad (1)$$

where δ_B is the change in momentum, in percent, from the central value of the beam momentum and x is the vertical distance in centimeters from the center of the pion beam. This vertical dispersion of the pion beam allows for an increase in beam intensity of 100X relative to the intensity of a monoenergetic pion beam in a similar channel. With careful measurement of the vertical position of a pion at the focal plane, a momentum resolution of $2\text{x}10^{-4}$, full width at half maximum (FWHM), may be achieved.

The EPICS Spectrometer

In order to carefully measure the momentum of a pion incident on a nucleus of interest, then to carefully measure the momentum of

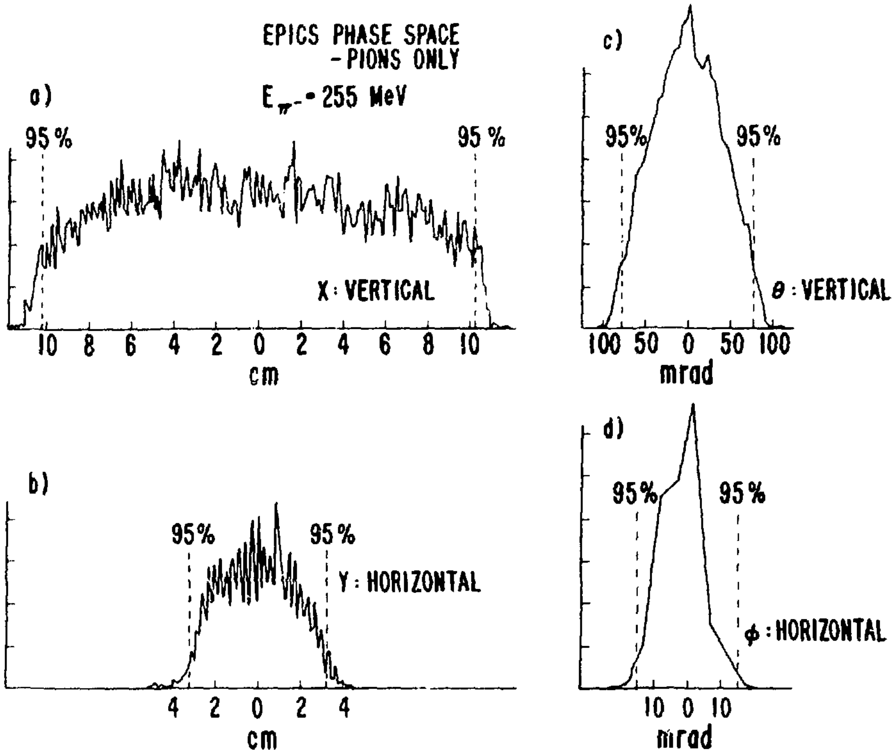

Fig. 5. Pion beam disposition at the focal plane. π^-, T_π = 255 MeV.

the scattered pion, the EPICS system must clearly have a device that determines the vertical position of each pion striking the scattering target, as well as a device which can measure scattered pion momentum. A large magnetic spectrometer at EPICS, depicted in Figure 6, satisfies both these requirements.

Spectrometer Construction

There are five magnets in the spectrometer, three identical quadrupole magnets and two similar dipole magnets. There are no multipole trim magnets as were found in the channel. The middle quadrupole magnet is rotated 90 degrees about the beam line relative to the other two. This quadrupole triplet translates and focuses the scattered pions from the scattering target. Figure 7 shows the coordinate system used to describe the spectrometer. Although it looks awkward, the coordinate system provides simplicity in the use of computer beam-transport codes, and for that reason was chosen. The optics of the quadrupole triplet cannot be equated with thin lens optics but the following matrix describes, to first order in the front coordinates, the effect of the triplet on pions transported from a scattering target in the xy plane to the front spectrometer focus.

$$\begin{pmatrix} x_T \\ \theta_T \\ y_T \\ \phi_T \end{pmatrix} = \begin{pmatrix} -1 & 0 & 0 & 0 \\ 0 & -1 & 0 & 0 \\ 0 & 0 & 0 & 0.2 \\ 0 & 0 & -5.0 & 0 \end{pmatrix} \begin{pmatrix} x_F \\ \Theta_F \\ y_F \\ \phi_F \end{pmatrix} \qquad (2)$$

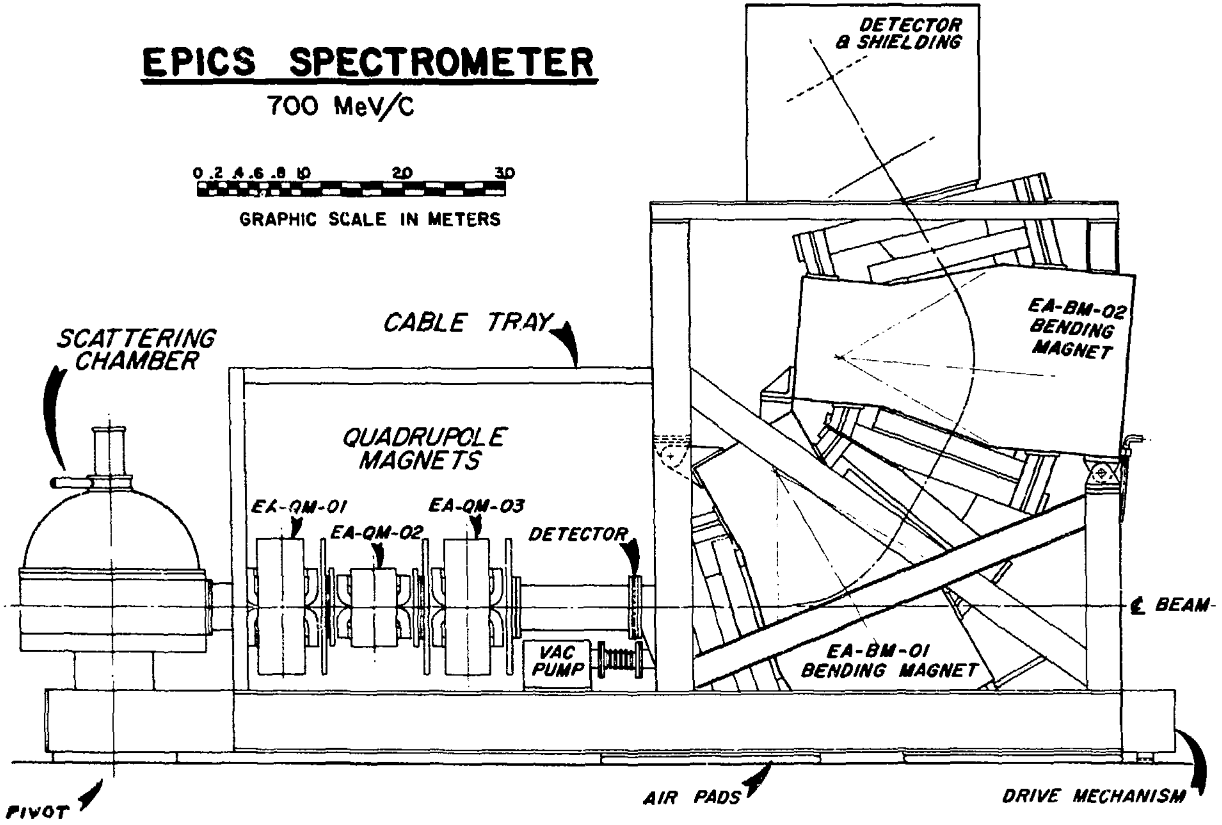

Fig. 6. The EPICS spectrometer measures the momentum of scattered pions.

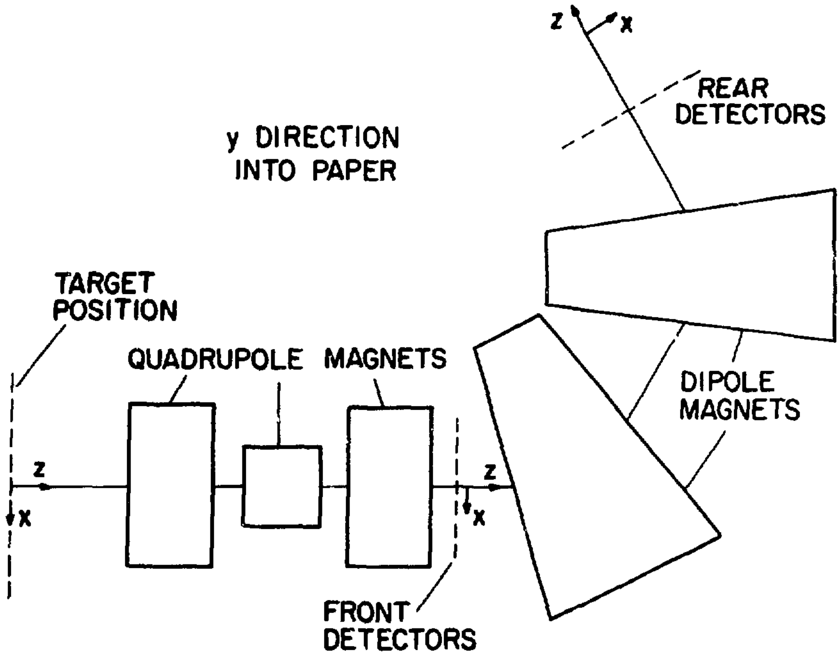

Fig. 7. The spectrometer coordinate system simplifies beam transport calculations.

Here, ϕ is the angle in the horizontal (yz) plane and θ is the angle in the vertical (xz) plane. The subscript T indicates a coordinate value at the scattering target, while the subscript F refers to a coordinate value at the front focus shown in Figure 6. Units of distance are cm and angles are given in mrad. A ray diagram through the quadrupole triplet would show parallel-to-point dependence in the yz plane from scattering target to first focus, but point-to-point dependence in the xz plane.

The two dipole magnets of the spectrometer are very similar in function to the dipole magnets of the EPICS channel. They serve to determine the momenta of pions in the spectrometer. Maximum field strength in the dipoles is 18 kG, just as it is in the channel dipole magnets, but because of the greater radius of curvature the spectrometer dipoles can handle pions of greater energy than the channel magnets. It would be possible to measure pion energies as high as 570 MeV in the spectrometer. This feature is useful for scattering experiments in which the scattered particles are other than pions. To first order, the optics of the dipole magnets in the zx plane is specified by the following matrix:

$$\begin{pmatrix} x_F \\ \theta_F \\ \delta \end{pmatrix} = \begin{pmatrix} -1 & 0 & 4 \\ -3 & -1 & 5 \\ 0 & 0 & 1 \end{pmatrix} \begin{pmatrix} x_R \\ \theta_R \\ \delta \end{pmatrix} \tag{3}$$

where $\delta = (P_\pi - P_{OS})/P_{OS}$, P_π is the momentum of a given pion and P_{OS} is the central momentum of the spectrometer (the momentum of a pion which travels through the nominal center of the spectrometer). The subscript R indicates a coordinate value at the rear focus of the spectrometer. The units of δ are percent. Notice that (3) means

$$\delta = (x_R + x_F)/4. \tag{4}$$

The spectrometer has a momentum acceptance of $\delta = \pm 6\%$.

The EPICS spectrometer weighs several hundred tons, but it may nevertheless be rotated about an axis centered on the scattering target. Figure 6 indicates this axis as the pivot. Compressed air is forced into pads under the spectrometer frame lifting the entire device slightly off the concrete floor so that an air engine may then rotate the spectrometer. This feature allows for the measurement of scattered pions at various angles relative to the direction of the pion beam incident on the scattering target. The spectrometer may be positioned at angles from -20 degrees through 0 degrees to +120 degrees. The pion beam path through the scattering chamber and spectrometer, 12.77 m in length, is almost entirely within high vacuum. The three exceptions are a short length of beam path, about 8 cm, near the spectrometer pivot, another section about 30-cm long near the front focus and a third section of about 40-cm long near the rear focus. The first two sections are filled with helium gas slightly above atmospheric pressure. The third section of beam path is in air at atmospheric pressure. Scattering of pions from gaseous particles is minimized by vacuum along the beam path.

Detection Equipment

Pion detection equipment mounted on the spectrometer is composed of eight multiwire proportional chambers and two plastic scintillators. The two scintillators, depicted in Figure 8, are located at the far downstream end of the beam path, near the rear focal plane of the spectrometer. Each scintillator[63] is made of 0.25-in.-thick polystyrene manufactured by Nuclear Enterprises Corporation (NE 110). Scintillator S2, the upstream scintillator, is 19-cm wide (y axis) and 140-cm long (x axis). Scintillator S3 has dimensions 21 cm by 140 cm. At both x axis ends of both scintillators there is a photomultiplier tube connected to the scintillator by a lucite light pipe. The phototubes are of 14 stages, model 9813 manufactured by E.M.I. Corporation, with a rise time of 2.4 nsec and gain of about 5×10^7. Charged particles passing through a scintillator create light, which is transmitted to both phototubes where an amplified electrical pulse is generated. The time integral of the current generated in a phototube, the total electrical charge, is proportional to the energy lost by the charged particle which passed through the scintillator. The detection efficiency of the EPICS scintillators is better than 99% for pions and protons.[64]

The other detectors in the spectrometer beam line are position-sensitive, delay-line wire chambers designed and fabricated by LAMPF

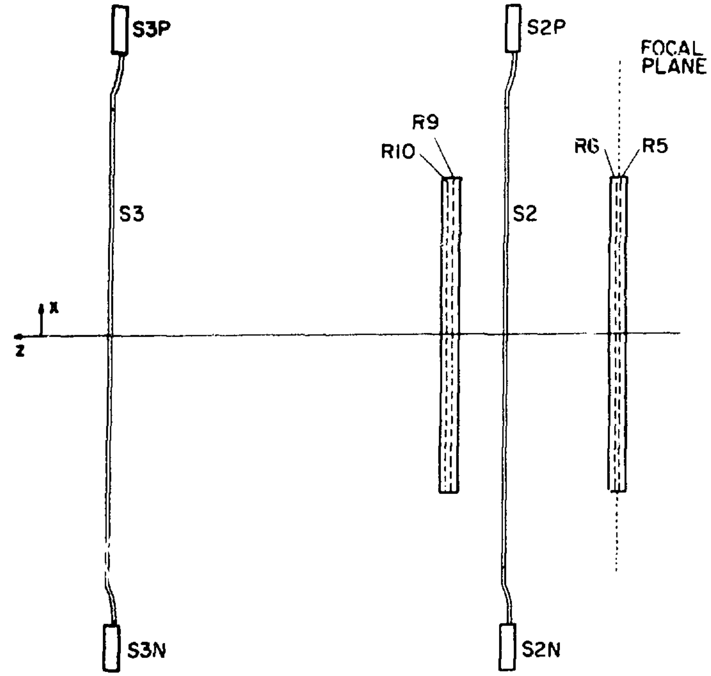

Fig. 8. There are six particle detectors near the rear focal plane of the spectrometer, four wire chambers, R5, R6, R9, and R10, and two scintillators, S2 and S3.

personnel.[65] The four rear chambers, R5, R6, R9, and R10, are schematically displayed in Figure 8. There are wires running in both the X direction and Y direction in every chamber mounted on the spectrometer, cathodes and anodes in opposite directions. Chamber R5 is 0.8 cm upstream of R6 and chambers R9 and R10 are separated by the same distance. The Z distance from R5 to R9 is 50.0 cm. Each rear chamber has an active area of 90 cm (X axis) by 30 cm (Y axis). Anode wires, 8 mm apart, parallel the Y axis in every rear chamber. Cathode wires, in the X direction, are 90-cm long having a 4 mm separation. These wires are typically 20 to 80 μm in diameter to insure few collisions between pions and the wire. Surrounding the wire grid of each chamber is a gas mixture.

A charged particle passing through a wire chamber ionizes the gas atoms along its path. Freed electrons from the gas drift to the anode wires where high amplification occurs. An electrical pulse is formed and travels down the wire and into delay circuitry. The pulse formed in the anode wires induces a positive pulse in adjacent cathode wires and these positive disturbances travel along the cathodes and into cathode delay circuitry. The anode delay circuitry is simply a serpentine conducting path printed on a circuit board. Soldered at uniform distances along the path are the ends of the anode wires. Wire chamber signals are detected at both ends of the delay path. Cathode delay circuitry is entirely analogous to the anode circuitry.

The difference in the time it takes for a signal to travel from an excited anode to one end of the delay path compared with the travel time to the other end of the delay line, t_{ad}, specifies which anode wire was closest to the charged particle which traversed the wire chamber. The sum of the travel times of the signals from an anode wire to each end of the delay line is constant for all anode wires. However, the sum of the times beginning when a charged particle ionizes the gas and ending when two signals reach separate ends of the anode delay line, t_{as}, is equal to a constant plus a time proportional to the length of electron drift from the point of ionization to the position of whichever anode wire is nearest. So, this last-described time sum may specify drift distance from the point of ionization to the adjacent anode wire.

With regard to cathode wires, the time difference between signals at either end of the cathode delay path, t_{cd}, specifies which cathode wires were nearest to the point where a signal was formed in the anode wire. Because the anode pulse induces signals of varying strengths in several cathode wires, depending on distance from the initially formed anode pulse, time difference of signals at the ends of the cathode delay line may be used to determine the position of the ionizing particle more closely than just the position of the nearest cathode wire. The time sum of the two signals beginning at ionization of the gas and ending when the signals are detected at either end of the cathode delay line, t_{cs}, is again a constant plus a time proportional to drift distance. But the difference,

$$t_c = t_{cs} - t_{as}, \tag{5}$$

is a constant for charged-particle induced ionization at any point in the wire chamber regardless of drift time. Using signals from scintillators S2, S3 to help define the instant ionization occurs in any of the wire chambers, the times t_{as} and t_{ad} are used to resolve the X position in a rear wire chamber to better than 0.5 mm. X position in the rear chambers determines the approximate pion momentum in the spectrometer. The Y position of an ionizing particle in a rear wire chamber may be resolved, given the time t_{cd}, to better than 3 mm. The wire chamber R9 was inoperative during this experiment, but this proved no significant handicap.

Four wire chambers, of similar construction to the rear chambers, are mounted in the spectrometer beam line near the front focus. These chambers, F1, F2, F3, and F4. in order of their proximity to the scattering target, are mounted in the XY plane. The chambers have active areas of 30 cm by 20 cm, the longest dimension measured vertically. Spacing between anode wires is 4 mm but cathode spacing is only 1 mm. Chamber F1, farthest upstream, is 26.04 cm ahead of F3. Chamber F2 is 1.90 cm behind F1 and chamber F4, positioned at the front focus, is likewise 1.90 cm downstream of F3. Unlike the rear chambers, cathode wires in the front chambers are not all parallel to the X axis. They are in the X axis direction in chambers F1 and F3, but are oriented along the Y axis in the other two front wire chambers. Position resolution is 0.5 mm using timed cathode signals but only 4 mm using anode signals. The drift-timing feature of the front chambers is not utilized since its superior resolution has not proved necessary. For a moderate particle flux, less than 10^5/sec, the wire chambers have detection efficiencies greater than 95 percent. Deadtime is 150 nsec. Deadtime is the period required for a wire chamber to recover from the effects of a charged particle passing through it.

Mounted directly in the EPICS channel beam line, downstream of the scattering target, are two ion chambers. Most pions whose paths intersect the scattering target pass right through the target and enter the first ion chamber. Those pions which are not stopped in the first ion chamber enter the second chamber. Each ion chamber is filled with a gas mixture held at constant pressure and has electrodes maintained at a constant electric potential. As charged particles ionize the gas, a current is set up between the electrodes, and this current is proportional to the flux of charged particles. Thus, one may measure the beam intensity of the channel by measuring ion chamber current. Because of the high intensity of the beam, scintillators would be unreliable as a beam monitor.

Measurement Techniques

It has been pointed out that the EPICS system depends on a measurement of the vertical position of a pion striking the scattering target in order to accurately determine the pion's incident momentum. This function is performed by the quadrupole triplet of the spectrometer and the four front wire chambers. To first order in Y_T, the Y component of momentum is zero for pions incident on the target, $P_{YB} = 0$. The Z component of momentum is approximately given by the relation

$$\delta_B \equiv (P_{ZB}-P_{OB})/P_{OB} = X_T/D_B \ , \qquad (6)$$

where P_{OB} is the pion central momentum of the channel and D_B is the momentum dispersion of the channel, 10.0 cm per percent. The X component of the momentum of incident pions to first order in X_T is specified by

$$\Theta_B \simeq P_{XB}/P_{OB} = X_T/A_B \ , \qquad (7)$$

with $A_B = 5.5$ mrad/cm. Using the quadrupole transport matrix (2), it is possible, by measuring the pion X position at chamber F4, to determine the momentum vector of a pion incident on the target. Notice that F4 measures X position with cathode, not anode, signals. The cathode signals provide better position resolution in the front chambers.

Figure 9 represents the fast electronic circuitry into which detector signals feed. As shown, both phototubes of the upstream scintillator, S2P and S2N, branch signals both to discriminators (DISC) and to an integrating analogue-to-digital converter (ADC). The signal to the converter is time-delayed, as indicated by a coiled wire in the figure. The ADC (model LRS 2249A) measures the time integral of the phototube current generated by a light scintillation in S2. So a function of this ADC value is proportional to the energy lost by a charged particle in traversing S2. The discriminator eliminates electronic noise and outputs two standard NIM[66] signals (digital logic signals) of -0.700 V into 50 Ω and of adjustable width. One output goes to a scaler (model LRS 2551), a device which simply counts every occurrence of a NIM signal it receives. The other output signal is sent to a mean timer (model LRS 624), where the modified signals from both phototubes are joined. The mean timer operates as a delayed logical .AND. If the two input signals occur within a specified time, in this case 16 nsec, then a NIM pulse is output after a standard delay. This ensures that no matter where a charged particle hits the scintillator, mean-timer output occurs at a constant time after scintillation. The mean timer feeds a pulse width adjusting discriminator whose output, indicating that S2 has detected a particle, branches to three devices. One device is a scaler, the other two are logical .AND. devices.

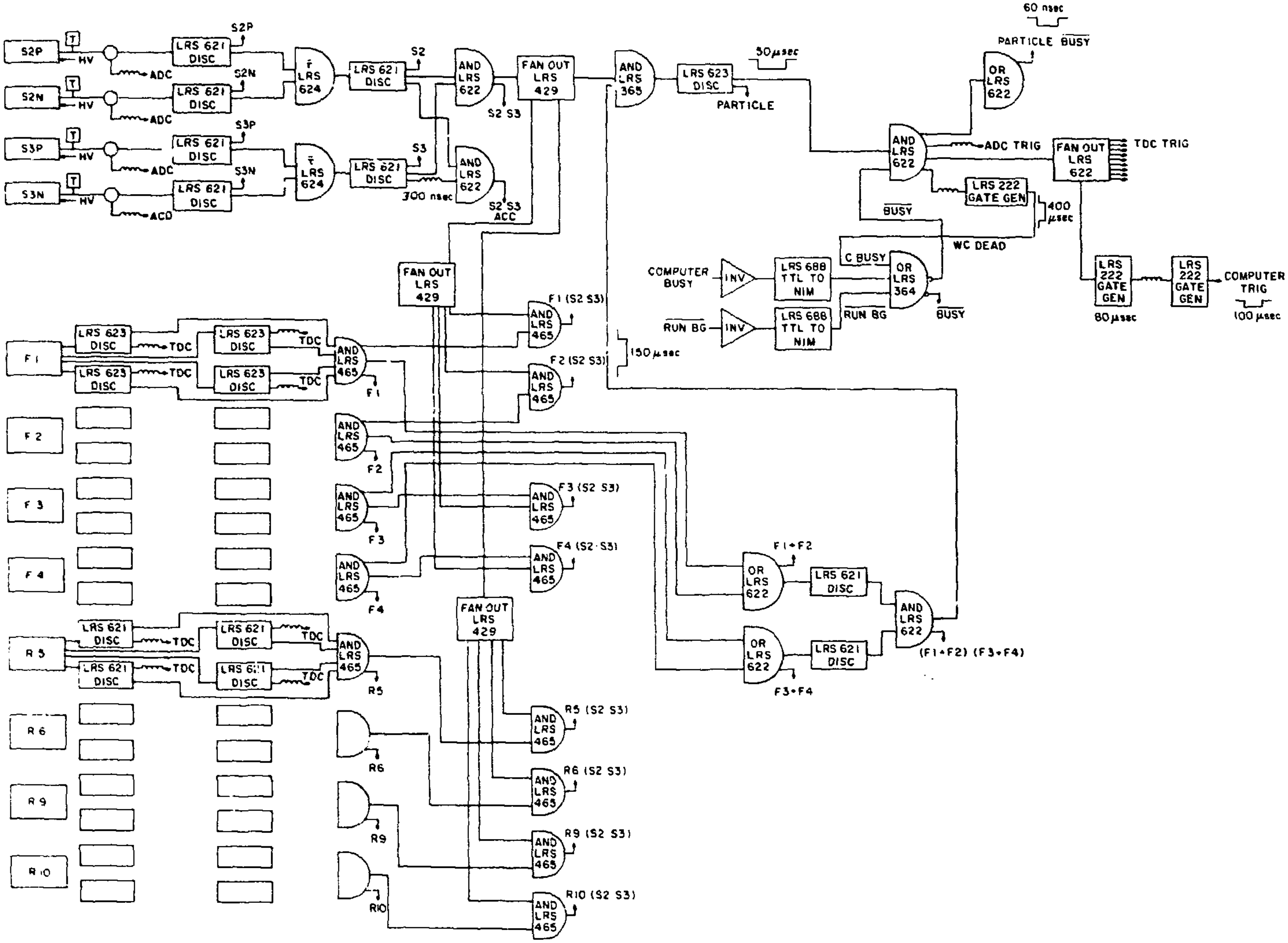

Fig. 9. Signals from the ten particle detectors of the EPICS spectrometer are fed into the fast electronics, depicted.

The outputs of the two phototubes, S3P and S3N from scintillator S3, follow circuitry identical with the S2 circuitry described above and give a signal indicative of a charged particle in S3. The S2 and S3 signals are input to two logical .AND. devices, one of which counts real particles traversing S2 and S3. Notice, though, that the other device accepts an S3 signal delayed 300 nsec before input. A real charged particle does not pass through S3 as long as 300 nsec after passing through S2, so coincidence of S2, and S3 delayed, measures accidental coincidences between the S2 and S3 signals. Such accidentals may be caused by two real particles 300 nsec apart or electronic noise.

Figure 9 shows that signals from either end of a wire chamber delay line are passed through a discriminator to shape the electrical pulse. Each discriminator output is sent to a time-to-digital converter (TDC, model EGG TD811). The TDC measures the time between the arrival of two electrical pulses, one called the start, and the other called the stop. In this case the discriminator pulse stops the TDC. All TDC start pulses are specified by the S2•S3 signal from the scintillators. Another signal from each discriminator enters a logical .AND. device. There is one .AND. for each wire chamber. One coincidence output signal from the .AND. feeds a scaler and indicates the detection of a particle in the chamber in question. Another output signal is fed into a logical .AND. device whose remaining input is the S2•S3 signal from the scintillators.

Output pulses from this coincidence are counted by a scaler, which indicates a particle in both scintillators and the wire chamber considered. For front wire chambers, a third output from the .AND. leads to a further coincidence network. A logical .OR. device indicates a particle in either F1 or F2 or both and another device indicates a particle in either F3 or F4 or both. The output signals from these two devices trigger an .AND. whose output is fed into another .AND. device along with the S2•S3 signal. A particle in the spectrometer is indicated by the output signal of this last .AND. device. The rest of the fast electronics circuitry is designed to produce the hardware trigger for the experiment.

Second only to the EPICS spectrometer and channel, the most important device used in this experiment is a very powerful minicomputer, the PDP 11/45,[67] manufactured by Digital Equipment Corporation. The measurements made with TDC's, ADC's and scalers are read by this computer. The CAMAC instrumentation system[68] supplies operating power for the measuring devices, provides an electrical network for reading and commanding the devices, and interfaces the electrical network with the computer through a microprogrammed branch driver (MBD).[69] Through the CAMAC interface the computer can read any measurement of a TDC, ADC or scaler in the system as though this information were in computer memory. The computer program called "Q",[70] written by LAMPF personnel, provides the command language for specifying location and type of measurement modules, and for resetting the modules or systematically reading their information into a software buffer in the computer. The metier of the CAMAC system is speed of data analysis.

Each hardware trigger prompts the computer to activate Q software and service measurement modules. The hardware trigger is the particle signal of the fast electronics, Figure 9, modified in several ways. Particle signals do not make hardware triggers if the computer or CAMAC system is busy processing data from the recent measurement of a particle in the spectrometer or if the wire chambers are temporarily dead after ionization. The structure of the LAMPF beam provides protons at the A-1 target only 6% of the time. A beam gate signal, labeled BG in Figure 9, causes no hardware triggers to occur if protons are not incident on the A-1 target. Finally, one may halt the processing of signals from the spectrometer detectors, by setting a switch, labeled RUN, to off. The hardware trigger is the actual signal which starts each TDC, but the timing of signals from the front wire chambers are set wide enough that it is the more accurate scintillator signals which determine trigger timing. In this way position in the wire chambers, including drift times in the rear chambers, is specified by the scintillator signals, indicating a charged particle has traveled through the spectrometer.

The computer software utilized in this experiment is characterized by sedimental and multilingual traits. Programs are written in three distinct languages, FORTRAN[71] and two others. User interactive Q data-handling programs speak in a language written by LAMPF programmers called QAL.[72] Many general utility programs are written in MACRO 11,[73] the machine language of the PDP-11 computer. The depth of the dependence of one layer of programming on others beneath it is startling. One of the more accessible blocks of programming includes a FORTRAN program called the event analyzer. Appendix A contains a copy of the analyzer for this experiment, called PROC06. The analyzer stores data from each CAMAC measurement as a word in a common buffer. The values of these words are the raw data for each particle measurement performed by the spectrometer. More importantly, the analyzer calculates values of quantities which are functions of the raw data and stores the calculated data in the same common. For example, the analyzer calculates a number proportional to the energy loss in scintillator S2 when a charged particle passes through it. Raw data for this calculation are the ADC readings from phototubes S2P and S2N. These two words are named IS2PA and IS2NA and energy loss in S2, named S2DELE, is calculated by

$$\mathrm{S2DELE} = (\mathrm{IS2PA} \times \mathrm{IS2NA})^{1/2} .$$

There is a small exponential loss as a light pulse travels to either end of the scintillator. At a phototube the light intensity is

$$Ie^{-(d \pm x)} ,$$

if I is the intensity at the position of scintillation, x_p, with $x \propto x_p$, and d proportional to the distance half way between each tube. The addition of the two light pulses at the two tubes yields

$$2Ie^{-d} \cosh x.$$

But the square root of the product of both pulses gives

$$Ie^{-d} ,$$

a term proportional to the light intensity of scintillation. It is this last term that is chosen to measure the energy loss in the scintillator.

The analyzer program calculates, among other quantities, the values of X_F, Y_F, Θ_F, Φ_F, X_R, Y_R, Θ_R, and Φ_R. Raw data for these calculations are the signals from all the wire chambers. Angles are calculated from position in the various chambers and their separation distances. A much more interesting calculation is performed by a subprogram of the analyzer. The computer stores the values of P_{OB}, angle of the spectrometer relative to particles incident on the scattering target, angle of the target, nuclear composition of the target, and P_{OS}, the momentum of a pion which travels down the center of the entire spectrometer. These values are input to the computer by the experimenter. An elaborate relativistic kinematics calculation carried out by the subprogram can determine the momentum, $P_{O\pi}$, of a pion scattered from the center of the target toward the exact center of the quadrupole magnets.

A program called DSP creates histogram and scatter plots, displayed on a CRT screen, using any data words stored by the analyzer. During this experiment, 280 data words were stored for every particle that caused a hardware trigger. Figure 10 displays the results of a histogram of S2DELE values for particles scattered from a target composed of ^{58}Ni. A scatter plot of X_F verses Y_F is shown in Figure 11 for particles scattered from a nickel target.

Another block of programs performs test operations on data words. One program counts the number of particles during an experimental run that have a measured, or calculated, value, such as S2DELE or X_T, lying between values specified by the experimenter. Such a test may be used to gate a histogram or scatter plot. It is possible, for example, to histogram the value S2DELE for those particles, and only those particles, whose X_T values lie between -1 cm and 1 cm. Protons which reach the scintillators of the spectrometer lose more energy in the scintillators than do pions, as can be seen from Figure 10. One may distinguish pions from protons by specifying limits to the value S2DELE for all particles that travel through the spectrometer.

Each hardware trigger activates the Q programs, causing each TDC and ADC to be read and reset after an appropriate delay to let measurements be made, causing the analyzer program to perform its operations and the test programs to perform theirs, and usually causing every raw data word to be written to magnetic tape. The Q programs are set up such that raw data words on tape can be used,

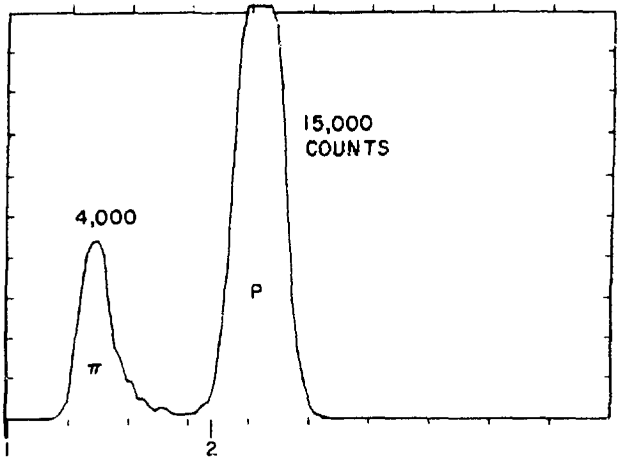

Fig. 10. The energy loss in scintillator S2 is histogrammed for particles scattered from ^{58}Ni. Protons are created by collisions in the target and are responsible for the peak at right. The other peak is caused by pions.

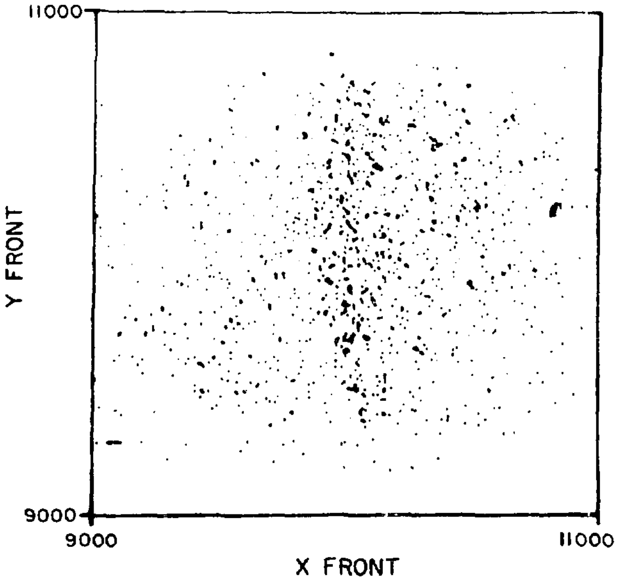

Fig. 11. A scatter plot of X_F versus Y_F for particles scattered from ^{58}Ni crudely shows the dimensions of the target.

off line, to mimic the acquisition of raw data from the spectrometer. This allows one to observe the effect of changing test limits, calculating different quantities with a different analyzer, or other such operations, without using the EPICS system. Scaler counts are read by the computer and, in the usual case, written to magnetic tape at uniform time intervals and at the end of an experimental run.

The analyzer program provides the means to measure X_T more accurately than is possible with the first-order quadrupole matrix (2). The optics of the quadrupole triplet are not fully described by the first-order matrix, and it is not possible to provide a fine tune to the quadrupole magnets with small multipole trim magnets, as exist in the channel, since there are no trim magnets in the spectrometer system. Instead, higher-order terms of the quadrupole optics may be equated with the coefficients of a linear equation, and the coefficients found by a fitting technique. Design calculations indicate that the prominent terms, to third order, affecting the measured value of X_T, are the following: X_F, Θ_F, X_R, X_R^2, Y_F^2, X_F^2, $X_R X_F$, Θ_F^2, $X_F \Theta_F$, $X_R \Theta_F$, $X_F^2 \Theta_F$, $X_F \Theta_F^2$, Θ_F^3, $Y_F^2 \Theta_F$, $\Phi_F^2 \Theta_F$, $X_F \Theta_F X_R$, $X_R^2 \Theta_F$, and $\Theta_F^2 X_R$. To calculate the coefficient of each of these terms in the linear equation specifying X_T, a procedure is used involving a thin horizontal rod as scattering target. The height of this rod relative to the center of the quadrupole triplet is carefully measured. A computer program is written which can read the data words X_F, Θ_F, Y_F, Φ_F, and X_R from the analyzer program. A large set of these values is accumulated by scattering pions from the rod target. Then, a fitting program is run which determines a best value of each coefficient such that X_T is the height of the rod target. A Q subprogram, known as "Event 18", stores the coefficient values in the computer so that the analyzer may calculate X_T for any particle entering the spectrometer. Using such an elaborate calculation, X_T may be measured with a resolution of 5 mm. (FWHM).

The other particle coordinates at the scattering target are found in the same way. A third-order linear equation is constructed for each of Φ_T, Y_T, and Θ_T, and the coefficients of each of these equations are stored in computer memory. Every time a particle in the spectrometer initiates the analyzer program, a third-order equation is used to determine each coordinate value at the target. Φ_T resolution was found to be better than 10 mrad (FWHM).

The momentum of a pion scattered from the target is calculated in a similar fashion. Again a third-order linear equation is constructed for the value to be found and coefficients of the equation are stored in the computer. The value measured is not strictly pion momentum, however, but rather the difference

$$\delta = (P_\pi - P_{OS})/P_{OS} \ , \qquad (8)$$

called DELTA in the analyzer program. Other values calculated by elaborate linear equations with fitted coefficients are the path length of a pion through the spectrometer and two angle predictions.

Given Θ_F and Φ_F, these last two calculations predict the values of Θ_R and Φ_R, which may be compared with the values measured by the rear chambers. Listed in Table 2 are the fitted coefficients used in each calculation.

During this experiment, the overall energy resolution, the measurement of the change in energy from the value possessed by an incident pion, to the value after scattering, was found to be 0.25% (FWHM). Calculations showed that multiple coulomb scattering and energy degradation in the vacuum windows contributes about 150 keV to the loss of resolution.

Table 2. The analyzer program calculates specified values using a linear equation of terms and fitted coefficients as shown. D_L is analogous to DELTA.

Delta Calculation

Term	Coefficient	Term	Coefficient
1	-0.2948	$Y_F\Phi_F$	0.00008533
X_F	0.2339	$\Phi_F\Phi_F$	0.1400
Θ_F	0.0008894	X_RX_R	0.001007
Y_F	-0.008157	$X_FX_F\Theta_F$	0.000006887
Φ_F	-0.0004591	$X_F\Theta_F\Theta_F$	0.0000008418
X_R	0.2345	$X_F\Theta_FX_R$	0.000001057
X_FX_F	0.001349	$\Theta_F\Theta_F\Theta_F$	0.00000004718
$X_F\Theta_F$	0.00001608	$\Theta_FY_FY_F$	-0.000005711
X_FX_R	0.0002318	$\Theta_F\Theta_F\Theta_F$	0.0000004762
$\Theta_F\Theta_F$	0.00005562	$\Theta_F\Theta_FX_R$	0.0000004048
Θ_FX_R	0.00004687	$\Theta_TX_RX_R$	0.0000009494
Y_FY_F	-0.0001106	$X_RX_RX_R$	0.000001689

Table 2 (continued).

X_T Calculation

Term	Coefficient	Term	Coefficient
1	0.03853	$X_F X_F \Theta_F$	0.00006907
X_F	-1.008	$X_F \Theta_F \Theta_F$	-0.000001147
Θ_F	-0.002943	$\Theta_F \Theta_F \Theta_F$	0.0000001064
$X_R X_R$	-0.00005678	$\Theta_F Y_F Y_F$	0.0001739
$Y_F Y_F$	0.001371	$\Theta_F \Phi_F \Phi_F$	0.000004742
$X_F X_F$	-0.001353	$X_F X_R \Theta_F$	-0.000007467
$X_R X_F$	-0.0004787	$X_R X_R \Theta_F$	-0.000005994
$\Theta_F \Theta_F$	-0.000005388	$X_R \Theta_F \Theta_F$	-0.0000007639

Θ_T Calculation

Term	Coefficient
1	-0.5435
X_F	-0.7357
Θ_F	-0.9774
$X_F X_F$	0.06257
$X_F X_R$	0.05558
$X_R X_R$	0.001392
$\Theta_F \Theta_F$	0.0001726
$\Theta_F X_R$	-0.0002686

Y_T Calculation

Term	Coefficient
1	-0.3920
Y_F	0.06151
Φ_F	0.1876
$X_R Y_F$	-0.01394
$X_R \Phi_F$	0.002396
$X_F Y_F$	-0.01706
$X_F \Phi_F$	0.004329

Table 2 (continued).

Φ_T Calculation

Term	Coefficient
1	5.331
Y_F	-5.325
Φ_F	0.04422
Y_FX_R	0.06709
Y_FX_F	0.08207
Φ_FX_R	-0.01167
Φ_FX_F	-0.01999

Θ_{RC} Calculation
(Predicts the measured value)

Term	Coefficient
1	-8.431
X_R	1.610
X_F	-1.291
Θ_F	-1.001
X_RX_R	-0.02314
X_FX_F	0.04468
$\Theta_F\Theta_F$	0.0006566
X_RX_F	0.003866
$X_R\Theta_F$	-0.007637

Φ_{RC} Calculation
(Predicts the measured value)

Term	Coefficient
1	9.446
Y_F	-2.628
Φ_F	-0.9352
X_FY_F	-0.09967
$X_F\Phi_F$	0.007082
X_RY_F	-0.003101
$X_R\Phi_F$	0.009789
Θ_FY_F	-0.004969
$\Theta_F\Phi_F$	0.001944

Path Length Calculation

Term	Coefficient
1	2.136
X_F	-0.006886
Θ_F	-0.003171
D_L	-0.01578
X_FX_F	0.0005288
$X_F\Theta_F$	0.00004625
$\Theta_F\Theta_F$	-0.000004341
D_LX_F	0.0003550
$D_L\Theta_F$	0.000006287

III. EXPERIMENTAL TECHNIQUE

Pion-nucleus scattering experiments are diverse and, as yet, most of the information from such work is not fully realized. There are numerous variations on scattering experiments, for example the measurement of total or charge-exchange cross sections. This thesis experiment concerns itself with one of the more fundamental scattering techniques, the measurement of elastic differential cross sections .

A Definition

Consider the following situation: A beam of pions of known momenta, and of intensity I_0 pions/cm^2-sec, is directed on a target containing a number, n_T, of nuclei in each cm^2 orthogonal to the incident beam. All pions scattered in one second into a solid angle $d\Omega$, located relative to the incident beam at scattering angle Φ_S, are detected and their momenta are measured. Some of the pions will induce an excitation of the nuclei with which they collide. The momenta of these pions will be less than that of the momenta of elastically scattered pions which do not excite the nucleus. The elastic differential cross section is defined as

$$(d\sigma/d\Omega)_E = N_E/n_T I_0 \ , \tag{9}$$

where $N_E d\Omega$ is the number of pions elastically scattered into the solid angle $d\Omega$ per second. An inelastic differential cross section measures the number of pions scattered into a solid angle $d\Omega$ in one second, which have lost a specified amount of energy to nuclear excitation.

By far, the easiest component of the differential cross section to measure is the value n_T. It requires only the determination of the mass of the target and its area incident to the incoming pion beam, assuming, of course, that the target thickness and density are uniform. Suppose such a uniform target contains a single species of nuclei of atomic mass A and has a mass of w grams. Its incident area is B cm^2. Then n_T may be calculated with Avogadro's number, N_a = 6.0222/gm-mole:

$$n_T = wN_a/BA \ . \tag{10}$$

In spite of the fact that B has the units of area, for purposes of calculating the cross section, n_T is taken to be a pure number. The density of targets used in this experiment is shown in Table 3. All targets were thin rectangular sheets measuring 8 in. in the vertical direction and were several millimeters thick. The lead and nickel targets were six inches wide. The beryllium, carbon, and silicon targets were four-and-a-half inches wide.

The Normalizing Ratio

It is not possible to measure the solid angle which the spectrometer presents to scattered pions. The optics of the spectrometer magnets are very complex, as has already been pointed out, and more than one aperture defines the solid angle acceptance in the

Table 3. The mass density of targets used in this experiment is listed below. The density is an area density incident to the incoming beam. Each target was relatively pure, containing better than 92% by weight of the particular nucleus shown. Error in the density is less than two percent for every target. The targets were a few millimeters thick. Average pion energy loss in each target is indicated for $\Phi_S = \Phi_T = 0$. $E_\pi = 162$ MeV.

Nucleus	Energy Loss (MeV)	Density (g/cm^2
^{9}Be	0.184	105
^{12}C	0.484	252
^{28}Si	0.634	366
^{58}Ni	0.461	292
^{208}Pb	0.341	289

spectrometer. Furthermore, the spectrometer solid angle is a function of the spectrometer central momentum and of the difference, δ, between central momentum and the momentum of a scattered pion. The solid angle may also be a function of the jaw settings in the EPICS channel, the charge sign of pions used, and of field strength in the channel separator. It is nevertheless possible to measure scattering cross sections of nuclei if the differential cross section of a single nucleus at a particular scattering energy is accurately known. In such a case, spectrometer scattering measurements may be compared with the accepted value of the cross section at a certain energy, enabling the measurement of differential cross sections on other nuclei at that energy.

There is one nucleus for which the differential cross section may be precisely calculated, ^1H. A physicist at the Los Alamos Scientific Laboratory has made a calculation of the cross section of pion scattering from hydrogen[74] based on the derived phase shifts of pion-proton scattering. His results, while considered more accurate than measurements of the pion-hydrogen cross section, such as those made by Bussey,[75] agree, within quoted error, with the measured values. Calculated cross sections have a total error less than 2%.

While it might seem possible to determine the spectrometer solid angle for a particular configuration of the EPICS system by comparing spectrometer measurements with the calculated cross section, even this is not practicable because it is not feasible to measure the pion beam intensity, I_0, on a scattering target. The intensity, I_0, is a function of the jaw settings in the channel, the separator field, and of the central momentum of the channel, and the shape and position of the scattering target. The measurement of I_0 is predicated on a knowledge of the ion chamber-target orientation and the relative number of different types of charged particles which compose the beam. But as was shown in Table 1, the percentage of pions in the beam is known to no better than ±3%. This alone introduces unnecessary error into a cross-sectional measurement. Comparing spectrometer scattering measurements on hydrogen with the calculated pion-hydrogen cross section obviates any need to measure solid angle or I_0. As long as parameters of the EPICS system that affect I_0 and $d\Omega$ remain unchanged, then the scattering information from a target containing hydrogen may be used to calibrate the scattering data from any of the other targets.

In this experiment, normalization was made to the pion-hydrogen cross section in a roundabout fashion. The differential cross section for pion scattering from ^{12}C at 162 MeV has been recently measured using the EPICS system.[76] Normalization of the ^{12}C cross section was derived from the pion-hydrogen cross-sectional calculations. Cross sections measured in this thesis experiment are directly normalized to the carbon cross section by measuring scattering from a carbon target. A ratio of the known cross section of pion-carbon scattering to the "yield" for pion-carbon scattering measured by the spectrometer in this experiment provides the cross section to yield ratio, which implicitly contains the solid angle and beam intensity information needed to normalize the scattering data from beryllium, silicon, nickel, and lead targets. The configuration of the EPICS system was maintained nearly unchanged during the entire experiment. That is, spectrometer central momentum, channel central momentum, separator field, and scattering target height were not changed.

A direct normalization to the pion-hydrogen cross-sectional calculations was not chosen for this experiment because the light hydrogen mass causes a large value of δ at large values of Φ_S, and requires the change of spectrometer magnetic fields in order to accept scattered pions. Changing large magnetic fields is a time-consuming process which slows down the acquisition of data.

The Scattering Yield

Some percentage of pions which scatter from any of the targets used in this experiment do so inelastically. They lose kinetic energy by exciting the scattering nucleus. It is worthwhile to distinguish inelastically scattered pions from those that are scattered elastically because it is thought that the mechanisms for the two types of scattering are different. It may be possible to learn about both mechanisms by gathering both types of scattering data.

Missing Mass

The kinetic energy of an elastically scattered pion is, of course, not the same as that of the incident pion. The scattered pion energy depends on the mass of the target nucleus as well as the direction of incident and scattered pion momentum. Additionally, some kinetic energy is lost as a pion passes through the finite thickness of the scattering target.

Except for a few measurements, the angle of the scattering target, relative to the incident particle beam ω_T, was half the value of the central spectrometer angle, ω_S, relative to the incident beam. This ensures a constant solid angle subtended at the spectrometer. It is also desirable to rotate the target half as much as the spectrometer because of pion energy loss to ionization in traveling through any target. If the spectrometer was at 90° and the target plane remained perpendicular to the incident beam, then a scattered pion might have to traverse the entire width of the target before entering the spectrometer. Fig. 12 shows a yz-plane cross section through the target and indicates the path of several scattered pions. The angular acceptance of the spectrometer in the yz plane is about seven degrees and all scattered pions which enter the spectrometer travel in a nearly parallel direction. It can be seen then, from Fig. 12, that the path length through the target is about the same

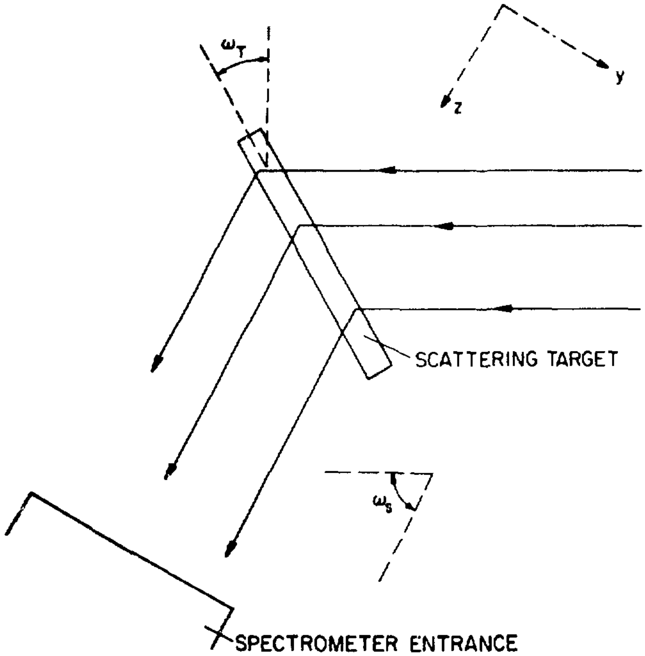

Fig. 12. *The path length through the target is approximately the* same for all pions scattered into the spectrometer.

for all scattered pions. This is true for all values of target angle, ω_T, such that $\omega_T = \omega_S/2$.

The average energy loss of pions passing through a target when $\omega_S = \omega_T = 0$, is listed in Table 3 for all five scattering targets. The average energy loss increases with ω_S where $\omega_T = \omega_S/2$. The mean value of the kinetic energy carried by a pion into a nuclear collision in the target is the pion's kinetic energy upstream of the target minus half the mean energy loss in that particular target. In a scattering experiment one must, in general, reach a compromise. The thicker the scattering target used, the greater is the intensity of particles scattered from the target, but also greater is the uncertainty in the exact value of incident particle energy at the scattering nucleus, and greater too, is the energy spread of scattered particles due to ionization losses in the target. In this experiment, the maximum change in the mean value of incident pion energy on a scattering nucleus was mainly due to the momentum dispersion of the incident pion beam, which corresponds to an energy dispersion of about 1.5% near 162 MeV. However, energy losses in the target before collision with a nucleus also contribute a small amount to the variation of incident energy. The target angle, ω_T, ranged from near 0° to 45° during the experiment. This represents a change in mean incident pion energy of 0.125 MeV in the silicon target. Rotation of any of the other targets resulted in smaller change.

The value measured by the EPICS system which is equivalent to pion energy lost to nuclear excitation is called the missing mass. An elaborate relativistic kinematics calculation determines missing mass. The values that must be fed into the computer for this calculation include the incident pion momentum, which is a function of the scattered pion momentum, and the direction of the momentum of the scattered pion. The experimenter must input the atomic mass of the target nucleus, the average pion energy loss in the target and the target angle, ω_T, the central momentum of the channel and spectrometer, and the central angle of the spectrometer relative to the incident charged particle beam, ω_S. The missing mass calculation compensates for pion energy loss in the target prior to the collision with a nucleus and for the energy lost in traversing part of the target after scattering. The calculation also transforms the values X_T, θ_T, Y_T, and θ_T, measured by the spectrometer, to the plane of the scattering target, which is not, in general, perpendicular to the central ray running through all the spectrometer magnets.

A histogram may be constructed of the missing mass values of pions entering the spectrometer. It is useful to divide the solid angle of the spectrometer into several partitions, each of which more closely defines the scattering angle Φ_S, of pions entering that partition. This division was made by using test software to restrict the Φ_T values of those pions whose missing mass values were histogrammed. Figure 13 displays a histogram of missing mass

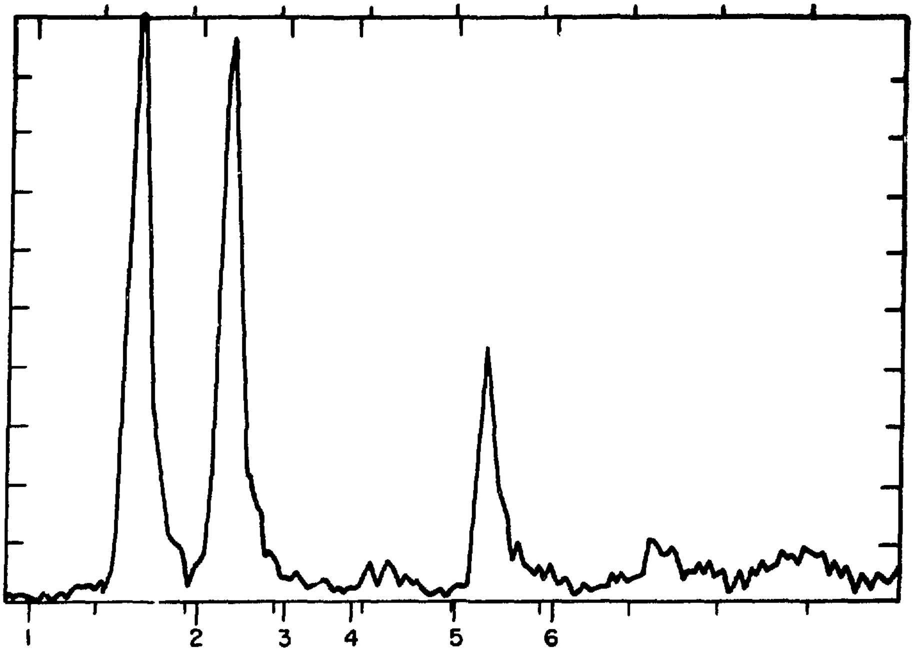

Fig. 13. A histogram of missing mass is shown for positive pion scattering from ^{28}Si. The incident pion energy is 162 MeV. The leftmost peak counts elastically scattered pions, while the first peak to its right indicates those pions which excited the first inelastic level of the nucleus at 1.78 MeV. A small bump between markers four and five is caused by pion excitation of the level at 4.61 MeV. The peak between markers five and six is due to pions which have lost 6.88 MeV to nuclear deformation. Angular acceptance is 2.4 deg. Φ_S = 35.6 deg. The six markers fall at energies -2.0 MeV, 1.2 MeV, 2.9 MeV, 4.2 MeV, 6.2 MeV, and 8.1 MeV relative to the zero value of elastic scattering.

values of those positive pions scattered from ^{28}Si whose angular values, Φ_T, lie between -1.2 deg and 1.2 deg. Since the central spectrometer angle, ω_S, was 35.6 deg in this instance, the scattering angles, Φ_S, of pions histogrammed lie between the two limits 34.4 deg and 36.8 deg.

The missing mass values were measured for those pions in one of three angular bins. A bin of width 2.4 deg centered on the spectrometer was set up to measure the missing mass of inelastically scattered pions. Two bins of 1.2 deg in width bisected the 2.4 deg bin. These smaller angular bins determined the missing mass of elastic pions. The smaller bins provide less uncertain measurement of Φ_S, but the number of elastic pions which are scattered into a 1.2 deg bin in a given time is only about half the number which would be scattered into the larger 2.4 deg bin. The cross section for elastic scattering is usually so much larger than an inelastic cross section that the better angular resolution at the expense of intensity is justified for elastic scattering.

Test software is also employed to ensure that of those charged particles causing a hardware trigger, protons initiate no histogramming. Protons which are accepted by the spectrometer loose more energy in the scintillators than do particles traveling nearer the speed of light, such as pions, muons, and electrons (see Fig. 10). A test gate is set on the value of energy loss in the scintillators and the result is that no significant number of protons initiate the histogramming and scatter plot programs. Though the charged particle beam contains measurable numbers of muons, electrons, and protons (see Table 1), scattering of muons and electrons into the spectrometer is small. The amount of muon and electron scattering may be calculated and its effect may be subtracted from measured scattering data to give purely pion-scattering cross sections. The calculation of the scattering of electrons and muons will be presented in a later chapter.

It might be expected that a good missing-mass calculation of pion-nucleus scattering would result in discrete values of missing mass. There is, after all, no energy lost to nuclear deformation in elastic scattering and the first few excited states of those nuclei examined in this experiment are reasonably well separated from the ground state and from each other. As Fig. 13 shows, pions which have excited the first inelastic state in ^{28}Si at 1.78 MeV, are clearly separable from elastically scattered pions. The central scattering angle is 35.6°. Scattering from excited states at 4.61 MeV and 6.88 MeV is also visible. However, every peak incorporates more than a single value of missing mass and each peak continuously melds into adjacent peaks. Even between widely separated peaks there is some background. Figure 14 shows a missing-mass histogram of the same pion scattering as Fig. 13 displays, except that the central scattering angle is 23.6°. Scattering to the inelastic states at this angle is very weak relative to elastic scattering, so that the elastic peak shape is better seen here.

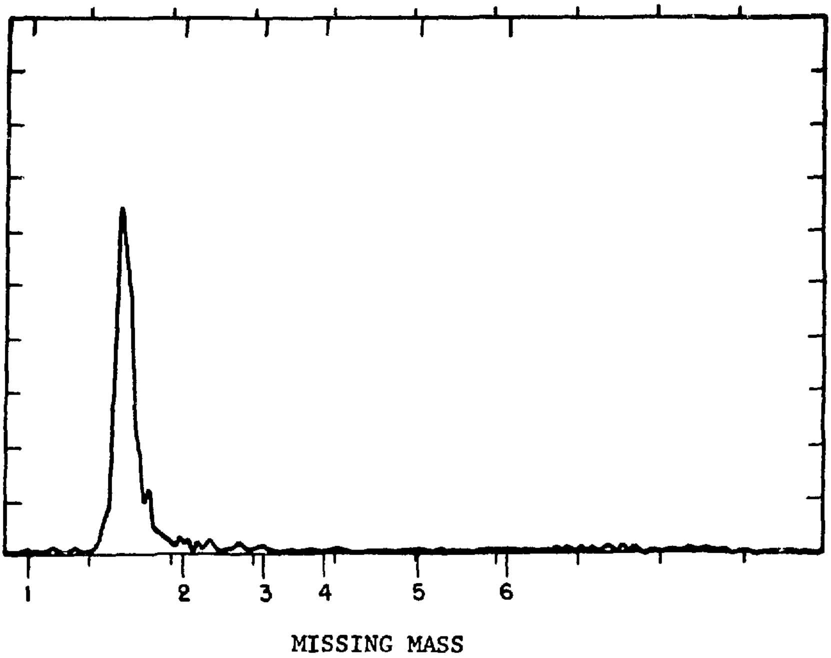

Fig. 14. A missing-mass histogram for positive pion scattering from ^{28}Si at 162 MeV incident pion kinetic energy is shown. The angular acceptance is 2.4 deg. Φ_S = 23.6 deg. Inelastic states are very weakly excited by pions at this angle. The six markers represent energies of -2.0 MeV, 1.2 MeV, 2.9 MeV, 4.2 MeV, 6.2 MeV, and 8.1 MeV.

The width of the missing-mass peaks is primarily a consequence of measurement error in the EPICS system. As has already been pointed out, the position resolution of the spectrometer wire chambers, coulomb scattering and energy degradation in the vacuum windows, uncertainties in the exact beam optics, and energy degradation in the scattering target, limit energy resolution of the EPICS system. There is also a source of natural line-broadening that is unrelated to any apparatus. When a charged particle is accelerated, such as occurs if it is scattered from a target, a number of photons are radiated according to statistical probability. There is a small chance that the particle will lose a great deal of energy to electromagnetic radiation and a much better chance that it will loose only a little energy in this way. For example, only 3.5% of all negative pions with 162 MeV kinetic energy, scattered at 90 deg from ^{208}Pb, lose more than 2 MeV of energy to radiation. Figure 14 gives an indication of the radiative tail on the missing-mass peak shape. Note that the right edge of the peak depicts those elastically scattered pions that have radiated significant amounts of energy.

It is thought that the missing-mass values so conspicuous on the left of the elastic peak in Fig. 14 are caused by muons. However, elastically scattered muons from the target should be assigned values about the same as the missing-mass values of elastic pions. Rather, it may be muons created by pion decay in the spectrometer that account for the few values to the left of the elastic peak.

When a pion decays into a muon and neutrino, the muon can have a higher momentum than the pion. Such an anomalously high momentum can result in misassignment of missing mass on the high energy side of the pion elastic peak. Most often the muon will diverge from the path of the pion that created it. If the pion decay occurs downstream of the front wire chambers in the spectrometer, it is possible to select out many of the product muons. The angle of a pion at the front chambers, and dipole magnet optics, allows for the prediction of pion angle at the rear chambers. If the pion decays downstream of the front chambers, it is likely that the angle of the muon through the rear chambers is not in agreement with the angle predicted by pion trajectory at the front chambers. All missing mass histograms are gated by a test on rear-focus angle prediction compared with the measured angle at the rear focus. That some muons seem to cause missing-mass assignment on the high energy side of the pion elastic peak is a sign that the angle test is not totally effective.

There are, in fact, quite a few tests which act as gates on the missing-mass histograms, excluding from the histograms the values of particles which cannot be identified as pions scattered from the target. Energy loss in the scintillators and the angle check are just two of many gates.

It is essential that all seven operating wire chambers function properly, if the momentum of a pion is to be measured correctly.

But the wire chambers are not 100% efficient and are, in fact, less efficient detectors of protons and muons that of pions because of the different speeds of the particles. Occasionally a wire chamber will malfunction when a charged particle passes through it. In such a case, the time check sum t_c [see equation (5)] will not attain its constant value. When this happens in any wire chamber, the particle that triggered the detection system will not contribute to any missing-mass histogram. Other tests set limits on the coordinate values of acceptable particles. If one of the coordinates S_T, Θ_T, Y_T, or Φ_T indicates a particle entering the spectrometer that did not come from the scattering target, then again, the missing-mass histograms are not augmented by the missing-mass value corresponding to that particle's momentum. The coordinates of a particle at the front and rear wire chambers are also tested for spurious values.

To determine the number of pions represented by a missing-mass peak, whether the elastic peak or any inelastic peak, a fitting program integrates the area under that peak between limits set by the experimenter, subtracting off the area of a specified background. Those muons that are products of pion decay in the spectrometer and are not tagged by the angle test can be handled by setting a proper background below each fitted area. The dotted line in Fig. 15 shows a typical background. The area under the dotted line is subtracted from the integrated area, in this case including two

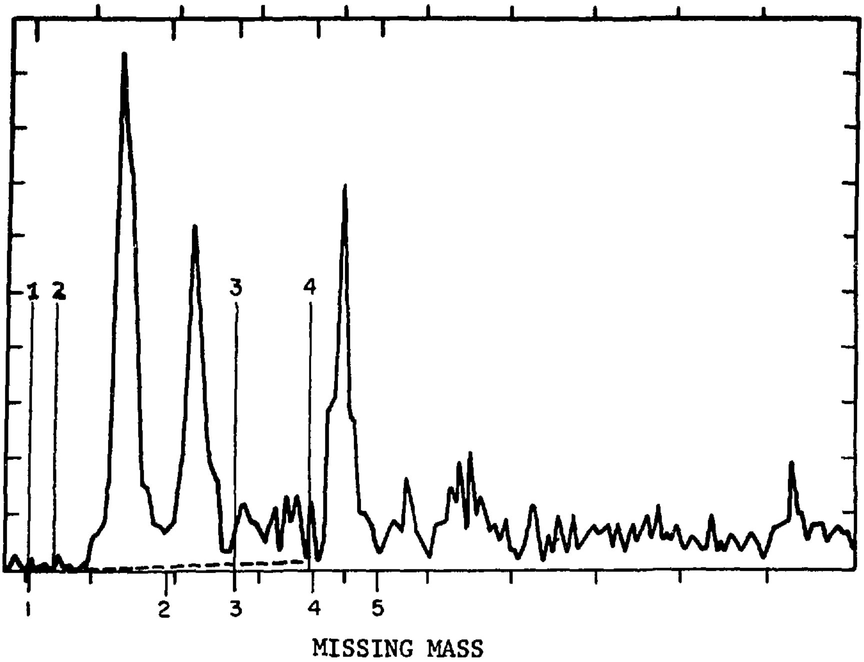

Fig. 15. An energy spectrum is shown for negative pion scattering from ^{58}Ni. A fitting program calculates the area between cursors two and three below the peaks and above the background (dotted line). The five lower markers represent the following energies: -2.0 MeV, 0.8 MeV, 2.2 MeV, 3.8 MeV, and 5.1 MeV.

peaks, between cursors 2 and 3 in the drawing. Even if the background area does not exactly correspond to all decayed muons, consistent fitting technique on carbon scattering along with scattering from the other four nuclei eliminates the problem with muons from pion decay. Suppose the background is consistently set too small. Then the cross section to yield ratio for carbon (the normalizing nucleus) will be smaller than its value had all decayed muons been accounted for properly. Since this ratio is used to normalize the cross sections for pion scattering on the other four nuclei, those cross sections (whose yields include muons) will be correct.

It is not unusual for the first inelastic peak in a missing-mass histogram to fall on top of the radiative tail of the elastic peak. The versatility of the histogram fitting routine allows both peaks to be fitted properly. Both Figs. 15 and 16 depict histograms generated by negative pion scattering from ^{58}Ni at 162 MeV. In the latter figure, the first inelastic peak is fit. The background, under the dashed line, is subtracted from the integrated area between cursors 2 and 3. The fitting method shown in Fig. 15 calculates the area under both the elastic and first inelastic peaks exclusive of background. The background shown in Fig. 16 represents the radiative tail of the elastic peak (see Fig. 14) so that the area above background is entirely due to scattering to the 1.45 MeV state in nickel. Subtracting this area from the area under both peaks yields the area due to elastic scattering.

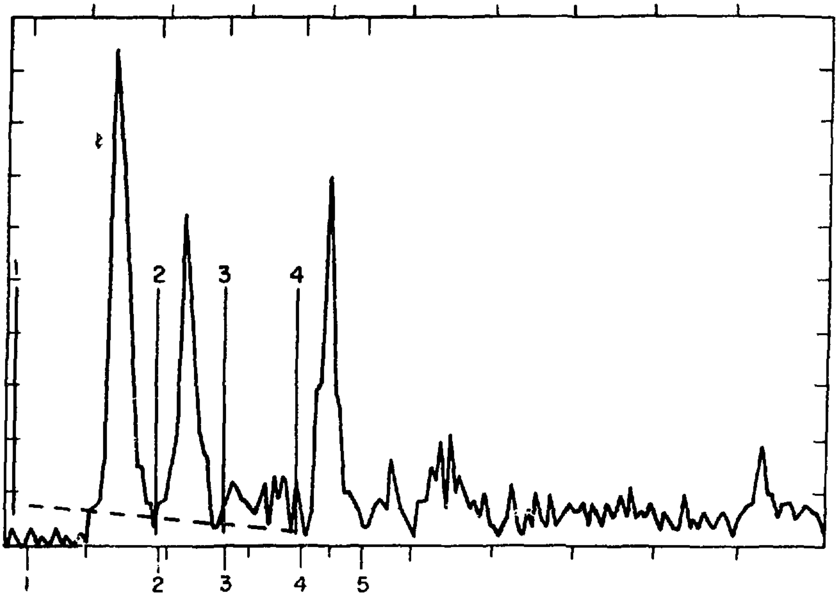

MISSING MASS

Fig. 16. The same spectrum as depicted in Fig. 15 appears here. The background under the first inelastic peak (1.45 MeV) represents the radiative tail of the elastic peak.

The typical background beneath another inelastic state is shown in Fig. 17. This histogram was generated by scattering positive pions from a target of ^{208}Pb. The integrated area is again between cursor 2 and cursor 3.

The overall energy resolution for this experiment, as embodied in the missing mass histograms, was nominally 400 keV at an incident energy of 162 MeV. Figure 18 represents the missing-mass spectrum of positive pion scattering from ^{9}Be.

Yield Corrections

The area under an elastic peak in a missing-mass histogram provides much of the information needed to calculate $N_E d\Omega$, the number of pions elastically scattered into the solid angle $d\Omega$ of the spectrometer. There are, however, a good many corrections which must be applied to the number of pions counted in an elastic peak before a proper yield value is determined. Yield need only be multiplied by cross section to yield ratio and target density to complete the cross-sectional calculation.

The number of pions which intersect the scattering target during the length of a particular experimental run is proportional to the integral over time of ion chamber current during the run, assuming that ion chamber-target orientation is standard. While it is not possible, nor necessary, to measure the beam flux, I_0, on the scattering target, it is essential that the number of pions

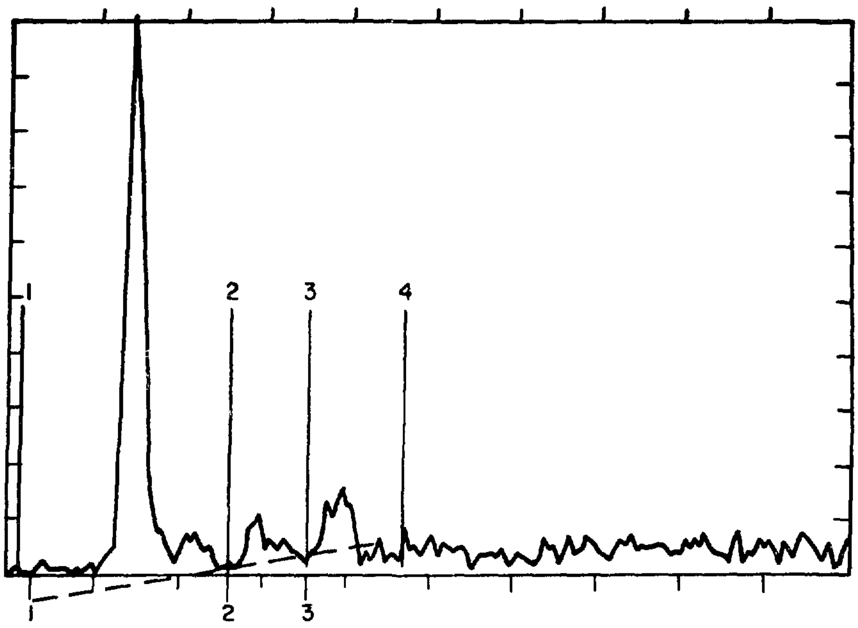

MISSING MASS

Fig. 17. The energy spectrum for scattering of π^+ from ^{208}Pb is shown. Under the inelastic peak at 2.62 MeV is a typical background. As usual, the area under the peak will be integrated between cursors two and three. The three markers below the plot frame indicate energies of -2.0 MeV, 2.0 MeV, and 3.62 MeV.

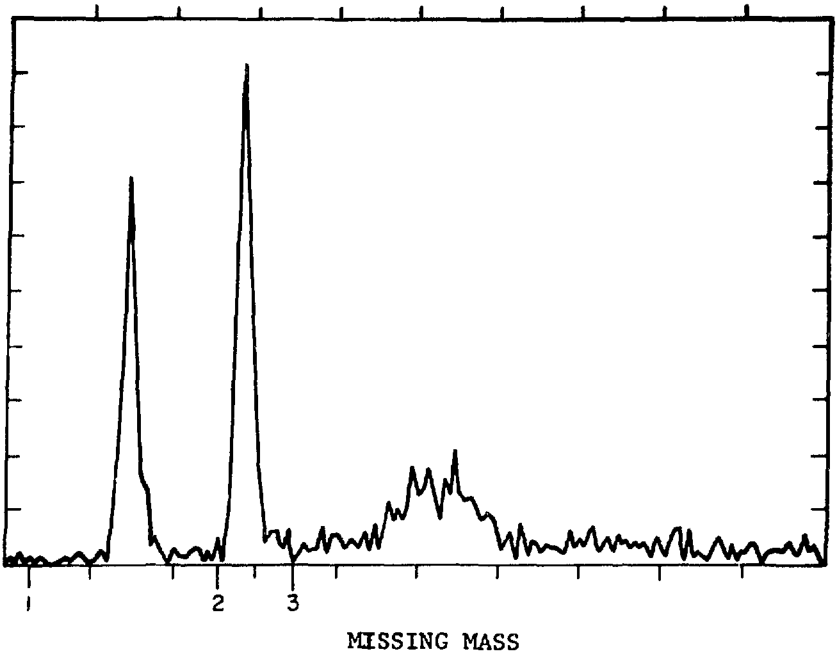

Fig. 18. Scattering of positive pions from Be generated this typical spectrum. The three markers indicate energies of -2.0 MeV, 1.9 MeV, and 3.5 MeV.

hitting the target during a run be measured. It was common for the LAMPF proton beam to shut off intermittently during an experimental run so that measuring the length of time of a run was no indication of the number of incident pions on a particular target.

During this experiment neither ion chamber proved itself vacuum tight. The gas inside each chamber slowly leaked. The rate of loss of gas was fairly constant, with the upstream chamber leaking faster than its downstream companion. The operating gas in each chamber was confined to a fixed volume so that as the gas pressure fell at a uniform rate, the density of gas also fell at a constant rate. This caused a steady rate of drop in ion chamber current per particle flux through the chamber.

An alternative method for measuring the relative flux of pions on the scattering target was provided, though in an erratic fashion, by a toroidal coil surrounding the proton beam, upstream of the A-1 production target. Recall that the A-1 target rotates in the 800 MeV proton beam, creating pions which are collected by the EPICS channel. The toroidal coil accurately measures the proton beam current; however, the proton beam position on the A-1 target was not steady and the coil measurement thus gives only a crude determination of the intensity of pions hitting the scattering target at the end of the EPICS channel. Shown in Fig. 19 is a plot of the ratio of the total charge passing through the toroid during an experimental run to a value proportional to the total charge generated by the downstream

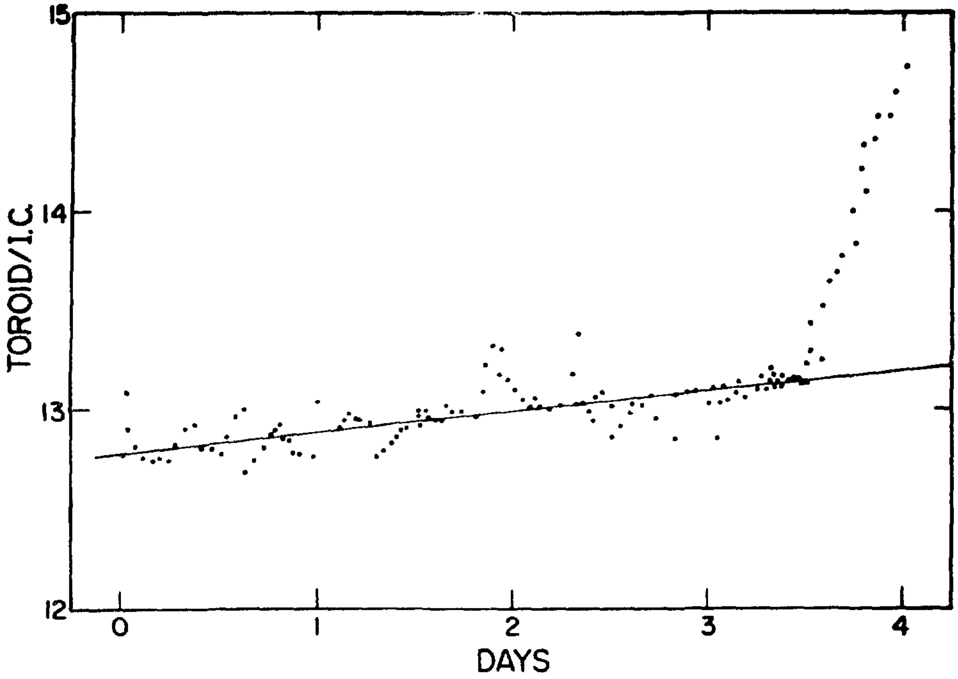

Fig. 19. *The ratio of proton beam intensity near the A-1 target to pion flux in the downstream ion chamber is plotted in arbitrary units for each experimental run. When the A-1 target quit rotating, the value of this ratio increased at an accelerated rate.*

ion chamber in the same time. Each point on the plot represents this ratio during a single run. Only runs of positive pion scattering are shown, but all these runs were contiguous in a time stretching over four days. Ignoring the erratic behavior caused by the change in the proton beam position on the A-1 target, the plotted values for the first three-and-a-half days are well represented by a straight line of moderate slope. This line is roughly sketched through the points. The slow decrease in gas pressure in the downstream ion chamber would justify a straight line compatible with the one sketched.

The precipitous increase in the specified ratio after three-and-a-half days, as indicated in Fig. 19, might present a quandry. Measurement of the pressure of the operating gas in the ion chamber did not confirm a much larger gas leak starting after three-and-a-half days. It was eventually discovered that the A-1 target mechanism was responsible for the anomalous measurements. The electric motor, which should rotate the target, malfunctioned, probably due to radiation damage. When that happened, protons began to destroy the target so that, with time, fewer pions were created for a given proton flux.

A correct scattering cross section cannot be calculated without compensating for the ion chamber leak. It is imperative that the relative number of pions intersecting the scattering target be determined in a fashion that is consistent for all runs. This could not be done if the falling ion chamber efficiency were ignored. The straight line sketched in Fig. 19 is used to correct for the ion chamber leak. For a particular run, some standard value, in this case the ordinate value of the line at zero days, divided by the line's ordinate value at that run, specifies the ratio, R_I, which corrects the scattering yield for ion chamber leak. Deterioration of the A-1 target has no effect on scattering measurements except to marginally decrease the flux in the EPICS channel, lengthening the time necessary for data acquisition. Negative pion-scattering measurements were performed immediately after the positive pion scattering. The ion chamber leak remained uniform during the entire experiment so that a straight line of slope the same as that of the line in Fig. 19 was used to correct the yield for negative pion scattering.

After each hardware trigger generated in the fast electronics by the spectrometer detection system (see Fig. 9), the computer initiates a busy signal while measurement data is processed. During this time, no additional scattered pions can be measured. But there is a signal, tagged "particle" in the electronics diagram, which indicates a scattered pion even if the computer is busy. The occurrence of each "particle" signal is counted by a scaler. Another scaler counts the number of pions which result in hardware triggers. The ratio, R_T, of this last scaler count to the number of occurrences of the "particle" signal during a particular run specifies the percentage of pions entering the spectrometer which were processed by the computer. It is assumed, of course, that the properties of those pions not causing hardware triggers correspond to the properties of measured pions. Thus, when the computer has time to analyze the properties of every pion entering the spectrometer, that missing-mass spectrum is assumed to look exactly the same as it would if, say, only 20% of scattered pions were analyzed.

Not every pion scattered into the spectrometer survives the trip from the scattering target to the rear wire chambers. In fact, most do not. Rather, the majority of scattered pions decay to muons before they have traveled completely through the spectrometer. The half life for charged pions is 1.808×10^{-8} sec in the pion rest frame. Suppose a beam contains positive pions of 161.5 MeV kinetic energy. Then the half life of the pions in the laboratory frame is

$$\Delta t = \Delta\tau/(1-\beta^2)^{1/2} , \qquad (10)$$

where $\Delta\tau = 1.808 \times 10^{-8}$ sec and $\beta^2 = v^2/c^2$. Half the pions in the beam have decayed during a length

$$L_H = v\Delta t = v\Delta\tau/(1-\beta^2)^{1/2} = Pc\Delta\tau/m_\pi , \qquad (11)$$

where P represents the pion momentum in units of MeV/c and m_π has the units of MeV/c^2. Thus,

$$L_H = 3.868P \text{ cm} , \qquad (12)$$

and, in this case, with $P = 267$ MeV/c, $L_H = 10.35$ m. Path length through the spectrometer is 12.77 m, so well over half of the pions which had a scattered energy of 161.5 MeV would decay before reaching the rear wire chambers.

If there are N pions scattered into the spectrometer, the number of pions that will decay in a certain time interval is proportional to the number of pions that exist at that time. Thus,

$$dN/dt = -\lambda N(t) \tag{13}$$

and

$$N(t) = N(0)e^{-\lambda t} \quad , \tag{14}$$

where λ is equal to $1/\tau$. τ is the mean lifetime for charged pions, 2.603×10^{-8} sec. Scattered pions with 161.5 MeV kinetic energy take 22.32 nsec in their own rest frame to travel from the scattering target to the rear of the spectrometer. According to equation (14), only 43% of these pions survive the trip. The survival fraction, $R_S = N(t)/N(0)$, specifies the fraction of scattered pions, at any momentum, which do not decay as they travel through the spectrometer. R_S was calculated by the computer, for each angular bin into which pions scattered using the calculated scattering energy. Since muons are eliminated from the missing-mass histograms by the angle test and proper fitting technique, the count of pions in a peak of the histogram must be divided by R_S to give the number of pions actually scattered into the spectrometer. Again, the assumption is made that pions which decay would yield the same missing-mass spectrum as those pions that survive.

It is not possible to include the entire radiative tail of a peak in the missing-mass histogram when intergating the area under that peak. A computer program has been written, based on the calculations of Borie[77] and Sogard,[78] which determines the area lost by cutting off a portion of the radiative tail. The calculated fraction of area lost, R_A, must be added to the fitted area under a given peak to ensure the proper scattering yield.

The solid angle of the spectrometer into which pions scatter is a function of δ, the difference between the scattered pion momentum and the central momentum of the spectrometer. Much of the configuration of the EPIcS system must not be varied while a scattering experiment is in progress. As detailed earlier, the actual values of spectrometer solid angle, $d\Omega$, and incident pion intensity, I_0, cannot be measured. Changes in jaw-setting in the channel, central spectrometer momentum, and other factors cause unknown changes in $d\Omega$ and/or I_0. Scattering from the normalizing carbon nucleus must be performed with the same setup as scattering from all other nuclei in order to keep $d\Omega$ and I_0 constant. There is, however, one problem. As the spectrometer itself is rotated toward larger values of ω_S, the momentum of elastic pions scattered into the spectrometer decreases. This means that δ decreases as the spectrometer is changed to larger scattering angles, and $d\Omega$ is a function of δ. Figures 20 and 21 show the relative change in $d\Omega$ with δ for two of the angular bins. Note that only changes in $d\Omega$ with δ are relevant. The actual value of the solid angle is never measured. The ratio, R_0, of the relative value of $d\Omega$ at a particular value of δ to some arbitrary number is used to correct scattering yield. For the 2.4° angular bin, the dependence of $d\Omega$ on δ is similar to that shown in Fig. 21.

Usually the scattering target angle, ω_T, was set to half the value of the spectrometer angle, ω_S. The pion beam is not as wide as any scattering target, so when the target is not perpendicular to the incident pion beam, more nuclei are in the beam. This corresponds to an effective change in n_T, the number of target nuclei in the pion beam. One may correct a scattering yield for this effect by multiplying by Cos ω_T.

At spectrometer angles, ω_S, greater than 90° mechanical problems prohibited the angle of the scattering target from being as large as half the value of ω_S. Measurements indicated that the solid angle of the spectrometer was a function of the difference $(\omega_T - \omega_S)/2$, though the solid angle changed no measurable amount with ω_T when ω_T was equal to $\omega_S/2$. Figure 22 shows the solid-angle dependence on the variable χ, where χ is the ratio $\mathrm{Cos}(\omega_S - \omega_T)/\mathrm{Cos}\,\omega_T$. For those few runs during this experiment for which χ was not equal to one, the solid angle of the spectrometer required correction. Again it should be pointed out that the values of $d\Omega$ in Fig. 22 are

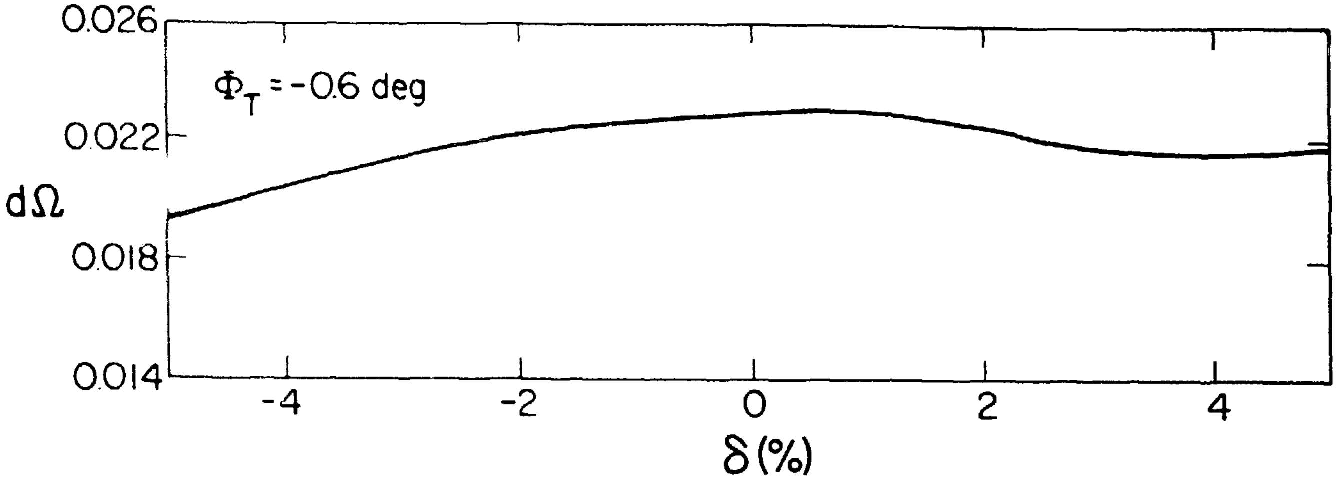

Fig. 20. The shape of this curve depicts the change in solid angle with δ for pions scattered into the angular bin centered on Φ_T = -0.6 deg.

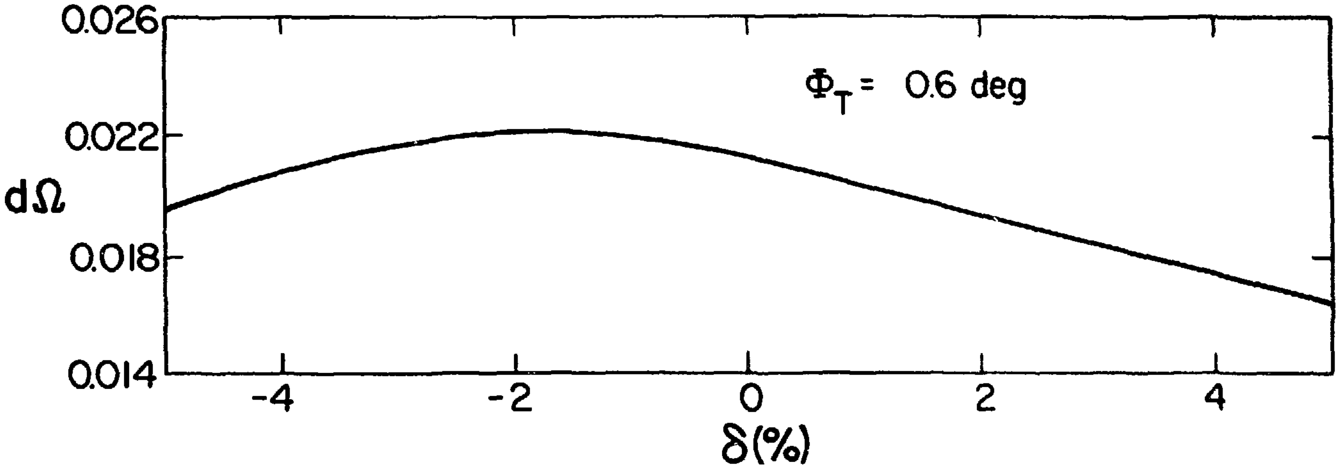

Fig. 21. This curve shows the relative change in solid angle with δ. The angular bin here is centered on $\Phi_T = 0.6$ deg.

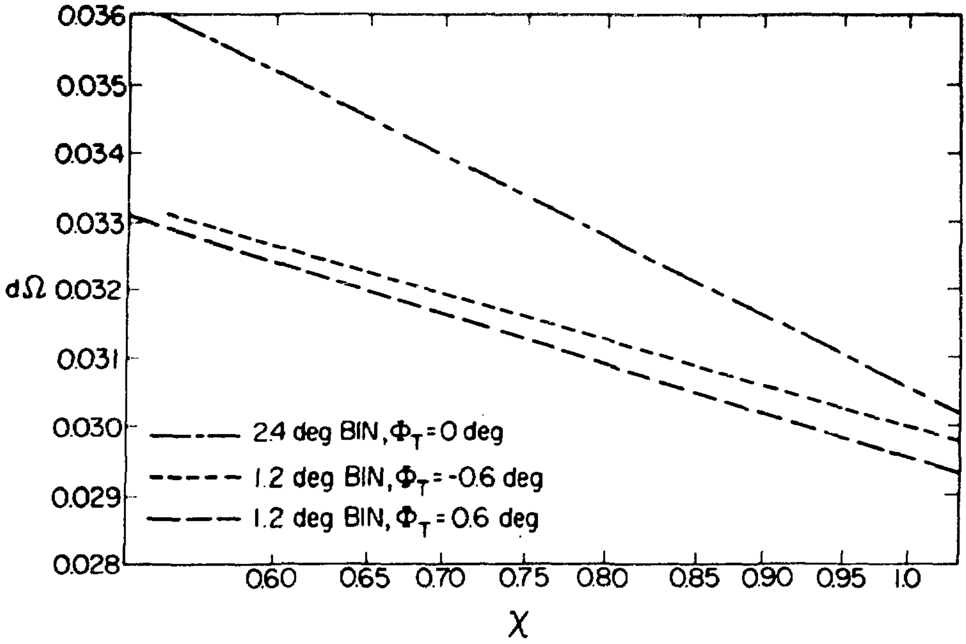

Fig. 22. Shown is the change in solid angle with χ. χ is equal to the ratio $\mathrm{Cos}(\omega_S - \omega_T)/\mathrm{Cos}\omega_T$. Values of $d\Omega$ are relative.

only relative values. $d\Omega$ is not assigned any absolute value. The ratio, R_χ, of $d\Omega$ at a certain value of χ, to the $d\Omega$ value for $\chi = 1$, was used to modify the scattering yield for those runs where the value of ω_T was not equal to half the value of ω_S.

The occurrence of a hardware trigger, generated by the detection equipment in the spectrometer, does not guarantee that each of the seven operating wire chambers in the spectrometer functioned properly. No wire chamber was 100% efficient as measured by the value of t_c in that chamber. When t_c did not have the constant value expected, the wire chamber which produced this spurious t_c value was considered to have malfunctioned. Under normal conditions, each of the four front wire chambers functioned properly better than 98% of the time. Each of the three rear wire chambers had a better than 93% efficiency. Every wire chamber must operate properly in order to measure pion momentum. So if not every wire chamber functions as it should when a pion passes through the spectrometer, then test software excludes from the missing-mass histograms the value of that pion. The ratio, R_C, specifies the fraction of pions for which all wire chambers performed adequately to the total number of pions scattered into the spectrometer.

It is more likely that a muon, decayed from a scattered pion, will cause any wire chamber to malfunction than it is that a pion will cause such a malfunction. Figure 23 shows a histogram of the value of the angle check during a particular experimental run.

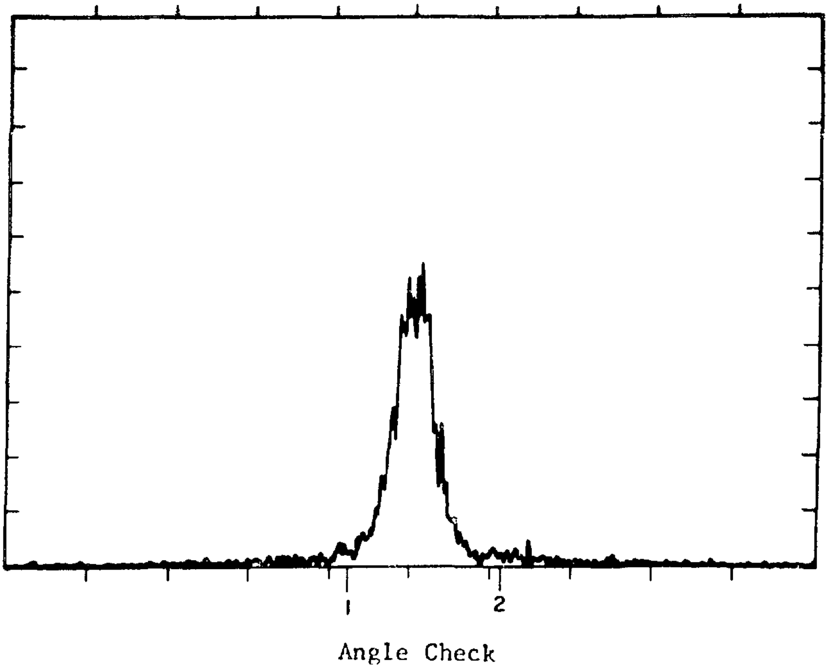

Fig. 23. The angle check histogram is depicted for a particular run. Particles whose values lie outside of the markers one and two do not contribute to the missing mass histograms.

Those particles whose predicted angle at the rear wire chambers agreed with the measured angle at the rear chambers are depicted within the peak between markers one and two. Most of the particles depicted outside of the markers are muons from pion decay downstream of the front wire chambers. There are also some muons whose angle check values fall within the peak shown. However, by selecting particles whose values lie in a very narrow width at the peak center most muons are excluded. It is found that the wire chamber efficiency is better for those particles with an angle check value near the center of the peak than it is for all particles whose values lie between markers one and two. Since pion scattering is to be measured, not muon scattering, the wire chamber efficiency for just pions is required. Thus, the value of the ratio, R_C, is modified to reflect wire chamber efficiency for pions only.

In most cases, the overall wire chamber efficiency was about 85%. Thus, if 100 pions scattered into the spectrometer, only 15 would induce any of the 7 wire chambers to malfunction. The wire chamber efficiency is a function of charged particle flux through the chambers. Occasionally during this experiment, because of high flux, overall wire chamber efficiency decreased to near 80%.

The pion-scattering yield is calculated from the area under a missing-mass peak, the ion chamber current during the experimental run, and the corrections outlined above. Let A_E be the area under the elastic peak, minus background, in a missing-mass histogram and let Q be a value proportional to the total charge generated in the downstream ion chamber during the run. The corrected elastic-scattering yield is given by the formula

$$Y_E = A_E R_I (1 + R_A) \mathrm{Cos}\omega_T / Q R_T R_C R_S R_0 R_X \ . \qquad (15)$$

An inelastic yield would be found by substituting for A_E the area under the particular inelastic peak of interest.

It now remains only to multiply a yield by the cross section to yield ratio and the target density in order to get a cross section.

The Cross Section

The cross section to yield ratio used to normalize a scattering yield is a function of the charge sign of incident pions. The beam flux transported through the EPICS channel is not the same for positive pions as it is for negative pions. The intensity of the negative pion beam is three to five times less than the positive beam.

The scattering yield for both positive and negative pions on ^{12}C was measured with a standard configuration of the EPICS system. The yield was determined at various spectrometer angles, ω_S, though the normalizing ratio of cross section to yield, R_Y, should not be a function of ω_S. There is no reason for either the incident pion intensity, I_0, nor the spectrometer solid angle, $d\Omega$, to vary with the spectrometer angle, ω_S. And, no correlation is found between the scattering yield and ω_S. Appendix B tabulates the pion differential cross section on ^{12}C. This cross section is the basis for the normalizing ratio R_Y.

The solid angle into which pions scatter in the spectrometer depends on which angular bin collects those pions. For this reason the ratio, R_Y, is different for each angular bin. Table 4 lists the measured values of the pion-carbon scattering yield for each angular bin and the cross section to yield ratio corresponding to each yield. The average ratio for each bin is the value used to normalize the scattering data of this experiment. For positive pion scattering the weighted average values of R_Y and the average relative errors are the following:

2.4 deg Bin	-1.2 deg Bin	1.2 deg Bin
1.199 ± 0.054 mb/sr	1.177 ± 0.057 mb/sr	0.9341 ± 0.046 mb/sr

For negative pion scattering the normalizing ratios are:

2.4 deg Bin	-1.2 deg Bin	1.2 deg Bin
1.141 ± 0.031 mb/sr	1.079 ± 0.032 mb/sr	0.8632 ± 0.026 mb/sr

That the normalizing ratios are different for each angular bin, testifies to the fact that the solid angle of each bin is different. It is worth noting, however, that R_Y is not correlated with ω_S.

The scattered particle flux into the spectrometer is very high at small scattering angles. In fact, it was impossible to measure positive pion scattering cross sections at angles near or below 20° without modifying part of the EPICS setup. Scattered beam intensity at small angles caused the front wire chambers in the spectrometer to completely malfunction in some instances. The main LAMPF proton

Table 4. The elastic yield and normalizing ratio is shown for carbon scattering at 162.1 MeV. Errors given are relative error.

π^+, ^{12}C - 2.4 deg Bin

Y_E	$\pm\Delta_r Y_E$	Φ_S (deg)	R_Y (mb/sr)	$\pm\Delta_r R_Y$ (mb/sr)
40.29	2.31	33.2	1.291	0.155
2.485	0.162	45.2	1.232	0.129
0.9730	0.0720	47.6	1.100	0.125
0.2349	0.0281	50.0	1.120	0.178
0.7298	0.0526	59.6	1.309	0.147
1.055	0.089	69.2	1.194	0.149
0.4474	0.0365	78.8	1.162	0.143

1.2 deg Bin, Φ_T = -0.6 deg

Y_E	$\pm\Delta_r Y_E$	Φ_S (deg)	R_Y (mb/sr)	$\pm\Delta_r R_Y$ (mb/sr)
46.41	3.08	32.6	1.239	0.131
3.159	0.230	44.6	1.209	0.136
1.249	0.105	47.0	1.144	0.137
0.3549	0.0476	49.4	1.057	0.185
0.6793	0.0611	59.0	1.289	0.167
1.110	0.115	68.6	1.152	0.165
0.5225	0.0521	78.2	1.100	

1.2 deg Bin, Φ_T = 0.6 deg

Y_E	$\pm\Delta_r Y_E$	Φ_S (deg)	R_Y (mb/sr)	$\pm\Delta_r R_Y$ (mb/sr)
45.60	3.09	33.8	1.041	0.112
2.559	0.198	45.8	0.9000	0.106
0.9762	0.0892	48.2	0.7888	0.103
0.1968	0.0355	50.6	0.9909	0.2184
1.007	0.083	60.2	1.023	0.123
1.315	0.1315	69.8	0.9278	0.130
0.4942	0.0492	79.4	0.9611	0.1345

Table 4 (continued).

π^-, ^{12}C - 2.4 deg Bin

Y_E	$\pm\Delta_r Y_E$	Φ_S (deg)	R_Y (mb/sr)	$\pm\Delta_r R_Y$ (mb/sr)
231.1	12.1	18.8	1.255	0.086
1.885	10.3	21.2	1.209	0.082
91.43	5.33	28.4	1.094	0.077
63.15	3.73	30.8	1.118	0.079
44.39	2.38	33.2	1.113	0.074
1.302	0.087	63.2	1.091	0.085
1.283	0.087	66.8	1.130	0.089

1.2 deg Bin, Φ_T = -0.6 deg

Y_E	$\pm\Delta_r Y_E$	Φ_S (deg)	R_Y (mb/sr)	$\pm\Delta_r R_Y$ (mb/sr)
229.1	13.5	18.2	1.331	0.095
226.6	12.9	20.6	1.068	0.074
108.3	7.26	27.8	0.9972	0.078
71.46	4.81	30.2	1.077	0.084
50.09	2.97	32.6	1.088	0.078
1.370	0.116	62.6	1.007	0.094
1.422	0.117	66.2	1.027	0.094

1.2 deg Bin, Φ_T = 0.6 deg

Y_E	$\pm\Delta_r Y_E$	Φ_S (deg)	R_Y (mb/sr)	$\pm\Delta_r R_Y$ (mb/sr)
303.8	17.3	19.4	0.8986	0.0625
272.4	15.1	21.8	0.7783	0.0532
101.4	6.69	29.0	0.8925	0.0689
73.07	5.18	31.4	0.8786	0.0715
51.82	3.15	33.8	0.8587	0.0625
1.607	0.134	63.8	0.8961	0.0827
1.539	0.137	67.4	0.9292	0.0906

beam intensity was decreased from about 300 μA to about 150 μA for a short period in order to facilitate the measurement of small-angle positive pion scattering on the EPICS system. This resulted in an attenuation of the positive pion intensity on the EPICS scattering target of about one half, and allowed the front wire chambers to operate properly. The negative pion beam delivered by the EPICS channel is less intense than the positive pion beam, and a lower proton beam intensity was not needed to measure negative pion scattering at small angles.

The scattering yield of positive pions on carbon was also measured at this reduced beam intensity and compared with the pion differential cross section at the appropriate angle. This particular normalizing ratio provided the basis for calculating all the cross sections measured at reduced beam intensity. The normalizing ratios at reduced intensity were the following:

π^+

2.4 deg Bin (mb/sr)	-1.2 deg Bin (mb/sr)	1.2 deg Bin (mb/sr)
1.440 ± 0.143	1.330 ± 0.143	1.079 ± 0.118

With the proper normalizing ratio, R_Y, the pion differential cross section is calculated by the prescription:

$$d\sigma/d\Omega = R_Y(n_C/n_T)Y \ , \tag{16}$$

where n_C is the number of carbon nuclei in a cm^2 of the carbon target and n_T is the number of nuclei in a cm^2 of the scattering target in question.

Error Analysis

It is customery to divide the error analysis of an experiment into two parts: systematic errors and random errors. While that division will be important in the analysis that follows, it is also necessary to make the distinction between relative and absolute errors. A differential cross section on a particular nucleus is a list of quite a few values, the measurements at each scattering angle. It turns out that part of the error in the cross-sectional values is the same for each value, regardless of scattering angle. This uniform error is referred to as absolute error.

The total error in the value of the normalizing ratio, R_Y, gives the absolute error in differential cross sections derived in this experiment. Since every measured scattering yield is multiplied by R_Y to produce a cross section, then, obviously, the error in R_Y will propogate into every cross section.

The total error in R_Y is the sum of both the absolute and relative errors caused by errors in the carbon cross section and the carbon yield. The absolute error in pion-carbon cross sections is estimated at four percent. The absolute error in any carbon yield is certainly smaller than relative errors in the yield, and will be assumed to be insignificant. So, the total error in a R_Y value is made up of the absolute error in the carbon cross section plus relative error.

Quite a few measurements of carbon-scattering yields were made for both positive and negative pion scattering. This redundancy allows one to handle the relative error in the normalizing ratio, R_Y, statistically. If differences between values of R_Y are considered to be due to purely random fluctuation, then the best value of both R_Y and its calculated relative error may be determined by standard statistical methods.[79] Differences between values of R_Y were found to be statistically consistent. The best values of R_Y and relative error, $\Delta_r R_Y$, were quoted earlier. The total error in R_Y is the sum of the absolute and relative error:

$$\Delta_t R_Y = 0.04\ R_Y + \Delta_r R_Y\ . \tag{17}$$

Total error of the normalizing ratio R_Y is about nine percent for both 1.2 deg angular bins. The total error of R_Y is slightly less than this for R_Y evaluated on the 2.4 deg angular bin.

The relative error that is assigned to a particular value of a pion-scattering cross section is caused by many factors. One contribution to the relative error is the statistical uncertainty of the peak area and the background of the missing-mass histogram considered. A Poisson probability distribution is assumed to govern the area of both the peak and background. The relative error in the number of elastic pions, or inelastic pions, scattered from a particular excited nuclear state, into a certain angular bin, is the square root of the area under the peak in question in the missing-mass histogram plus the square root of the subtracted background. Another contribution to the relative error in the cross section is the uncertainty in ion chamber measurement. The error in the charge flow measured in an ion chamber during a given experimental run, due both to random fluctuations and systematic effects, was found to be about three percent. The change in solid angle of the spectrometer with momentum difference δ, has an error of two percent. At those large scattering angles for which it was impossible to take the target angle as half the spectrometer angle, an additional relative error of five percent is introduced into the cross section.

The wire chamber efficiency measurement also adds its part to the relative error of a cross-sectional value. The uncertainty in efficiency of the chamber for pions only is the source of the error. The efficiency of the chambers for all charged particles which produce hardware triggers is well known. This last efficiency is accurately determined by counts of CAMAC scalers, but some particles inducing hardware triggers are not pions. The error due to uncertainty in the true pion efficiency of the chambers is about two percent.

The relative error in a differential cross-sectional value is given by the formula,

$$\Delta_r(d\sigma/d\Omega) = d\sigma/d\Omega[(\Delta_r A/A)^2 + (0.03)^2 + (0.02)^2 + (0.03)^2]^{1/2}$$

or

$$\Delta_r(d\sigma/d\Omega) = d\sigma/d\Omega[(\Delta_r A/A)^2 + (0.041)^2]^{1/2} \quad , \qquad (18)$$

where $\Delta_r A$ is the relative error predicted by statistics in the area, A, of a missing-mass peak. Each contribution to the relative error of the cross section is added in quadrature because each contribution is independent of the others. For those measurements where ω_T was not equal to half the angle, ω_S, the relative cross-sectional error is increased by the value 0.05 added in quadrature.

By definition, the absolute error of those cross-sectional values which were measured at a reduced proton beam current of 150 μA is the same as the absolute error for all other cross-sectional values; the relative error of these few values is quite a bit larger than the relative error in other cross-sectional measurements. One must add in quadrature the relative error in R_Y, calculated at a single angle during low beam intensity, (call this $D_r\hat{R}_Y$), and the relative error in the average value of R_Y, determined during normal intensity runs, (call this $D_r\langle R_Y\rangle$), to determine the relative value of those cross sections measured at low intensity. Thus,

$$D_r(d\sigma/d\Omega)_{Low} = (d\sigma/d\Omega)_{Low}[(D_r\hat{R}_Y)^2 + (D_r\langle R_Y\rangle)^2 + (D_r Y_{Low})^2]^{1/2} \quad , \qquad (19)$$

where Y_{Low} is the scattering yield from some nucleus calculated at low beam intensity.

IV. THEORETICAL ANALYSIS

The scattering of pions from nuclei is a complicated many-body problem that has admitted no analytical solution from first principles, without broad initial and intermediate assumptions. This is true in spite of the fact that the free pion-nucleon interaction is reasonably well understood. Even in the region of the pion-nucleon (3,3) resonance, where very few of the affected pions are scattered elastically, the situation is improved only slightly.

Elastic Pion Scattering

A beam of pions incident on a nucleus may be described in quantum mechanical terms as a plane wave impinging on a scattering center. If the nucleus elastically scatters incoming pions via a spherically symmetric potential, then the resultant wave will be of the form[80]

$$\psi_{\underline{k}}(\underline{r}) = e^{i\underline{k}\cdot\underline{r}} + f_k(\theta)\,\frac{e^{ikr}}{r}\ , \qquad (20)$$

which represents both the unscattered portion of the incident wave and the spherical wave scattered from the nucleus. Here k is the wave number of the incident plane wave and $f_k(\theta)$ is, of course, the scattering amplitude. Furthermore, the differential cross section is given by $\frac{d\sigma}{d\Omega} = |f_k(\theta)|^2$.

In analogy with Gibbs,[81] it can be shown that the scattering amplitude is actually proportional to the matrix element of the scattering potential.

In a non-relativistic approximation the pion-nucleus interaction may be described by the Schrödinger equation:

$$(\underline{K} + \underline{V}(r) - \underline{E})\ \psi_{\underline{k}}(\underline{r}) = 0. \tag{21}$$

Note that the wave function may be expanded in spherical harmonics:

$$\psi_{\underline{k}}(\underline{r}) = 4\pi \sum i^{\ell}\ \psi_{\ell}(r)\ Y_{\ell}^{m}(\hat{k})\ Y_{\ell}^{m*}(\hat{r}). \tag{22}$$

Now, since,

$$\begin{aligned}(\underline{E} - \underline{K})\psi_{\underline{k}}(\underline{r}) &= (\underline{E}-\underline{K})e^{i\underline{k}\cdot\underline{r}} + \underline{V}(r)\ \psi_{\underline{k}}(\underline{r}) = \\ &\quad V(r)\ \psi_{\underline{k}}(\underline{r}),\end{aligned} \tag{23}$$

the wave function may be expressed formally with an explicit plane-wave initial boundary condition:

$$\psi_{\underline{k}}(\underline{r}) = e^{i\underline{k}\cdot\underline{r}} + (\underline{E} - \underline{K})^{-1}\ \underline{V}(r)\ \psi_{\underline{k}}(\underline{r}). \tag{24}$$

Equation (24) is expanded by the insertion of unity, where,

$$1 = \int\delta(\underline{r}-\underline{r}')d\underline{r}' = \frac{1}{(2\pi)^3}\int e^{i\underline{k}'\cdot(\underline{r}-\underline{r}')}d\underline{k}'d\underline{r}'. \tag{25}$$

With the kinetic energy and total energy operators explicitly specified, the scattered wave function is

$$\psi_{\underline{k}}(\underline{r}) = e^{i\underline{k}\cdot\underline{r}} + \frac{2\mu}{\hbar^2}\int \frac{e^{i\underline{k}'\cdot\underline{r}}}{k^2-k'^2}\, d\underline{k}'\, \frac{1}{(2\pi)^3}\int e^{-i\underline{k}'\cdot\underline{r}'} V(r')\psi_{\underline{k}}(\underline{r}')d\underline{r}', \tag{26}$$

where μ is the reduced mass.

The transition matrix is defined to be the last integral in the final equation:

$$t(\underline{k}',\underline{k}) = \frac{1}{(2\pi)^3}\int e^{-i\underline{k}'\cdot\underline{r}'}\, V(r')\, \psi_{\underline{k}}(\underline{r}')\, d\underline{r}' . \tag{27}$$

So,

$$\psi_{\underline{k}}(\underline{r}) = e^{i\underline{k}\cdot\underline{r}} + \frac{2\mu}{\hbar^2}\int \frac{t(\underline{k}',\underline{k})\, e^{i\underline{k}'\cdot\underline{r}}}{k^2-k'^2+i\eta}\, d\underline{k}'. \tag{28}$$

The addition of $i\eta$ in the denominator above, ensures that far from the scattering center, where total energy and kinetic energy may be equal, no singularity results. The wave function at infinity will be represented by an outgoing wave. The transition matrix is a common tool of scattering theory.[82] It plays essentially the same role as the scattering amplitude, as will be shown below.

Recalling the expression of $\psi_{\underline{k}}(\underline{r})$ in spherical harmonics, the transition matrix may be written

$$\begin{aligned} t(\underline{k},\underline{k}') &= \frac{(4\pi)^2}{(2\pi)^3}\sum_{\ell m} Y_\ell^m(\hat{k}')\, Y_\ell^{*m}(\hat{k}) \int_0^\infty r'^2\, V(r')\, \psi_\ell(r')\, j_\ell(k',r')\, dr' \\ &= \sum_{\ell m} t_\ell\,(k',k)\, Y_\ell^m\,(\hat{k}')\, Y_\ell^{m*}(\hat{k}), \end{aligned} \tag{29}$$

so that

$$t_\ell\,(k,k') \equiv \frac{2}{\pi} \int_0^\infty r^2\, V(r')\, \psi_\ell(r')\, j_\ell(k',r')dr'. \qquad (30)$$

By actually performing the integration in equation (28), one can see the relationship of the transition matrix to the scattering amplitude. Set

$$I \equiv \frac{2\mu}{\hbar^2} \int \frac{t(k',k)\, e^{i\underline{k}'\cdot\underline{r}}}{k^2-k'^2+i\eta}\, d\underline{k}' = \frac{2\mu\; 4\pi}{h^2} \sum_{\ell m} i^\ell\, Y_\ell^m(\hat{k})\, Y_\ell^{m*}(\hat{r}) \;\cdot$$

$$\int_0^\infty \frac{k'^2\, j_\ell\,(k',r)\; t_\ell(k',k)}{k^2-k'^2+i\eta}\, dk' \,. \qquad (31)$$

Since the integral is even,

$$I = \frac{2\mu\; 2\pi}{\hbar^2} \sum_{\ell m} i^\ell\, Y_\ell^m(\hat{k})\, Y_\ell^{m*}(\hat{r}) \int_{-\infty}^\infty \frac{k'^2\; j_\ell(k',r)\; t_\ell(k',k)}{k^2-k'^2+i\eta}\, dk' \,,$$

and

$$I = \frac{2\mu\pi}{\hbar^2} \sum_{\ell m} Y_\ell^m(\hat{k})\, Y_\ell^{m*}(\hat{r}) \int_0^\infty \frac{k'^2(h_\ell^+(k',r) + h_\ell^-(k',r))\; t_\ell(k',k)\; dk'}{k^2-k'^2+i\eta} \,.$$

As r goes to infinity,

$$I \overset{r\to\infty}{=} \frac{2\mu\pi}{\hbar^2} \sum_{\ell m} \frac{Y_\ell^m(\hat{k})\; Y_\ell^{m*}(\hat{r})}{r} \int_{-\infty}^\infty \frac{k'(i^{-1}e^{ik'r}+i^{2\ell+1}e^{-ik'r})t_\ell(k',k)dk'}{k^2 - k'^2 + i\eta} \,.$$

(32)

Since

$$t_\ell(-k',k) = (-1)^\ell \; t_\ell(k',k), \qquad (33)$$

one may integrate the first piece in (32) in the upper half-plane so that $k'\to+i$, and the second piece is integrated in the lower half-plane, using (33) to yield

$$I = \mu(2\pi)^2 \; \frac{e^{ikr}}{r} \; \sum_{\ell m} Y_\ell^m(\hat{k}) \; Y_\ell^{m*}(\hat{r}) \; t_\ell(k,k). \qquad (34)$$

Notice that for elastic scattering, $k\to k'$ for large values of r.

From (20), (22), (28), (31), and (34) it is seen that

$$f(\theta) = \mu(2\pi)^2 t(\underline{k}',\underline{k}); \; k'=k, \qquad (35)$$

which is the anticipated result.

The Watson Series

To obtain the Lipmann-Schwinger equation it is only necessary to multiply equation (28) by $(2\pi)^{-3}$ $V(r)$ $e^{-i\,\underline{k}''\cdot\underline{r}}$ and integrate over $\underline{r}$:

$$t(\underline{k}'',\underline{k}) = V(\underline{k}'',\underline{k}) + \frac{2\mu}{\hbar^2} \int \frac{V(\underline{k}',\underline{k}'')t(\underline{k}'',\underline{k})}{k^2 - k''^2 + i\eta} \, d\underline{k}' \qquad (36)$$

This equation usually appears in scattering theories in its operator notation:

$$\underline{t} = \underline{V} + \underline{VG_0}\,\underline{t} \;, \qquad (37)$$

where

$$\underline{G}_0 \equiv \frac{1}{\underline{E} - \underline{K}} \ . \tag{38}$$

Also define

$$\underline{G} \equiv \frac{1}{\underline{E} - \underline{K} - \underline{V}} \ . \tag{39}$$

If a pion interacts with a nucleus other than hydrogen, multiple scattering off more than a single nucleon must be considered. Because of this, pion-nucleus scattering is complicated. It is possible, however, to develop an infinite series which describes the repeated pion-nucleon scatterings inside a nucleus to all orders. This series is known as the Watson multiple-scattering series[83] and, following Gibbs' development once again, the series may be generated from the Lipmann-Schwinger equation, (36), (37).

For a nucleus composed of A nucleons the Schödinger equation has the form

$$(\underline{K} + \sum_{i=1}^{A} \underline{V}_i + \underline{H}_N - \underline{E})\ \psi = 0. \tag{40}$$

The interaction between a pion and an individual free-nucleon is reasonably well known, but the pion-nucleon potential, $\underline{V}_i$, is modified by its nuclear environment in a poorly understood fashion. Furthermore, the nuclear Hamiltonian, $\underline{H}_N$, incorporates much of the information still to be learned from nuclear science. $\underline{H}_N$, therefore, is by no means known a priori. But, assume $\underline{H}_N$ has the following eigenstates:

$$\underline{H}_N \phi_n (r_1, r_2, \ldots, r_A) = E_n \phi_n (r_1, r_2, \ldots, r_A) \qquad (41)$$

and define

$$\underline{G}_N \equiv \frac{1}{\underline{E} - \underline{K} - \underline{V} - \underline{H}_N}, \quad \underline{g}_N \equiv \frac{1}{\underline{E} - \underline{K} - \underline{H}_N} . \qquad (42)$$

With the plane-wave boundary condition as before, the pion-nucleus wave function is

$$\psi = \phi_0 \, e^{i\underline{k}\cdot\underline{r}} + \underline{g}_N \sum_{i=1}^{A} \underline{V}_i \, \psi. \qquad (43)$$

The transition matrix for this particular quantum-mechanical system is defined as before:

$$T(\underline{k}',\underline{k}) = \frac{1}{(2\pi)^3} \int e^{-i\underline{k}'\cdot\underline{r}} \sum_{i=1}^{A} V_i \, \psi \, d\underline{r} = \sum_{i=1}^{A} T_i(\underline{k}',\underline{k}). \qquad (44)$$

Multiplying equation (43) by $\frac{1}{(2\pi)^3} e^{-i\underline{k}'\cdot\underline{r}} \Sigma Vi$ and integrating over $\underline{r}$, then, for each nucleon in the nuclear medium,

$$\underline{T}_i = \underline{V}_i + \underline{V}_i \, \underline{g}_N \sum_{j=1}^{N} \underline{T}_j . \qquad (45)$$

To eliminate $\underline{V}_i$ in favor of $\underline{T}_i$, define

$$\underline{\tilde{t}}_i \equiv \underline{V}_i + \underline{V}_i \, \underline{g}_N \, \underline{\tilde{t}}_i . \qquad (46)$$

Then,

$$\tilde{\underline{t}}_i = \underline{V}_i + \tilde{\underline{t}}_i \, \underline{g}_N \, \underline{V}_i = (1 + \tilde{\underline{t}}_i \, \underline{g}_N) \, \underline{V}_i . \tag{47}$$

Substituting for V_i in equation (45) yields

$$\underline{T}_i = \tilde{\underline{t}}_i + \tilde{\underline{t}}_i \, \underline{g}_N \sum_{j \neq i}^{A} \underline{T}_j . \tag{48}$$

The last equation may be iterated to display the multiple-scattering nature of the process which is occuring in the interaction :

$$\underline{T}_i = \tilde{\underline{t}}_i + \sum_{j \neq i} \tilde{\underline{t}}_i \, \underline{g}_N \, \tilde{\underline{t}}_j + \sum_{\substack{j \neq i \\ k \neq j}} \tilde{\underline{t}}_i \, \underline{g}_N \, \tilde{\underline{t}}_j \, \underline{g}_N \, \tilde{\underline{t}}_k + \cdots \tag{49}$$

The first term in this equation represents scattering from each of the A nucleons in the nucleus. The next term indicates that the pion wave impinging on each nucleon contains a component due to single scattering from the A-1 remaining nucleons. Going a step further, the pion wave incident on each separate nucleon also contains components of double scattering from combinations of two nucleons. $\underline{t}_i$ is interpreted as the pion-nucleon transition matrix in the nuclear medium.

Equation (49) is the Watson multiple-scattering series. It represents a step forward in solving the pion-nucleus scattering problem only if the series can be quickly truncated, meaning that higher orders of multiple scattering are not as important as the lower orders of scattering. This is often the case in pion scattering and is particularly so near the (3,3) resonance.

Elastic pion scattering requires that the nucleus return to the ground state after the interaction with an incident pion. To particularize the exact multiple-scattering equation, (48), to elastic scattering, project out the ground state expectation values:

$$\langle o|\underline{T}_i|o\rangle = \langle o|\underline{\tilde{t}}_i|o\rangle + \sum_{\substack{n\\ j\neq i}} \frac{\langle o|\underline{\tilde{t}}_i|n\rangle\langle n|\underline{T}_j|o\rangle}{\underline{E} - \underline{K} - E_n + i\eta} . \tag{50}$$

The probability that a particular nuclear state, $|n\rangle$, will be excited by pion interaction is, in general, unknown, and therefore the gross assumption must be made that even during multiple scattering the nucleus remains in its ground state. In effect, E_n is set to zero and the nuclear Hamiltonian, $\underline{H}_N$, is ignored. This assumption is called the coherence approximation, and since intermediate states other than the ground state are ignored, the resultant calculation of $\langle o|\underline{T}_i|o\rangle$ will be too absorptive. Scattering to intermediate excited states is treated as lost flux. With the coherence approximation,

$$\langle T_i\rangle = \langle \tilde{t}_i\rangle + \langle \tilde{t}_i\rangle \underline{G}_o \sum_{j\neq i} \langle T_j\rangle , \tag{51}$$

where $\underline{G}_o = \frac{1}{\underline{E} - \underline{K} + i\eta}$. The wave function is antisymmetrized so all $\langle T_i\rangle$ are identical as are all $\langle \tilde{t}_i\rangle$. Thus

$$\langle T\rangle = A\langle \tilde{t}\rangle + A\langle \tilde{t}\rangle \underline{G}_o \frac{A-1}{A} \langle T\rangle . \tag{52}$$

If the following definition is made:

$$\langle\tilde{T}\rangle \equiv \frac{A-1}{A}\ \langle T\rangle, \qquad (53)$$

then, in analogy with the Lipmann-Schwinger equation,

$$\langle\tilde{T}\rangle = (A-1)\langle\tilde{t}\rangle + (A-1)\langle\tilde{t}\rangle\, G_0\, \langle\tilde{T}\rangle\ . \qquad (54)$$

The term $\frac{A-1}{A}$ is known as the KMT factor, and, in a minor way, takes into account scattering of higher than first order. To solve the last equation, the second term on the right is dropped, effectively ignoring all but first-order scattering. Pions that interact with nuclei, especially those pions whose energy is near the (3,3) resonance energy of about 180 MeV, are predominantly absorbed by the nucleus. Thus, the pion-nucleus interaction near the (3,3) resonance can be justifiably thought to have little multiple elastic scattering.

The first order optical potential, U_0, is defined to be the first term on the right of equation (54):

$$U_0 \equiv (A-1)\langle\tilde{t}\rangle. \qquad (55)$$

Knowing the form of U_0 is now all that is necessary to solve the Schrödinger equation. (Assuming, of course, that the first-order optical potential is a sufficiently good approximation to the pion-nucleus potential.)

Kisslinger observed that at resonance the pion-nucleon interaction is dominated by the p-wave, and therefore postulated that the first-order optical potential ought to take the form:[84]

$$U_0 = (A-1)\ (b_0 + b_1\ \underline{q}\cdot\underline{q}')S(\underline{q}'-\underline{q}), \tag{56}$$

where $\underline{q}$ is incident pion momentum and

$$S(\underline{q}'-\underline{q}) = \int e^{i(\underline{q}'-\underline{q})\cdot r}|\phi|^2 d\underline{r}. \tag{57}$$

The two strength parameters, b_0, b_1 are complex constants. In coordinate space the Kisslinger potential becomes

$$\underline{U}_0\psi = (A-1)(b_0\ \rho + b_1\ \underline{\nabla}\cdot\rho\underline{\nabla})\psi, \tag{58}$$

with ρ representing the nuclear mass density.

The Optical-Model Fitting Program

Several computer programs exist which may be used to analyze the data generated by elastic pion scattering. Some of these programs calculate scattering cross sections based on an initial set of input parameters that include values of the nuclear mass distribution and the strength parameters, b_0, b_1, of the first-order optical potential.[85,86] Another program, called FITPI,[87] calculates cross sections after fitting the scattering data for the best values of the strength parameters and other parameters. None of these programs have been used for final analysis of the data of this experiment for several reasons.

The values of the optical potential strength parameters which are correct for free pion-nucleon scattering are not expected to accurately describe pion-nucleus scattering. Because of the coherence approximation, the first-order pion-nucleus optical potential will be too absorptive. This will be reflected in the imaginary values of the strength parameters. Additionally, the nuclear environment affects the way pions interact with an individual nucleon,[88] and the strength parameters for pion-nucleus scattering must reflect this nuclear environment. Therefore, a program which fits the scattering data for the best values of the optical potential strength parameters is necessary. The FITPI program is not considered adequate for this task because its formulation does not include a consideration of the finite range of the pion-nucleon interacton. Instead, a first-order optical-model fitting program which compensates for the finite interaction range[89] has been applied to the elastic scattering data of this experiment. This program was written by physicists at the Los Alamos Scientific Laboratory.[90]

The non-relativistic Schrödinger equation is not an adequate starting point for the calculation of pion scattering at 162 MeV incident energy - pions are relativistic at that energy. Instead, the Klein-Gordon formula is used. But the first-order optical model, based on truncation of the Watson multiple-scattering series, retains its validity. The first-order optical potential is inserted in the Klein-Gordon equation and this is the foundation of the fitting program used to analyze the pion-scattering data.

The Klein-Gordon equation has the form

$$\underline{E}^2 - \underline{p}^2 c^2 = m_0{}^2 c^4. \qquad (59)$$

The momentum operator is familiar: $\underline{p} = -i\hbar\nabla$. But the energy operator must include the strong interaction as well as the electromagnetic interaction. The Coulomb potential, V_c, is included with the energy, where it transforms as the time-like component of a four-vector. The nuclear interaction presents a bit more trouble. If the optical potential is to be included with E, it must transform in the proper manner. It is assumed that, indeed, $\underline{U_0}$ does transform as the time-like portion of a four-vector simply because little is actually known about the Lorentzian properties of $\underline{U_0}$.[91] Substituting $\underline{E} \rightarrow E - V_c - \underline{U_0}$ the Klein-gordon equation now is

$$(E-V_c-\underline{U_0})^2\ \psi = (m_0{}^2c^4 - c^2h^2\nabla^2)\ \psi\ . \tag{60}$$

The terms $2V_c\underline{U_0}$ and $\underline{U_0}^2$ are arbitrarily dropped so that

$$(E^2-2V_cE + V_c{}^2 - 2E\underline{U_0})\psi = (m_0{}^2c^4 - c^2h^2\nabla^2)\psi\ . \tag{61}$$

The Kisslinger potential with the range formalism is used, $\underline{U_0} \rightarrow (A - 1)(b_0 + b_1\frac{\underline{q}\cdot\underline{q}'}{k^2})\frac{(\alpha^2 + k^2)^2}{(\alpha^2 + q^2)(\alpha^2 + q'^2)}\ S(\underline{q}' - \underline{q})$, where α is the range and k is the incident pion wavenumber, and the mass density distribution, ρ, is taken to be a two-parameter Fermi distribution. While it is true that the optimum density distribution for all nuclei is not the two-parameter fermi, pions incident on nuclei are quickly absorbed and experience only the outer fringes of the density distribution. It is reasonable to expect that the two-parameter Fermi distribution will adequately describe the fringe of all nuclear matter distributions.

The electromagnetic interaction of pions with nuclei is, of course, weaker than the nuclear interaction. Thus a very simple, spherical, uniform-charge distribution is used to calculate the Coulomb potential.

As mentioned above, an important part of the first-order optical calculation of pion-nucleus scattering is a pion-nucleon interaction range. The actual value of the range was in dispute at the time of this experiment, so provision was made in the computer program to allow insertion of various range values.

The optical-model program uses the least-squares method[92] to fit parameters of the model to the differential cross-sectional data. Only five parameters may be fit by this particular computer program. They are the real and imaginary parts of the two strength parameters b_o and b_1 and the absolute normalization of the cross-sectional data. It is possible, however, to fit other parameters "by hand". For example, different values of the pion-nucleon range may be inserted into the program and the quality of the fit of the optical model to the data may be evaluated for each different range value. In a similar fashion, the two parameters of the Fermi distribution, namely the half-density radius and skin thickness, may be varied to provide a best fit to the scattering data.

Additional Calculations

Pions interact differently with neutrons and protons. The free pion-nucleon interaction is such that, in the region of the (3,3) resonance, where the p-wave predominates, the scattering amplitude for positive pions on protons is about three times larger than the scattering amplitude for positive pions on neutrons. Likewise, negative pions are scattered from neutrons with a scattering amplitude about three times larger than the amplitude for negative pion scattering from protons. Because of this, pion-nucleus scattering may provide evidence of differences in the matter distributions of protons and neutrons that compose nuclei, if such differences exist. Electron-and proton-scattering experiments indicate that there are differences.[93] However, the Kisslinger potential, as implemented in the optical-model fitting program used here, provides the same matter density for both the proton and neutron distribution.

Calculating the Effective Mass Distribution

If a given sign of pion-scattering data is manually fit for the best mass distribution parameters, (by using different distribution parameters as initial values in the fitting program) the parameters will, in the main, represent either the proton or neutron nuclear distribution, depending on which kind of nucleon interacts most strongly with that sign of pion. By comparing both the positive and negative pion-fitted mass distributions it is possible to calculate the values of the effective proton and neutron distributions of a given nucleus. This is so in spite of the fact that the computer fitting program accommodates only a single-mass distribution to describe the nucleus. If ρ_+ is the distribution fitted to positive pion scattering by the program and ρ_- is the fitted distribution for the negative pion-scattering data on the same nucleus, then the effective neutron and proton distributions for the nucleus are related by the approximate equalities:

$$\rho_+ \approx \frac{3Z\,\rho_p + N\,\rho_n}{3Z + N}\ , \qquad (62)$$

$$\rho_- \approx \frac{Z\,\rho_p + 3N\,\rho_n}{Z + 3N}\ , \qquad (63)$$

where Z is the number of protons and N the number of neutrons in the nucleus. It is assumed that the incident pion energy puts the interaction in the vicinity of the (3,3) resonance where the p-wave dominates, and a given pion interacts about three times more strongly with one kind of nucleon than the other. The computer program allows only a two-parameter Fermi distribution, so,

$$\rho(r) = \frac{\rho_0}{1+e^{\frac{r-c}{z}}} \qquad (64)$$

with c the half-density radius, z the diffuseness, and ρ_0 the normalization.

Expanding $\rho(r)$ to second order about r=c gives

$$\rho(r) \approx \frac{\rho_0}{2} - \frac{\rho_0}{4z}\cdot(r-c). \qquad (65)$$

Expanding the three distributions in each of the two equations, (62) and (63), generates two equations in six unknowns (including ρ_0 as an unknown variable):

$$\begin{aligned} &3Z\,\rho_{op}\,[\tfrac{1}{2} - \frac{1}{4z_p}(r-c_p)] + N\rho_{on}\,[\tfrac{1}{2} - \frac{1}{4z_n}(r-c_n)] \\ &\quad\approx (3Z+N)\,\rho_{o+}\,[\tfrac{1}{2} - \frac{1}{4z_+}(r-c_+)], \end{aligned} \qquad (66)$$

$$Z\,\rho_{op}\left[\tfrac{1}{2} - \frac{1}{4z_p}(r - c_p)\right] + 3N\,\rho_{on}\left[\tfrac{1}{2} - \frac{1}{4z_n}(r - c_n)\right] \approx (Z+3N)\,\rho_{o-}\left[\tfrac{1}{2} - \frac{1}{4z_-}(r-c_-)\right]. \qquad (67)$$

These two approximate equations are linear in r and true for all values or r in the neighborhood of c, so both the slope and intercept may be equated in each case. Equating the slope in equation (66) gives

$$\frac{2\,Z\,\rho_{op}}{z_p} = 3(3Z+N)\,\frac{\rho_{o+}}{4z_+} - (3N + Z)\,\frac{\rho_{o-}}{4z_-}. \qquad (68)$$

Similarly, for the intercept, the equation is

$$2Z\,\rho_{op}\left(2 + \frac{c_p}{z_p}\right) = (3Z + N)\;3\,\rho_{o+}\left(\tfrac{1}{2} + \frac{c_+}{4z_+}\right) - (3N + Z)\,\rho_{o-}\left(\tfrac{1}{2} + \frac{c_-}{4z_-}\right). \qquad (69)$$

Solving for the effective proton distribution parameters leads to

$$z_p = \frac{2\,Z\,\rho_{op}}{(3Z-N)\,\frac{3\rho_{o+}}{4z+} - (3N+Z)\,\frac{\rho_{o-}}{4z_-}} \qquad (70)$$

$$c_p = \frac{z_p\left[3(3Z+N)\rho_{o+}\left(\tfrac{1}{2} + \frac{c_+}{4z_+}\right) - (3N+Z)\rho_{o-}\left(\tfrac{1}{2} + \frac{c_-}{4z_-}\right)\right]}{2\,Z\,\rho_{op}} - 2z_p. \qquad (71)$$

In an entirely analogous fashion the effective neutron distribution parameters may also be determined.

$$z_n = \frac{2\,N\,\rho_{on}}{(3N+Z)\,\frac{3\rho_{o-}}{4z_-} - (3Z+N)\,\frac{\rho_{o+}}{4z_+}} \qquad (72)$$

$$c_n = \frac{\left[3(3N+Z)\,\rho_{o-}(\tfrac{1}{2} + \frac{c_-}{4z_-}) - (3Z+N)\,\rho_{o+}(\tfrac{1}{2} + \frac{c_+}{4z_+})\right] z_n}{2\,N\,\rho_{on}} - 2z_n . \qquad (73)$$

The normalization factor, ρ_o, is specified by the volume integral

$$1 = \int_0^\infty 4\pi\, r^2\, \rho(r)\, dr, \qquad (74)$$

and an iterative process is used to generate three-parameter values from only two equations. As an example, consider the neutron distribution. For a starting value take $\rho_{on} \approx \frac{3}{2}\,\rho_{o-} - \frac{1}{2}\rho_{o+}$. Using this value, z_n is calculated from equation (72). Then, c_n is calculated from equation (73). Using the new-found values of c_n and z_n a better value of ρ_{on} is determined by numerical volume integration (equation (74)). The new value of ρ_{on} may be applied to equations (72), (73) and so on until sufficient accuracy in the distribution parameters is obtained.

It is interesting and informative to compare the density distribution determined by electron scattering on a nucleus with the effective distribution resulting from fitting pion-scattering data. In order to do this, the proton charge form factor must be eliminated from the nuclear charge distribution to yield a mass distribution. The root mean square (RMS) mass radius of a proton distribution may be calculated from a nuclear charge RMS radius by folding out, quadratically, the proton charge RMS radius. But this method is not useful in calculating, for example, a mass-distribution half-density radius (assuming a Fermi distribution) from a charge distribution half-density radius. Instead, a technique suggested by William R. Gibbs is employed.

The appropriate charge distribution is Fourier transformed to momentum components and the proton-charge form factor, appropriately transformed, is divided out. Next, several mass distributions of interest, each constrained to have a proper value of the RMS mass radius, are Fourier-transformed, and their momentum components are compared with those of the transformed charge distribution. That mass distribution whose momentum components most nearly match the charge distribution components in a certain neighborhood is considered to be the best description of the nuclear mass distribution.

Suppose an electron-scattering experiment indicates that a Gaussian model with specified parameters is the best fit to the ^{28}Si proton charge distribution. The RMS mass radius for the ^{28}Si proton distribution is determined by quadratically unfolding the proton charge radius from the nuclear charge RMS radius. If a two-parameter Fermi distribution is deemed adequate to describe the nuclear mass distribution of ^{28}Si, then a family of Fermi parameter sets (half-density radius and skin thickness) is collected, each set of two parameters being constrained to give the specified RMS mass radius. The Fourier transform technique is applied to each parameter set, and that set of parameters whose distribution conforms to the Gaussian charge distribution is considered to best describe the mass distribution of protons. For this thesis experiment, momentum components of two distributions were compared in the neighborhood of 267.6 MeV/c, the incident laboratory momentum of pions.

It is also useful to compare mass distributions of diverse functional form. Proton-scattering experiments indicate the mass distribution of nucleons in certain nuclei. But if these distributions are not of the two-parameter Fermi form, then direct comparison with the results of this experiment is impossible, since the optical-model analysis used here accomodates only the Fermi distribution. But, both distributions may be Fourier-transformed and their momentum components compared.

Partial-Wave Approximation

It may be recollected from previous chapters that the differential scattering cross-sectional values measured by this experiment are averaged over a small, but non-negligible, scattering angle. It is impossible, of course, to physically measure the cross section for particle scattered into a vanishingly infinitesimal solid angle, although the optical model for pion scattering calculates the cross section in this limit. To accommodate measured cross-sectional values to the optical-model theory, the data must be modified in accordance with the angular resolution of the measuring apparatus. (The differential cross-sectional values measured in this experiment are averaged over an angular bin of ± 0.6 deg.)

The differential scattering cross section for pions on a nucleus may be approximated by a series of Legendre polynomials in a partial-wave analysis.[94,95] Based on the partial-wave approximation, the effect on cross-sectional measurements of an angular resolution of

± 0.6 deg. may be assessed, and the scattering data appropriately modified.

The fitting of arbitrary scattering-amplitude compoments to pion-nucleus scattering data in a parial-wave analysis is described by Gibbs et al.[96], and it is their method that has been applied here. A least-squares best fit is determined for the partial wave series such that χ^2 is minimized, where

$$\chi^2 = \sum_{i=1}^{M} \left[\frac{\sigma_d(\theta_i) - \sigma_p(\theta_i)}{\Delta_i} \right]^2 . \tag{75}$$

The differential scattering cross section measured at a given angle, θ_i, is $\sigma_d(\theta_i)$, Δ_i is the error in this measurement, $\sigma_p(\theta_i)$ is the cross sectional value calculated from the partial-wave series, and M is the number of measured cross-sectional values. The values of the complex ampltitudes, f_ℓ, are searched and determined in order that the calculated cross section will minimize χ^2. The partial-wave series is

$$f_p(\theta) = f_c(\theta) + \frac{1}{2ik} \sum_{\ell=o}^{\ell_m} (f_\ell - f_{\ell c})\, (2\ell + 1)\, P_\ell(\cos\theta), \tag{76}$$

(76)

with the Coulomb scattering amplitude given by

$$f_c(\theta) = - \frac{\eta_0}{2k \sin^2\left(\frac{\theta}{2}\right)} \, e^{2i\sigma_0 - 2\eta_0 \log \sin(\frac{\theta}{2})} , \tag{77}$$

and, as usual,

$$\sigma_p(\theta) = |f_p(\theta)|^2 . \tag{78}$$

The partial-wave series is truncated at ℓ_m, the angular momentum of the last partial wave included, $f_{\ell c}$ is the component of f_c, and η_0 is the Sommerfeld parameter, which incorporates information about the particular nucleus being studied.

The pion-scattering data from a particular nucleus may be fitted for the best values of f_ℓ and the calculated differential scattering cross section generated by that fit may then be used to correct the data for poor angular resolution. It is assumed that the differential cross-sectional value, measured at angle θ_i,$\sigma_d(\theta_i)$, is a weighted average of those calculated cross-sectional values in the interval $\sigma_i-.6\leq\theta\leq\theta_i+.6$:

$$\sigma_d(\theta_i) \approx < \sigma_p(\theta_i) > \equiv \frac{\int_{\theta_i-.6}^{\theta_i+.6} g_L(\theta)\sigma_p(\theta)}{\int_{\theta_i-.6}^{\theta_i+.6} g_L(\theta)} . \tag{79}$$

The weighting function $g_L(\theta)$ is the Lorentzian line shape:

$$g_L(\theta) \equiv \frac{1}{\pi} \frac{0.6}{(\theta-\theta_i)^2 + (0.6)^2} . \tag{80}$$

According to this procedure, the first-order modification to the scattering data will follow the formula,

$$\sigma_M(\theta_i) = \frac{\sigma_p(\theta_i)}{<\sigma_p(\theta_i)>} \sigma_d(\theta_i), \tag{81}$$

and an iterative process is pursued until $\sigma_M(\theta_i)$ converges to a value of sufficient accuracy. Namely, $\theta_M(\theta_i)$ is substituted for the differential cross section measured experimentally at every angle θ_i, then these new cross sectional values are again fitted with the partial-wave approximation and the data is modified again according to equation (81), and so on.

Besides using the partial-wave approximation to correct experimental data for angular resolution, it also provides an indication of the very best optical-model fit that may be obtained for the modified data. The optical-model fitting program can be thought of as providing the value of f_ℓ in equation (76) based on a specified potential U_o. Since the partial-wave fit searches over all values of f_ℓ, and is not constrained to those values which satisfy the optical potential, then it must provide a fit at least as good as the optical-model fitting program.

Contaminant Scattering

The EPICS pion channel transports no more than 30 percent muons and electrons at a central momentum of 268 MeV/c (see Table I, Chapter II). Unfortunately, every electron or muon which scatters from the target into the spectrometer is interpreted to be a pion by the experimental detectors. These electromagnetically scattered particles, if in suffucient numbers, could cause a background error to the calculated pion-nucleus cross sections.

The differential cross section for scattering of electrons and muons from atomic nuclei is given, in the Born approximation, by the following formula,[97]

$$\frac{d\sigma}{d\Omega} = \left(\frac{Ze^2}{2E}\right)^2 \frac{\cos^2\left(\frac{\theta}{2}\right)}{\sin^4\left(\frac{\theta}{2}\right)} \frac{|F(q)|^2}{1 + \frac{2E}{Mc^2}\sin^2\left(\frac{\theta}{2}\right)} , \tag{82}$$

where M is the nuclear mass, E is the total energy of the incident particle, and F(q) is the charge form factor. Even on a lead nucleus, at the energy of this experiment, equation (82) should be accurate to about 25 percent for $0 \leq \theta \leq 60$ deg., and on lighter nuclei better agreement will occur.[98] Because of the dependence on Z^2, consider the situation of electron scattering from lead as a worst case. At an electron momentum of 268 MeV/c, E is 268 MeV, and

$$\left(\frac{d\sigma}{d\Omega}\right)_{e^-,Pb} \approx .049 \; |F(q)|^2 \, \frac{\cos^2 \frac{\theta}{2}}{\sin^4 \frac{\theta}{2}} \; \frac{mb}{sr} \quad . \tag{83}$$

At θ = 20 deg., F(q) = .279 (using a Gaussian density distribution), and $\left(\frac{d\sigma}{d\Omega}\right)_{e^-,Pb}$ is about 40 mb/sr. This number is divided by four before comparison with the negative pion cross section for ^{208}Pb at 20 deg. because the particle beam incident on the scattering target contains less than 30 percent electrons. At 20 deg. the pion-lead cross section is about 110 mb/sr (see Appendix C). Thus, for this single measurement, electron and muon contamination results in an error of about ten percent. For the two cross-sectional measurements on either side of the first minimum of the angular distribution, electron and muon scattering adds no more than five percent to the measured value. No other measurement contains as much as a one percent contribution due to electron and muon scattering. Furthermore, the cross sections measured for pion scattering from nuclei lighter than lead can contain only negligible error contributions due to contaminant electrons and muons in the incident pion beam.

V. EVALUATION AND CONCLUSIONS

It is remarkable how well a simple optical-model calculation can reproduce elastic pion scattering on the diverse nuclei of this experiment. Various efforts have been made over the past few years to calculate the elastic differential cross-section for pion scattering from nuclei, all with less than complete success.[99,100,101] It would now seem, however, that the fitting program used here represents a distinct and happy improvement.

The Best Fits to the Scattering Data

The values of the differential cross sections for elastic scattering from ^{9}Be, ^{28}Si, ^{58}Ni, and ^{208}Pb are tabulated in Appendix C, both the data modified for electron and muon scattering and for the angular resolution of the experimental apparatus and the original unmodified data. Figures 24-31 show the modified scattering data and the best fit obtained with the optical-model program. The worst correspondence between the calculation and data occurs for negative pion scattering from ^{208}Pb and the quality of the fit is specified by a χ^2 per degree of freedom value of 1.44. This value is atypical; the next worst value being 1.17 and a more usual value of χ^2 per degree of freedom is about 1.

It can be shown[102] that the probability of obtaining a worse χ^2 fit to the 56 data points for negative pion scattering from ^{208}Pb,

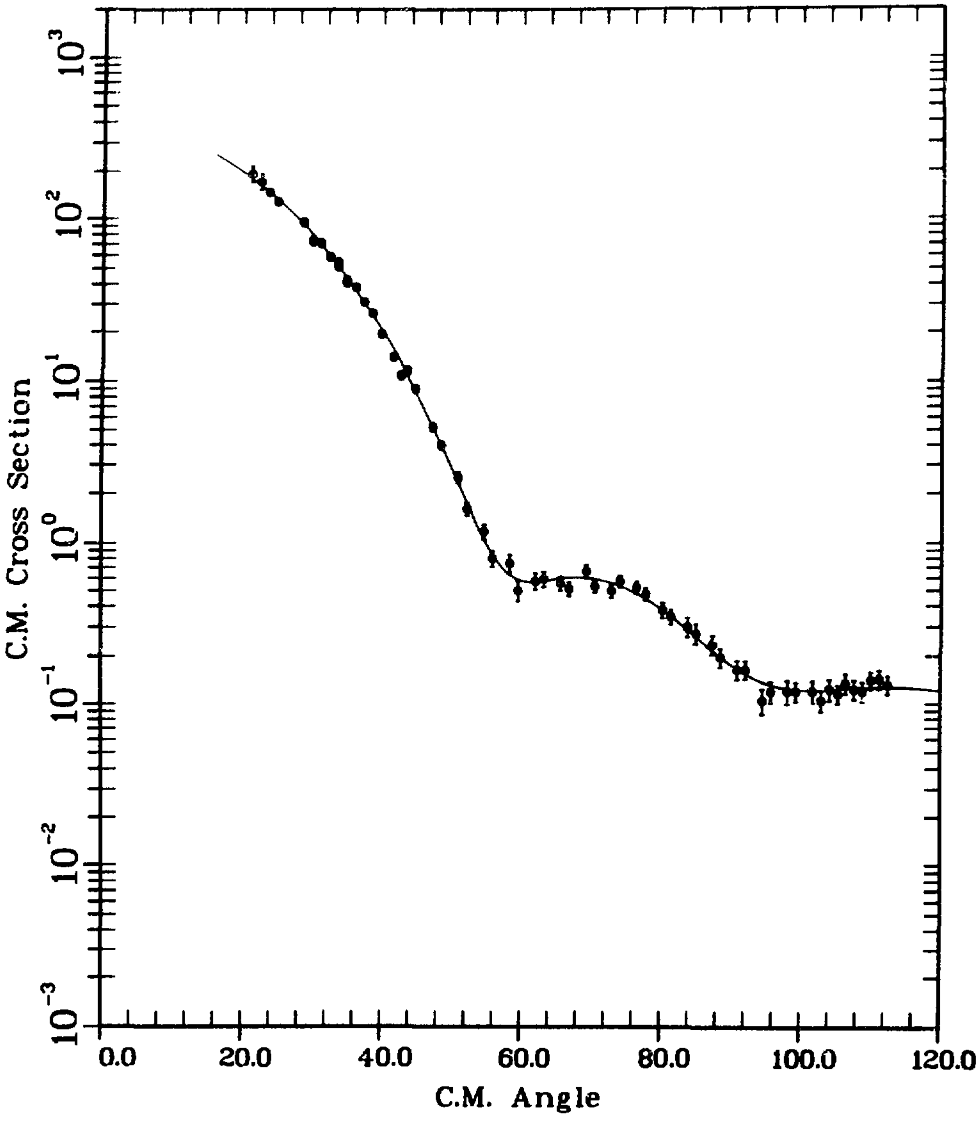

Figure 24 Pi+ elastic scattering from 9Be. The solid line is the optical-model fit.

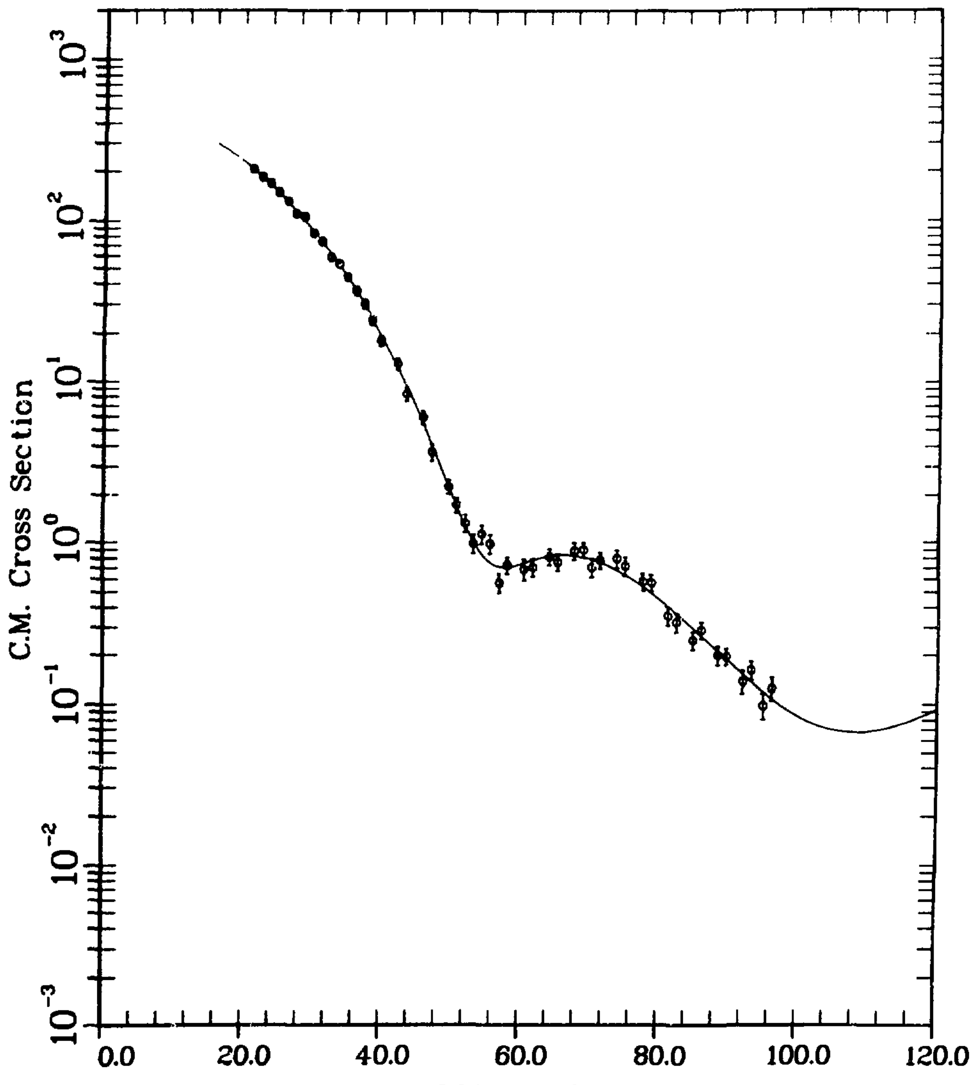

Figure 25. Pi– elastic scattering from 9Be. The solid line is the optical-model fit.

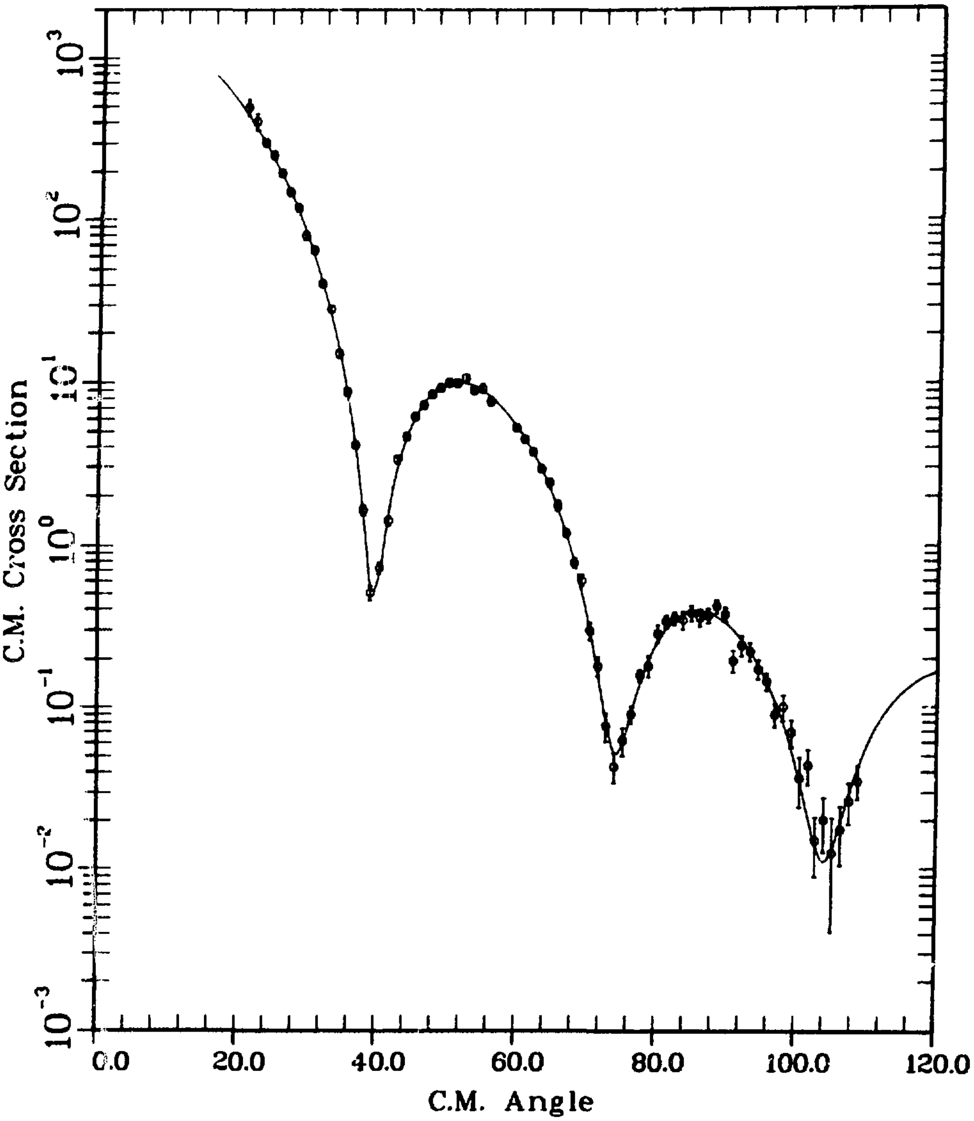

Figure 26. Pi+ elastic scattering from 28Si. The solid line is the optical-model fit.

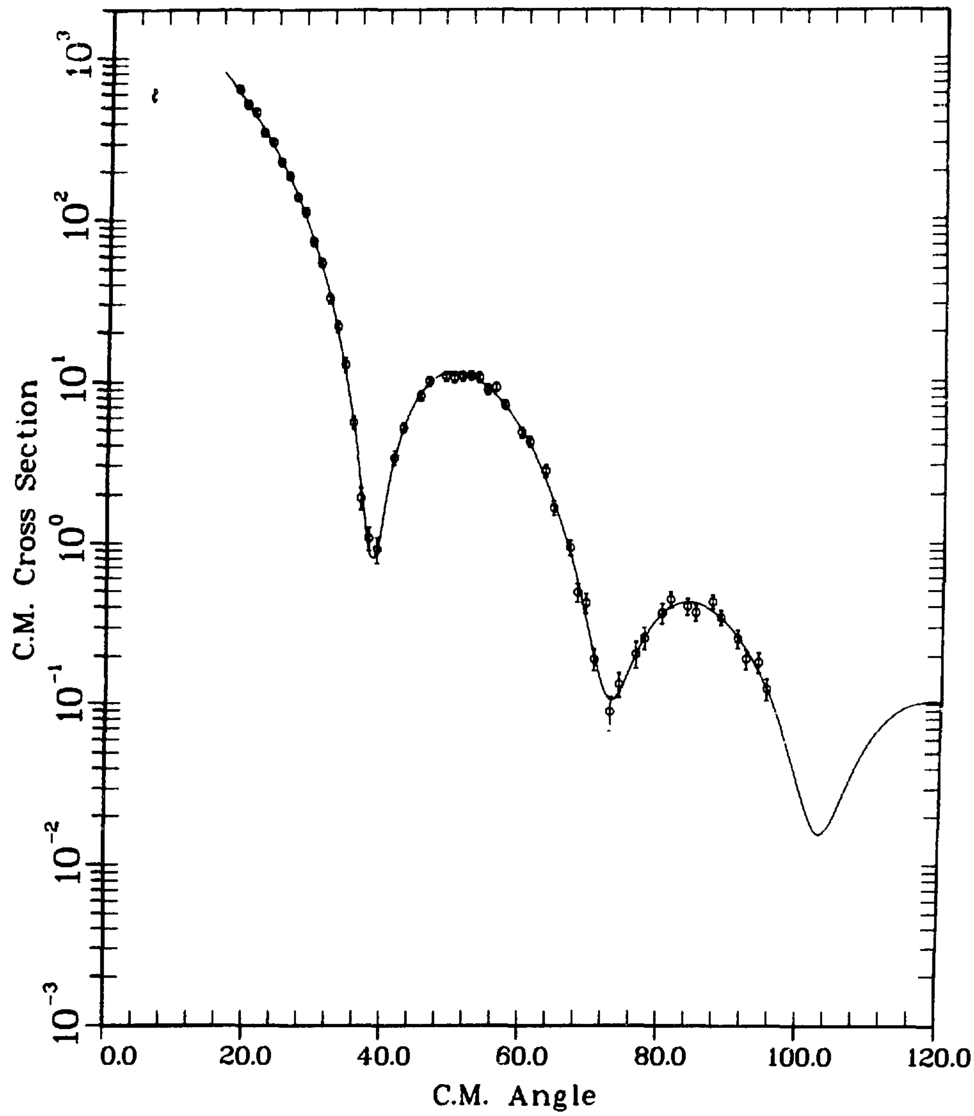

Figure 27. Pi− elastic scattering from 28Si. The solid line is the optical-model fit.

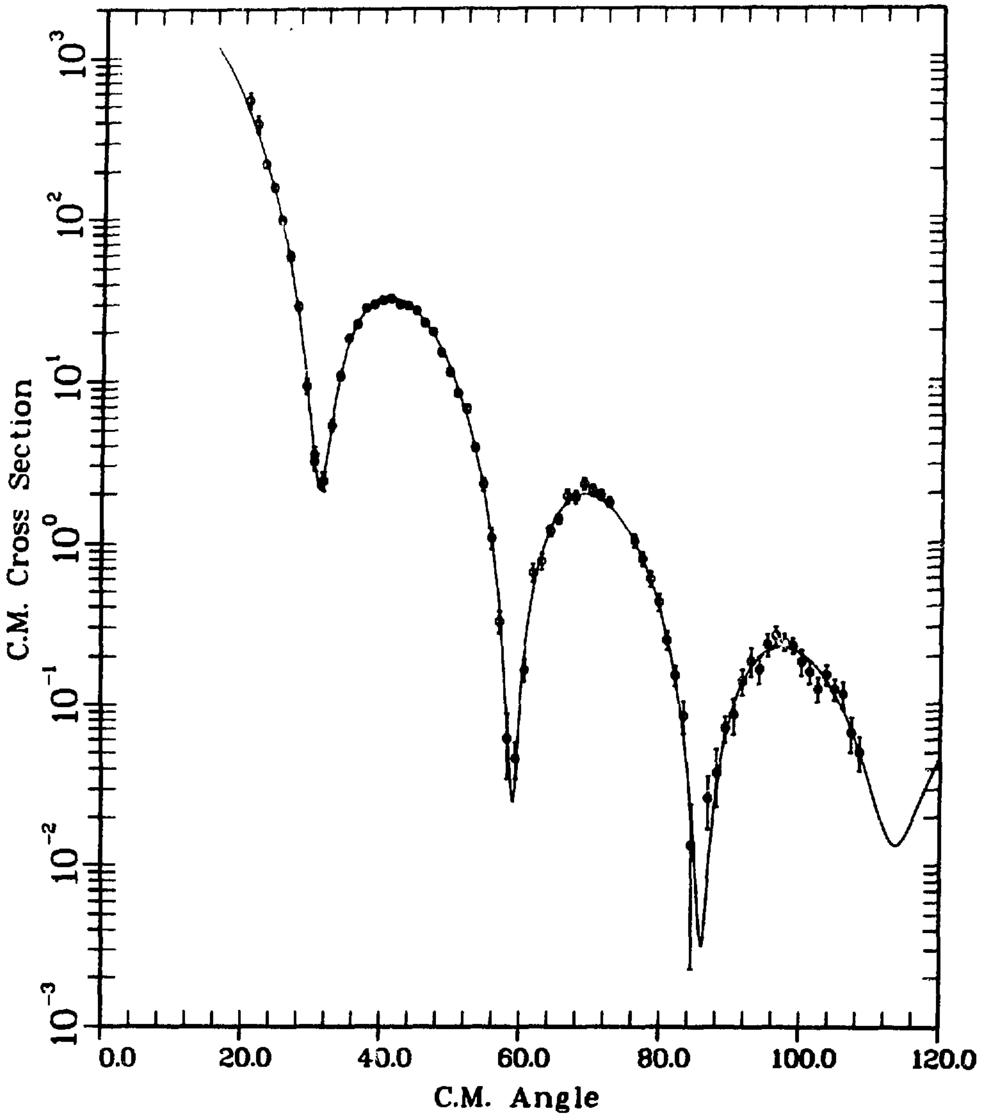

Figure 28 Pi+ elastic scattering from 58Ni. The solid line is the optical-model fit.

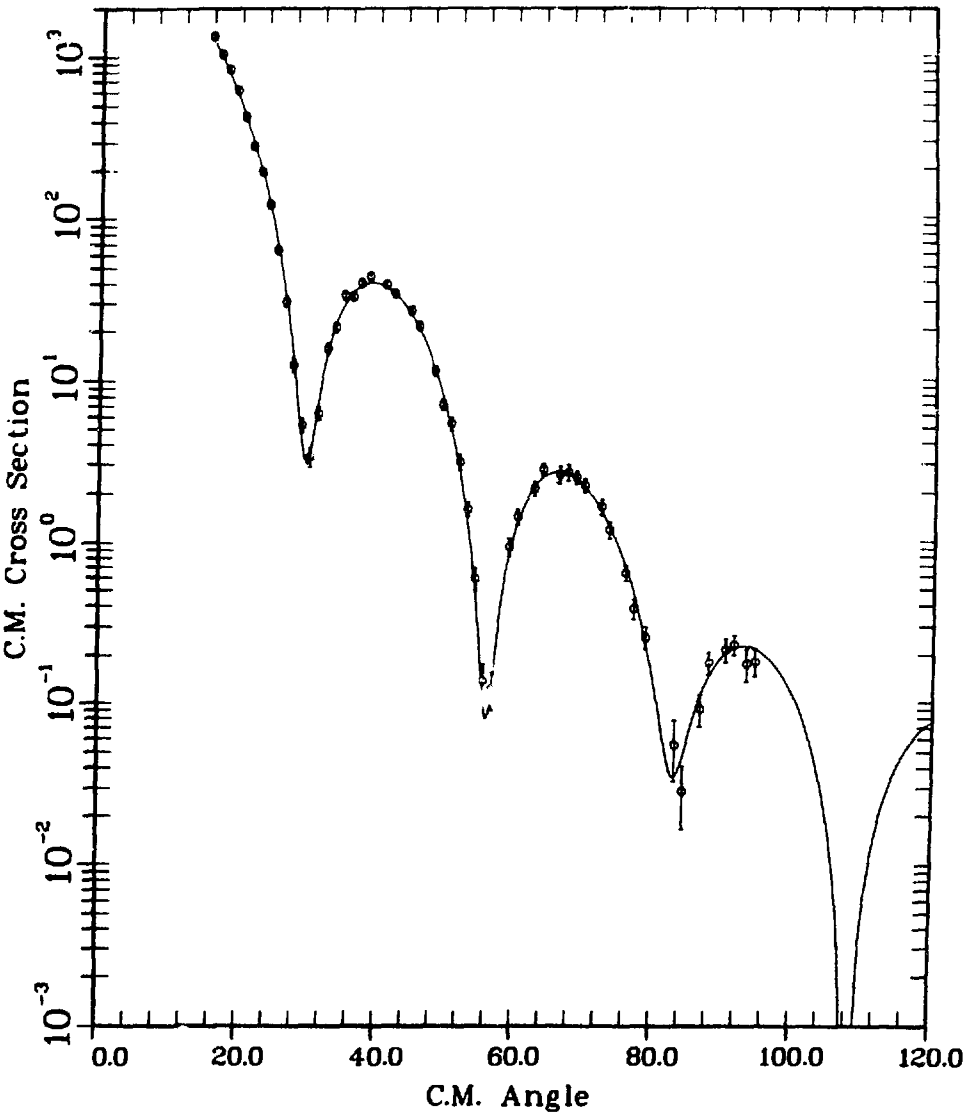

Figure 29. Pi− elastic scattering from 58Ni. The solid line is the optical-model fit.

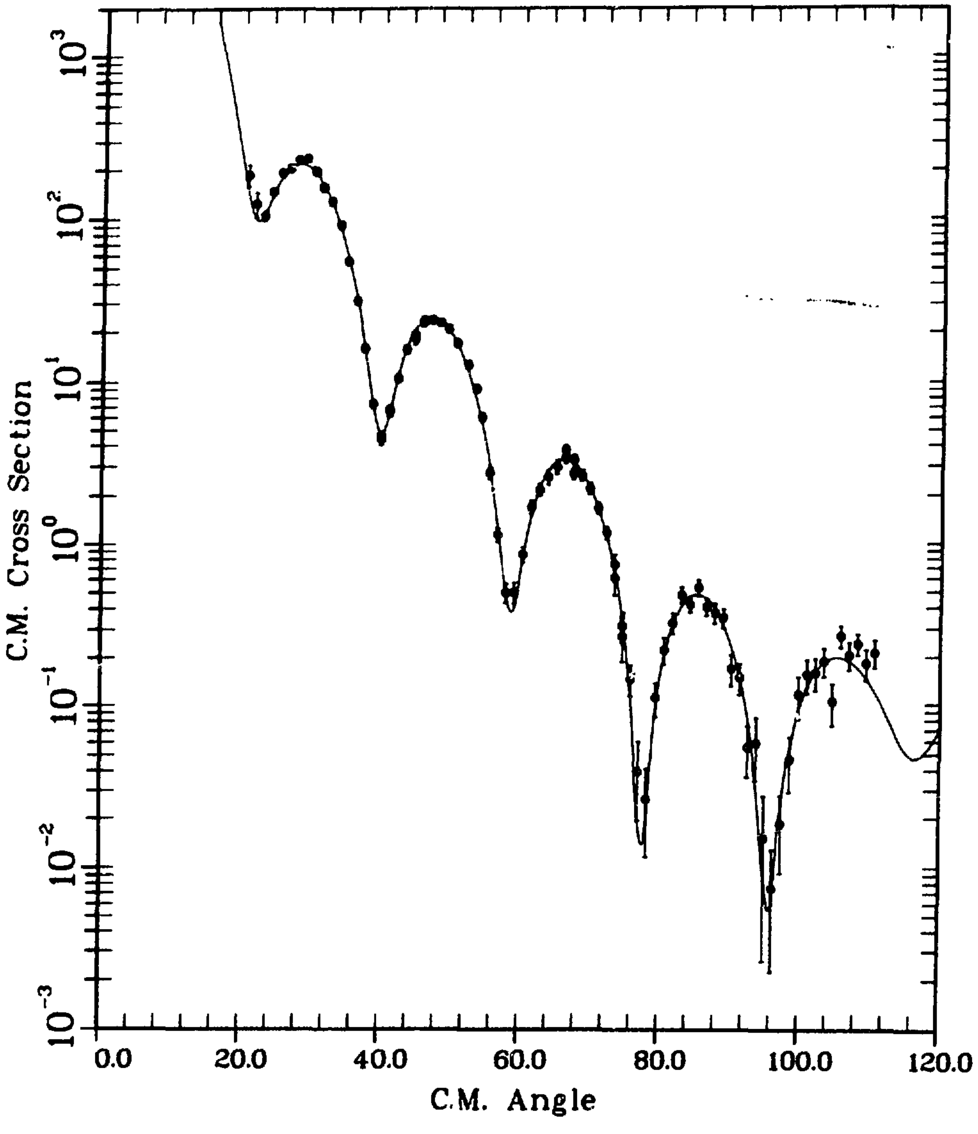

Figure 30. Pi+ elastic scattering from 208Pb. The solid line is the optical-model fit.

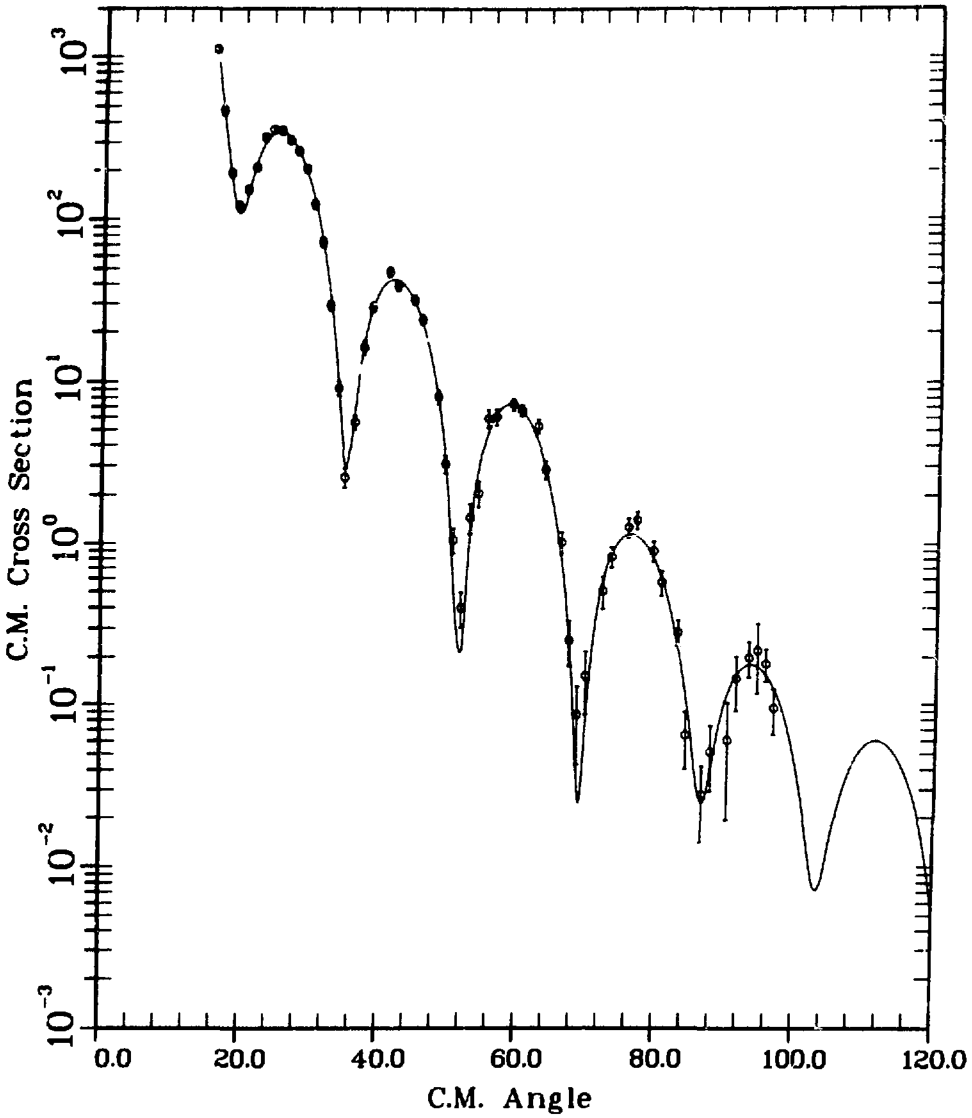

Figure 31 Pi− elastic scattering from 208Pb. The solid line is the optical-model fit.

should the scattering data be measured anew, is only two percent. So, statistical arguments indicate that a future experiment to remeasure this cross section may yield a more useful data set.

It might be argued that the optical-model fitting program is at fault for the poor correspondence between data and calculation, but this is unlikely. The data has also been fit with a partial-wave analysis for arbitrary scattering amplitudes and the very best fit yielded by this data set corresponded to a value of χ^2 per degree of freedom of 1.45. Thus one may conclude that this particular data set is statistically poor. On the other hand, the cross-sectional data for negative pion scattering from ^{28}Si is fit exceedingly well by the optical-model program. A value of 0.70 χ^2 per degree of freedom (also called the reduced χ^2, symbolized by χ^2_ν) is obtained. There is a 93 percent chance that χ^2_ν would be worse if this cross section were remeasured.

Table 5 is a tabulation of the probality for a worse χ^2 optical-model fit to all the cross-sectional data of this experiment and to the measured cross sections for pions on ^{12}C, used to normalize the data of this experiment. The spread of probability values over the nuclei of this experiment may indicate a proper calculation of the relative error in cross-sectional values.

The best values of all fitted parameters are listed in Table 6. It is these parameters which provide the calculated cross sections plotted in Figs. 24-31. The absolute normalization value, R_n, for the π^-, ^{9}Be cross section is not the result of an optical-model fit.

Table 5. The probability that a remeasured cross section would provide a worse fit to the optical model is tabulated for both positive and negative pion scattering. The measured carbon cross sections were used to normalize the data of this experiment.

	π^+	π^-
^{9}Be	60.0	80.0
^{28}Si	35.0	93.0
^{58}Ni	70.0	20.0
^{208}Pb	15.0	2.0
^{12}C	greater than 99.0	99.0

Table 6. The fitted parameters are indicated for each cross section. The effective mass distribution parameters, half-density radius, c, and diffuseness, z, are measured in fm. The pion-nucleon range, α, is measured in MeV/c. R_n is the absolute renormalization value, b_0, b_1 are the optical potential strength parameters and χ^2_ν is the reduced chi-squared value.

$\pi^+, {}^9\text{Be}$

χ^2_ν = 0.956 R_n = 1.25
c = 1.92 z = 0.490
b_0 = -2.722 -2.963i
b_1 = 3.917 10.29i
α =250.

$\pi^-, {}^9\text{Be}$

χ^2_ν = 0.814 R_n = 1.22
c = 1.91 z = 0.510
b_0 = -3.990 -4.621i
b_1 = 4.118 12.712
α = 200.

$\pi^+, {}^{28}\text{Si}$

χ^2_ν = 1.06 R_n = 1.34
c = 3.02 z = 0.465
b_0 = -1.100 -1.400i
b_1 = 4.610 9.579i
α = 250.

$\pi^-, {}^{28}\text{Si}$

χ^2_ν = 0.700 R_n = 1.31
c = 3.110 z = 0.465
b_0 = -0.9335 -0.3992i
b_1 = 4.351 8.075i
α = 300.

Table 6 (continued).

$\pi^+, {}^{58}\mathrm{Ni}$

$\chi^2_\nu = 0.914$ $R_n = 1.26$

$c = 4.03$ $z = 0.515$

$b_0 = -0.2727$ $-1.067i$

$b_1 = 4.108$ $7.922i$

$\alpha = 250.$

$\pi^-, {}^{58}\mathrm{Ni}$

$\chi^2_\nu = 1.17$ $R_n = 1.24$

$c = 4.00$ $z = 0.520$

$b_0 = -0.4942$ $-0.8502i$

$b_1 = 3.441$ $8.517i$

$\alpha = 250.$

$\pi^+, {}^{208}\mathrm{Pb}$

$\chi^2_\nu = 1.17$ $R_n = 1.19$

$c = 6.59$ $z = 0.550$

$b_0 = -0.5500$ $-1.217i$

$b_1 = 4.159$ $6.287i$

$\alpha = 250.$

$\pi^-, {}^{208}\mathrm{Pb}$

$\chi^2_\nu = 1.44$ $R_n = 1.12$

$c = 6.28$ $z = 0.630$

$b_0 = -1.420$ $-1.241i$

$b_1 = 5.611$ $10.94i$

$\alpha = 350.$

There is little structure in the π^-, ^{9}Be angular distribution and the cross section was not measured to as large an angle as the π^+, ^{9}Be cross section. There is not enough information in this angular distribution to allow a fit simultaneously to all the strength parameters and the absolute renormalization value. Therefore, R_n was chosen to have a value of 1.22 based on the renormalization values for other cross sections and on the general behavior of the fitting program.

The parameters of the optical-model calculation for negative pion scattering from lead are determined with the least certainty. The fitted value of the pion-nucleon range lies between the values 200 MeV/c and 300 MeV/c for all cross sections except that one with the largest value of reduced chi squared, namely the cross section for π^-, ^{208}Pb. Additionally, the renormalization value for this cross section is quite different from the renormalization value for the positive pion cross section on lead, a difference not as noticeable for any other nucleus.

Cross-Sectional Renormalization

There is a result of the optical-model fits that is unsettling, at least at first glance: the fitted renormalization values for the various nuclei fall in the interval 1.12-1.34 despite a measured absolute renormalization error of ±0.09 about a nominal value of 1.00 (see chapter III). The actual renormalization error inherent in the measured data is the same value for all cross sections of a particular pion charge sign. So, while all the positive (or negative) pion cross sections may be either lower or higher than their measured values, the difference is the same for all four cross sections. The fitted renormalization values and their standard deviations for the cross sections measured by this experiment, and for the $\pi^{\pm}$, ^{12}C cross sections are shown in Table 7.

Two difficulties seem to exist. First, all the fitted renormalization values for cross sections of a given pion charge sign are not the same within errors. Second, the average value of these four renormalization values does not fall in the range 0.91-1.09 as anticipated. It is possible that both of these problems may yield to the same solution. The optical-model fitting program is only as valid as the coherence approximation. A calculation[103] which accounts for elastic scattering through intermediate excited nuclear states, in contrast to the coherence approximation, indicates that the first-order optical model will calculate anomalously high cross sections. This result of taking the coherence approximation should be a function of the topography of the excited states of a given nucleus. A glance at Table 7 indicates that the fitted renormalization values (with the exception of values for the carbon cross sections) are similar for the cross sections on a particular nucleus.

Another calculation,[104] which corrects the first-order optical model for the coherence approximation by actually determining the

Table 7. The fitted values of the renormalization constant, R_n, and its approximate standard deviation are shown for the various cross sections of this experiment and for the ^{12}C cross sections.

	π^+	π^-
^{9}Be	1.25 ± 0.04	1.22
^{28}Si	1.34 ± 0.05	1.31 ± 0.04
^{58}Ni	1.26 ± 0.04	1.24 ± 0.05
^{208}Pb	1.19 ± 0.05	1.12 ± 0.06
^{12}C	1.22 ± 0.05	1.32 ± 0.05

amount of pion absorption, leads to the same result. It indicates a first-order optical model will calculate cross sections that are too large.

The Fitted Strength Parameters

The fitted optical-model strength parameters mock up some effects not explicitly accounted for by the first-order optical model. Table 8 is a list of the strength parameters of the optical potential derived from the fitting program and the free-strength parameters based on the work of McKinley.[105] As expected, the fitted value which is most nearly the same as its corresponding free value is the real part of b_1. Pion absorption effects not handled formally by the first-order model appear mainly as modifications to the imaginary part of the strength parameters.

Additionally, since each nucleon from which a pion scatters is immersed in the nuclear environment, the consequences of nucleon-binding result primarily in fitted values of b_o different from the free values. Because a nucleon is bound to its neighbors inside the nucleus, the angle of pion scattering from the nucleon is different than it would be from a free nucleon. Explicitly calculating this effect is known as making the nuclear "angle transform". In particular, the "angle transform" neglected in the first-order optical model causes a subtraction of part of the p-wave strength parameter b_1 from the s-wave strength b_o, leaving fitted values of b_o which are smaller and more negative than the free b_o values. In spite

Table 8. The fitted strength parameters, and free values are shown. b^f are the free values.

$\pi^+, {}^{9}$Be		
b_0 =	-2.722	-2.963i
b_1 =	3.917	10.29i
b_0^f =	-0.3277	0.5876i
b_1^f =	3.988	7.933i

$\pi^-, {}^{9}$Be		
b_0 =	-3.990	-4.621i
b_1 =	4.118	12.71i
b_0^f =	-0.6609	0.5652i
b_1^f =	4.676	8.851i

$\pi^+, {}^{28}$Si		
b_0 =	-1.100	-1.400i
b_1 =	4.610	9.579i
b_0^f =	-0.4884	0.5745i
b_1^f =	3.992	8.542i

$\pi^-, {}^{28}$Si		
b_0 =	-0.9335	-0.3992i
b_1 =	4.351	8.075i
b_0^f =	-0.4884	5.745i
b_1^f =	3.992	8.542i

$\pi^+, {}^{58}$Ni		
b_0 =	-0.2727	-1.067i
b_1 =	4.108	7.922i
b_0^f =	-0.4357	0.5771i
b_1^f =	3.759	8.447i

$\pi^-, {}^{58}$Ni		
b_0 =	-0.4942	-0.8502i
b_1 =	3.441	8.517i
b_0^f =	-0.5366	0.5703i
b_1^f =	3.955	8.739i

Table 8 (continued).

$\pi^+, {}^{208}\mathrm{Pb}$		
b_0 =	-0.5500	-1.217i
b_1 =	4.159	6.287i
b_0^f =	-0.1767	0.5945i
b_1^f =	3.220	7.711i

$\overset{-}{\pi}, {}^{208}\mathrm{Pb}$		
b_0 =	-1.420	-1.241i
b_1 =	5.611	10.94i
b_0^f =	-0.7942	0.5526i
b_1^f =	4.412	9.504i

of the changes in strength parameters induced by the fitting process, all scattering matrix elements corresponding to the fitted optical potential are computed to be unitary.

Results of the Fit

It is possible to calculate the effective mass distributions which yield a best fit to the scattering data for the optical model. The method, based on the different fits to positive and negative pion scattering on a single nucleus, was outlined in the last chapter. Figures 32 and 33 show the effective two-parameter Fermi distributions for ^{58}Ni obtained with the optical-model fit and a comparison with the neutron and proton densities given by proton-and electron-scattering experiments. The proton charge size is removed from electron-scattering results to yield a proton mass density as outlined in the previous chapter. All plotted densities are normalized so that the volume integral $4\pi \int_0^\infty r^2\rho(r)dr$ is equal to one.

At energies near the (3,3) resonance, an elastic pion is likely to be lost before it penetrates far into any nucleus. The center of the nuclear mass distribution is not probed effectively by pions at the energy of this experiment. The pion is expected to be more sensitive to the nuclear density in the neighborhood of the 0.2 density point and Figs. 32 and 33 seem to bear this out.

Figure 34 is a plot of the proton mass density of ^{28}Si given by electron scattering and of the effective proton and neutron mass distributions from the-optical model fit. The effective proton

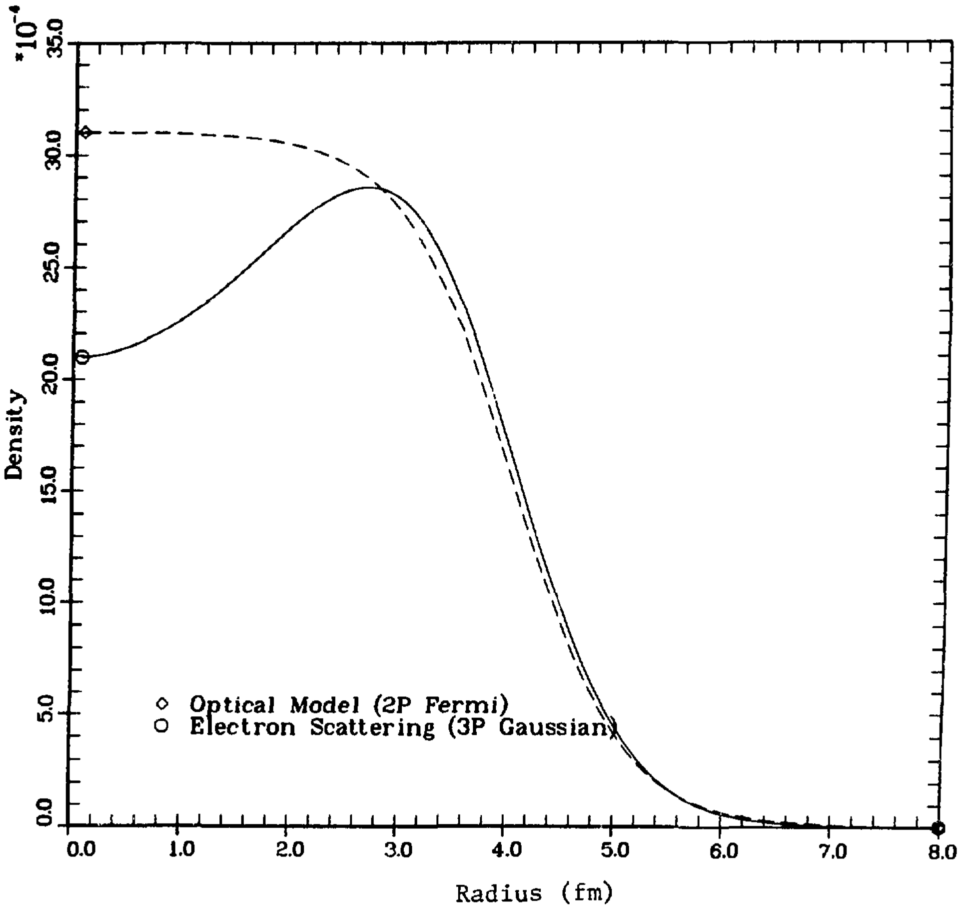

Fig. 32. Proton mass density for ^{58}Ni and the effective optical-model density.

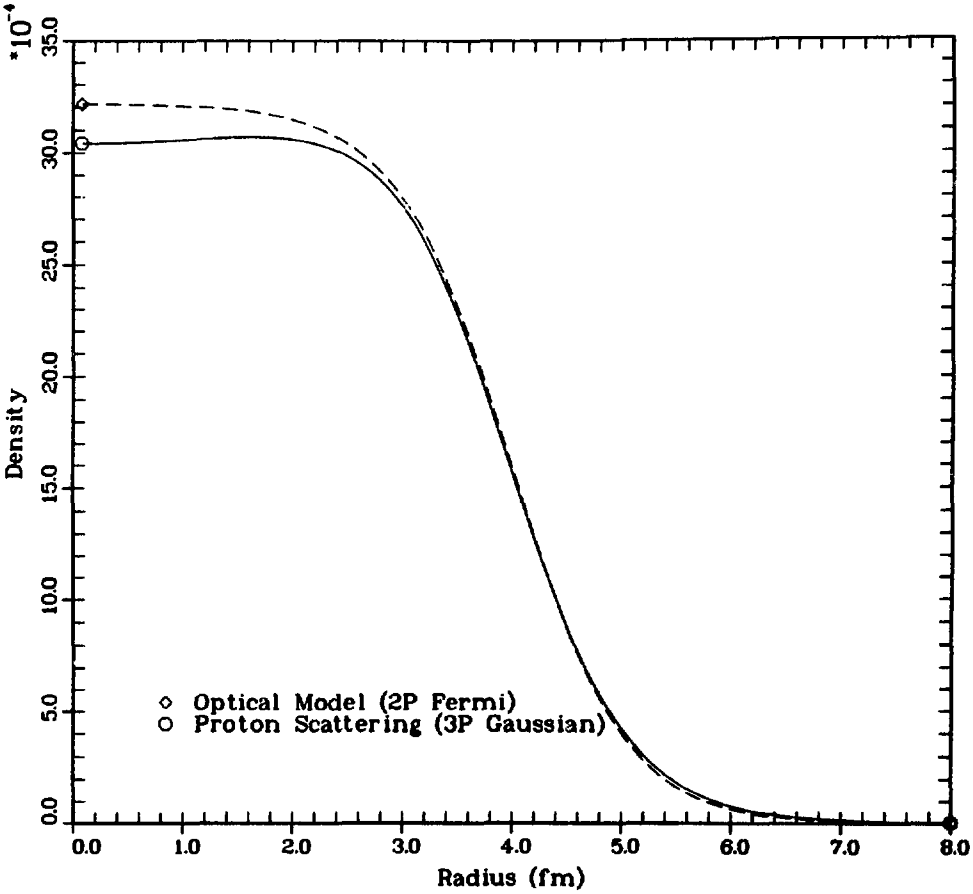

Fig. 33. Neutron mass density for ^{58}Ni and the effective optical-model density.

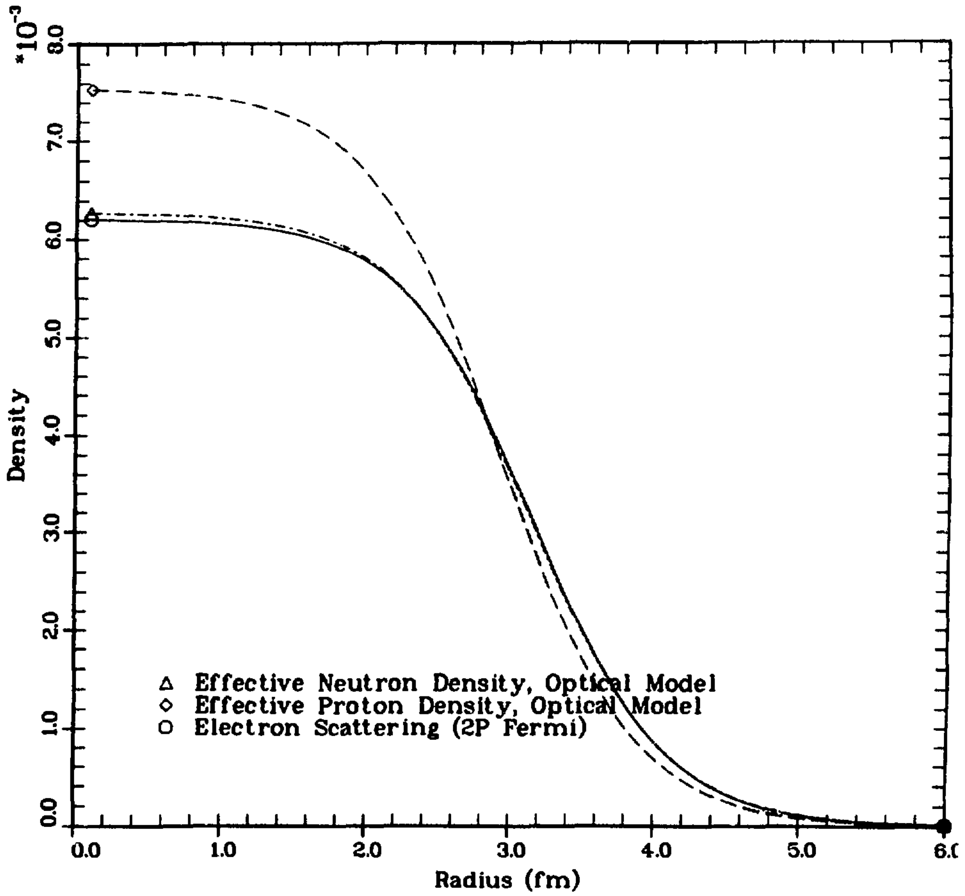

Fig. 34. Proton and neutron mass densities for ^{28}Si. Error in the dashed line lies between the two dotted lines.

density specified by the optical-model fit is clearly unacceptable when compared with electron-scattering results. However, the effective neutron distribution from the optical model matches the proton distribution given by electron scattering, just as one expects the real neutron distribution to do for this particular nucleus.

The compilation of effective proton and neutron distribution parameters and electron-[106] and proton-scattering[93,107] results in Table 9 includes approximations of the standard deviation errors. The root mean square (RMS) proton radius of the ^{28}Si nucleus, as given by the Fermi parameters of the effective density from the optical-model fit, differs from the best value from electron scattering by about two standard deviations. The optical-model fit for $\pi^{\pm}$, ^{28}Si was the only case where more than one local minimum was found in the parameter-space of the fit. Some small possibility exists that this may account in an unknown way for the discrepancy between the real proton RMS radius and the effective value determined with the optical model.

The optical-model-generated effective mass distributions for ^{9}Be are shown in Fig. 35. No good electron-scattering determination of these distributions exists. The RMS proton mass radius shown in Table 9 has been calculated from an electron-scattering experiment[108] with only the limited momentum transfer range of 0.26 - 0.70 fm^{-1}.

Table 9. The effective Fermi density parameters (c,z) are shown for the neutron and proton distributions. R_p is the effective value of the proton distributions RMS radius as R_n is the effective neutron distribution RMS radius. R_{es} is the RMS proton distribution radius from electron scattering and R_{ps} is the value, from proton scattering, given to the RMS radius of the neutron distribution. Errors shown are roughly the standard deviation.

^{9}Be

$c_p = 1.92 \pm 0.03$

$z_p = 0.481 \pm 0.008$

$R_p = 2.36 \pm 0.05$

$R_{es} = 2.37 \pm 0.01$

$c_n = 1.90 \pm 0.04$

$z_n = 0.521 \pm 0.01$

$R_n = 2.43 \pm 0.05$

^{28}Si

$c_p = 2.94 \pm 0.04$

$z_p = 0.463 \pm 0.008$

$R_p = 2.86 \pm 0.06$

$R_{es} = 3.00 \pm 0.03$

$c_n = 3.150 \pm 0.06$

$x_n = 0.465 \pm 0.01$

$R_n = 2.99 \pm 0.06$

^{58}Ni

$c_p = 4.05 \pm 0.07$

$z_p = 0.513 \pm 0.012$

$R_p = 3.68 \pm 0.08$

$R_{es} = 3.69 \pm 0.01$

$c_n = 3.99 \pm 0.07$

$z_n = 0.523 \pm 0.012$

$R_n = 3.69 \pm 0.08$

$R_{ps} = 3.70 \pm 0.08$

Table 9 (continued).

^{208}Pb

$c_p = 6.73 \pm 0.20$

$z_p = 0.511 \pm 0.03$

$\mathcal{R}_p = 5.55 \pm 0.15$

$\mathcal{R}_{es} = 5.45 \pm 0.02$

$c_n = 6.10 \pm 0.30$

$z_n = 0.673 \pm 0.03$

$\mathcal{R}_n = 5.34 \pm 0.15$

$\mathcal{R}_{ps} = 5.611 \pm 0.08$

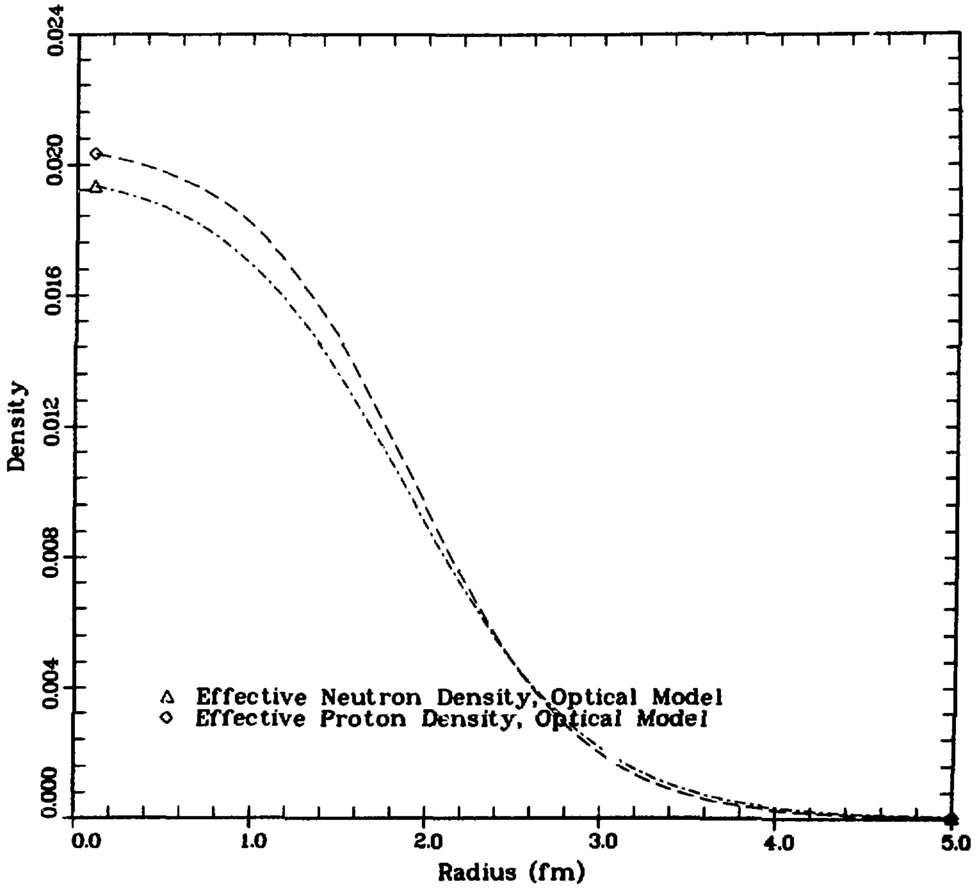

Fig. 35. The proton and neutron mass densities for ^{9}Be.

As mentioned before, the $\pi^-, {}^{208}$Pb cross section measured by this experiment provides an atypically poor fit to both the optical model and the partial-wave calculation. Such a poor fit discredits all the fitted parameters of the calculated cross section, including effective-density parameters. Since the proton as well as the neutron effective-density parameters depend on both positive and negative pion-scattering results, the effective proton density, as well as the effective neutron density of ^{208}Pb, is not believable. For the sake of completeness, the effective-density parameters for lead, generated by the optical-model fit, are listed in Table 9 and the densities are plotted in Figs. 36 and 37. Additionally, these figures show the densities derived from electron and proton scattering. Figure 36 also indicates the best two-parameter Fermi distribution that may be fit to the tail of the three-parameter Gaussian distribution from electron scattering.

The value of the pion-nucleon range fit by the optical model is independent of nucleus. Excluding the poor fit to the $\pi^-, {}^{208}$Pb scattering data, all fitted values of the range lie in the interval 200 MeV/c - 300 MeV/c, with a best value of 250 MeV/c corresponding to a length of 0.8 fm. Table 10 shows the values of the range which give best fits for the particular functional form of the optical model.

Wave functions, phase shifts, and various cross sections calculated by the optical model are also valuable. Appendix D

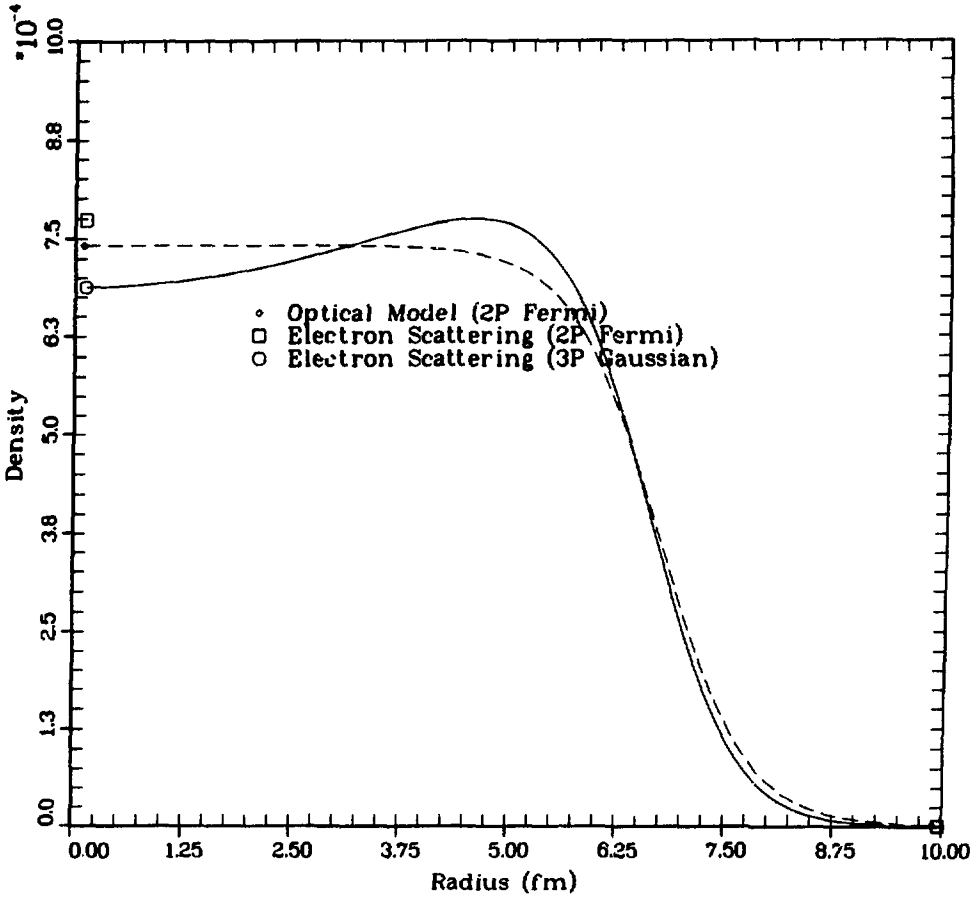

Fig. 36. Proton mass density for ^{208}Pb and the effective optical-model density.

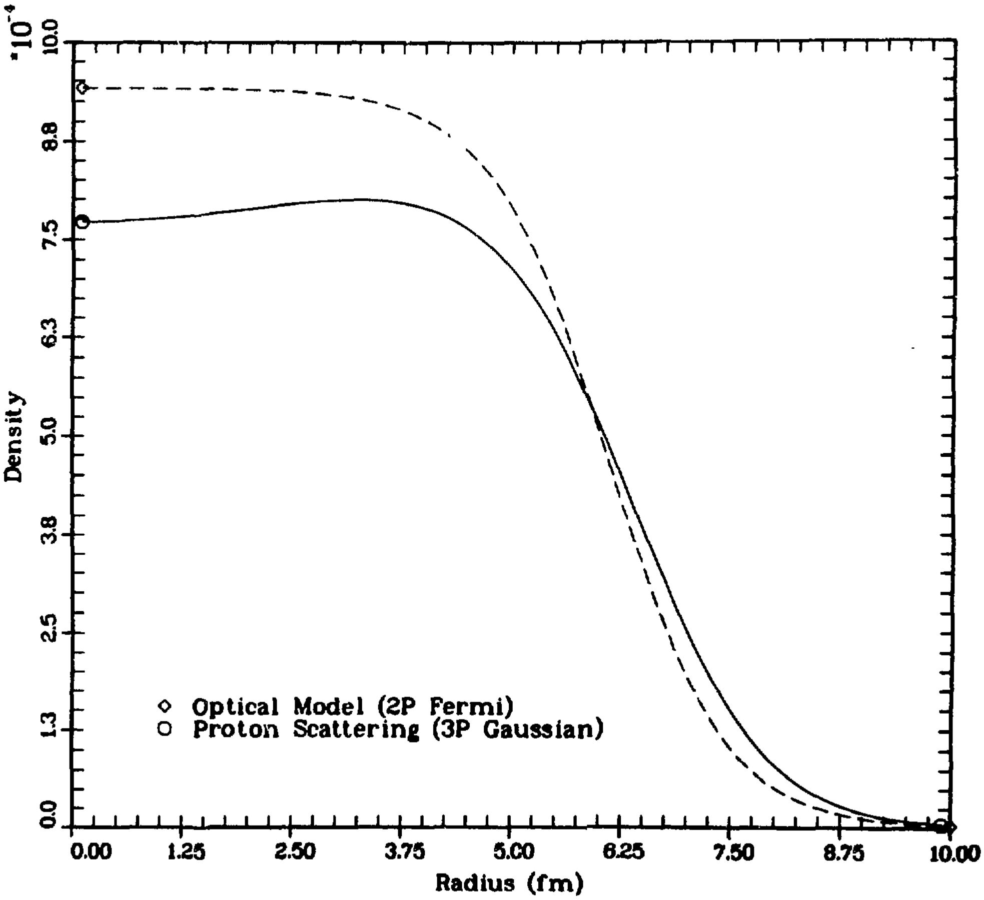

Fig. 37. Neutron mass density for ^{208}Pb and the effective optical-model density.

Table 10. Shown are the values of the pion-nucleon range for each cross section. In parenthesis is the standard deviation error.

	π^+	π^-
^{9}Be	250. (+500, -75)	200. (+100, - 60)
^{28}Si	250. (+ 50, -25)	300. (+100, - 75)
^{58}Ni	250. (+ 75, -40)	250. (+ 75, - 40)
^{208}Pb	250. (+ 60, -60)	350. (+700, -100)

lists the total cross section and forward scattering amplitude based on the best optical-model fits to all the scattering data.

Conclusions

The optical model used here to fit the elastic pion-scattering data is not, strictly speaking, just a first-order model. Allowing the renormalization parameter in the model to assume values which cannot really specify the true renormalization of the data appears to mock up effects of second-order scattering in a nucleus. While only the first term in the Watson series is explicitly incorporated into the model, the free parameters account for some higher-order terms.

Notice that the two-parameter Fermi distribution used to specify the nuclear mass density in the optical model does not often correspond to the optimum functional form of the nuclear distribution as given by electron or proton-scattering measurements. So the optical potential in this model is not precisely of first order, because it does not use the exact nuclear mass density. But, except for the peculiar case of the effective proton distribution for ^{28}Si and the discredited lead fitted parameters, the effective mass density values fit by the optical model are reasonably close to the expected values, at least near the 0.2 density point.

It is no surprise that a strict first-order optical model will not adequately fit pion-nucleus scattering at intermediate energies. What is remarkable is that a first-order model with a significant modification for the pion-nucleon range and adequate flexibility i its fitted parameters to account for effects not explicitly calculated, fits all the quality scattering data with physically reasonable parameter values. (This excludes, of course, the aberrant fitted proton distribution parameters of ^{28}Si, and even these values lie outside accepted limits by little more than two standard deviations).

Taking a large value for the pion-nucleon range in the optical-model program gives an approximation to those fitting programs which do not include the formalism of range. Symptoms of neglecting the finite range of the pion-nucleon interaction include smaller values of the half-density radius for the effective mass distributions compared with those radii fit to the optical model with a finite pion-nucleon range. Additionally, an optical-model fit with no finite range formalism yields values of real b_1 that are quite a bit larger than either the free values or the values fit with the modified optical model.

It may be possible to learn about the physics of the pion-nucleus system from the parameter values fit by the optical model. For example, the fitted values of the s-wave strength parameter, b_o, seem to argue the importance of the "angle transform" in the multiple-scattering calculation, and the fitted evaluation of the pion-nucleon range should be useful in future calculations of the optical potential. Furthermore, the weakness of the coherence approximation, and the importance of multiple scattering to intermediate excited nuclear states, is hinted at by the fitted renormalization values.

The very careful analysis of the scattering data of this experiment seems to have borne fruit. When analyzed with the particular optical model that contains the pion-nucleon range formalism, encouraging results are obtained. It may even be true that the tedious, exacting, and extended work of this thesis was really worthwhile.

REFERENCES

1. J. Dalton, *A New System of Chemical Philosophy* (1808).
2. J. J. Thompson, Phil. Mag. 44, 293 (1897).
3. J. J. Thompson, Phil. Mag. 7, 237 (1904).
4. H. Nagaoka, Phil. Mag. 7, 445 (1904).
5. H. Geiger and E. Marsden, Proc. R. Soc. A 82, 495 (1909).
6. H. Geiger and E. Marsden, Philos. Mag. 25, 604 (1913).
7. E. Rutherford, Phil. Mag. 21, 669 (1911).
8. N. Bohr, Phil. Mag. 26, 1 and 476 (1913).
9. M. Planck, Verhandl. Deut. Physik Ges. 2, 237 (1900).
10. A Sommerfeld, Ann. Phys. (Leipz.) 51, (1916).
11. M. Born, Z. Phys. 37, 863 (1926).
12. M. Born, Nature (Lond.) 119, 354 (1927).
13. J. Chadwick, Proc. R. Soc. A 136, 692 (1932).
14. D. Iwanenko, Nature (Lond.) 129, 798 (1932).
15. W. Heisenberg, Z. Phys. 77, 1 (1932).
16. See, for example, P. Marmier and E. Sheldon, *Physics of Nuclei and Particles* (Academic Press, New York, 1969), Vol. II, Chap. 15.
17. J. Allred, *LAMPF: The Meson Factory*, (Los Alamos Scientific Laboratory Report LA-6590, 1977).
18. M. Livingston, *Origins and History of the Los Alamos Meson Physics Facility*, (Los Alamos Scientific Laboratory Report LA-5000, 1972).

19. See, for example, T. Ericson, *Proceedings of the International Conference on Nuclear Structure*, Kingston, Canada, Aug. 29-Sept. 3, 1960.
20. H. Yukawa, Proc. Math. Soc. Japan *17*, 48 (1935).
21. M. Lattes et al., Nature (Lond.) *159*, 594 (1947).
22. N. Kemmer, Proc. Camb. Philos. Soc. *34*, 354 (1938).
23. T. Trippe et al., Rev. Mod. Phys. 48, S26 (1976).
24. G. Backenstoss et al., Phys. Lett. B *36*, 403 (1971).
25. T. Trippe et al., Rev. Mod. Phys. *48*, S21 (1976).
26. F. Becker and Yu. Batusov, Nuovo Cimento *1*, 309 (1971).
27. A. Reitan, "Double Charge Exchange Scattering of Pions by Nuclei," in *Proceedings of the International Seminar on Pi Meson-Nucleus Interactions*, Strasbourg, France, September 1971 (V-1-15), Sect. 3, 1.
28. A. Abashian et al., Phys. Rev. *104*, 855 (1956).
29. M. Sternheim and E. Auerbach, Phys. Rev. C *4*, 1805 (1971).
30. G. Dugan et al., Phys. Rev. C *8*, 909 (1973).
31. T. Kopaleishvili, Soviet Journal of Particles and Nuclei Vol. 2, Part 2, 87 (1973).
32. G. Chew and F. Low, Phys. Rev. *101*, 1570 (1956).
33. F. Binon et al., J. Nucl. Phys. B *17*, 168 (1970).
34. M. Blecher et al., Phys. Rev. C *1C*, 2247 (1974).
35. S. Rohlin et al., Nucl. Phys. B *37*, 461 (1972).
36. G. Dugan et al., Phys. Rev. C *8*, 909 (1973).

37. F. Binon et al., Phys. Rev. Lett. 35, 145 (1975).

38. S. Iverson et al., Phys. Rev. Lett. 40, 17 (1978).

39. J.-P. Egger et al., Phys. Rev. Lett. 39, 1608 (1977).

40. S. Dytman et al., Phys. Rev. Lett. 38, 1059 (1977).

41. J. Piffaretti et al., Phys. Lett. B 67, 289 (1977).

42. M. Jakobson et al., Phys. Rev. Lett. 38, (1977).

43. C. Wilkin et al., Nucl. Phys. B 62, 61 (1973).

44. E. Boschitz, Proceedings of the VII International Conference on High-Energy Physics and Nuclear Structure, Zurich, Switzerland (1977).

45. L. Kisslinger, Phys. Rev. 98, 761 (1955).

46. E. Auerbach et al., Phys. Rev. 162, 1683 (1967).

47. E. Auerbach et al., Phys. Rev. Lett. 21, 162 (1968).

48. See, for example, J. Eisenberg, "Introductory Review of Multiple-Scattering Theory for Pion-Nucleus Scattering" in W. Gibbs and B. Gibson ets., Lectures from the LAMPF Summer School on the Theory of Pion-Nucleus Scattering (Los Alamos Scientific Laboratory Report LA-5443-C, 1973).

49. J. Huffner, Physics Reports 21, No. 1, 1 (1975).

50. M. Sternheim and R. Silbar, Ann. Rev. Nucl. Sci. 24, 249 (1974).

51. F. Tabakin, "Pion-Nucleus Elastic Scattering" in P. Barnes et al. eds., AIP Conference Proceedings 33, 38 (1976).

52. W. Gibbs and B. Gibson eds., *Lectures from the LAMPF Summer School on the Theory of Pion-Nucleus Scattering* (Los Alamos Scientific Laboratory Report LA-5443-C 1973).

53. N. Tanner, "Pions and Nuclei" in S. Devons ed., *High Energy Physics and Nuclear Structure*, 346 (Plenum Publishing Co., New York, 1970).

54. C. Wilkin, "Pion-Nucleus Scattering: Theory" in *Proceedings of the International Seminar on Pi Meson-Nucleus Interactions*, Strasbourg, France, September 1971, (V-1-15), Sect. 2,1.

55. G. Brown, *Unified Theory of Nuclear Models and Forces* (American Elsevier, New York, 1971).

56. W. Lock and D. Measday, *Intermediate Energy Nuclear Physics* (Metuen and Co. Ltd., London, 1970).

57. J. Stroot, "Experiments in Pion Nucleus Physics" in W. Gibbs and B. Gibson eds., *Lectures from the LAMPF Summer School on the Theory of Pion-Nucleus Scattering* (Los Alamos Scientific Laboratory Report LA-5443-C, 1974).

58. F. Binon, "Pion-Nucleus Scattering: Experiment" in *Proceedings of the International Seminar on Pi Meson-Nucleus Interactions*, Strasbourg, France, September 1971, (V-1-15), Sect. 2, 25.

59. D. Koltun, Advan. Nucl. Phys. *3*, 71 (1969).

60. H. Thiessen and S. Sobottka, "A Proposal for EPICS: A High-Resolution Pion Beam and Spectrometer Facility for Nuclear Structure Studies," Los Alamos Scientific Laboratory Report (LA-4534-MS, 1970).

61. See, for example, C. Slichter, "Principles of Magnetic Resonance," (Harper & Row, New York, 1963).

62. H. Thiessen et al., "EPICS Pion Channel Performance," Los Alamos Scientific Laboratory Report (LA-6663-MS, 1977).

63. D. Smith et al., Nucl. Instrum. Methods 64, 157 (1968).

64. For a description of scintillators, see J. Kallne et al., "Scintillators and Photomultipliers - Some Tests for EPICS Tune-up," Los Alamos Scientific Laboratory Report (LA-6356-MS, 1976).

65. For a description of the EPICS wire chambers and their function, see C. Morris et al., "Position Sensitive Gas Proportional Chambers," IEEE Transactions on Nuclear Science NS-25, No. 1, 1 (1978).

66. "Standard Nuclear Instrument Modules" TID-20893 (Rev. 4) (United States Department of Energy, Washington, D.C., 1978).

67. "PDP-11 Handbook," 112X01269 AJOFJ150, (Digital Equipment Corporation, Maynard, Mass., 1978.)

68. "CAMAC - A Modular Instrumentation System for Data Handling," Euraton Report (EUR 4100e 1969).

69. S. Schlaer, "An MBD Primer," Los Alamos Scientific Laboratory Report (LA-511-MS, 1974).

70. M. Kellogg et al., "Introduction to Q," Los Alamos Scientific Laboratory Report, (LA-7001-M, 1978).

71. "PDP-11 Fortran Language Reference Manual," DEC-11-LFLRA-B-D, (Digital Equipment Corporation, Maynard, Mass., 1974).

72. M. Kellogg et al., "QAL and the Analyzer Task," Los Alamos Scientific Laboratory Report, (LA-6887-M, 1977).

73. "RSX-11M, MACRO-11 Reference Manual," DEC-11-OMMAA-A-D, (Digital Equipment Corporation, Maynard, Mass., 1974).

74. The results have been presented in a private communication by Don Dodder, Mail Stop 542, Los Alamos Scientific Laboratory, Los Alamos, NM 87545

75. P. Bussey et al., Nucl. Phys. B 58, 363 (1973).

76. H. Thiessen et al., to be published in Phys. Rev. Lett.

77. E. Borie, Phys. Lett. B 68, 433 (1977).

78. M. Sogard, Phys. Rev. D 9, 1486 (1974).

79. See, for example, P. Bevington, "Data Reduction and Error Analysis for the Physical Sciences," (McGraw-Hill, New York, N.Y., 1969).

80. See, for example, E. Mertzbacher, "Quantum Mechanics," Chap. 11 (John Wiley & Sons, Inc., New York, 1970).

81. W. R. Gibbs, "Introduction to Multiple Scattering and the Pion Nucleus Optical Potential," Los Alamos Scientific Laboratory Report (LA-UR-78-1665, 1977).

82. See M. L. Goldberger and K. M. Watson, "Collision Theory," (John Wiley & Sons, Inc., New York, 1964).

83. K. M. Watson, Phys. Rev. 105, 1388 (1957).

84. L. S. Kisslinger, Phys. Rev. 98, 761 (1955).

85. R. A. Eisenstein and G. A. Miller, Computer Physics Communications 8, 130 (1974).

86. R. A. Eisenstein, PIPIT, Computer Physics Communications 12, 237-257 (1976).

87. M. D. Cooper and R. A. Eisenstein, "FITPI" Modifications to the Optical Model Program PIRK for Parameter Searches and Total Cross Sections," Los Alamos Scientific Laboratory Report (LA-5929-MS, 1971).

88. See the discussion of the "angle transform" in the article on double charge-exchange scattering from ^{4}He, W. R. Gibbs et al., Phys. Rev. C15, 1384 (1977).

89. For the mathematical formalism of the pion-nucleon range, see W. R. Gibbs et al., "Pion-Nucleus Multiple Scattering using Separable t-Matrices I. Multiple Scattering Formalism," Los Alamos Scientific Laboratory Report (LA-UR-75-1874, 1974).

90. G. J. Stephenson, Jr., to be published.

91. E. H. Auerbach, D. M. Fleming, and M. M. Sternheim, Phys. Rev. 171, 1781 (1968).

92. A. Bjorck, "Numerical Methods,"Chap. 4 (Prentice Hall, Inc., Englewood Cliffs, New Jersey, 1974).

93. L. Ray, to be published in Phys. Rev. C.

94. K. Crow et al., Phys. Rev. 180, 1349 (1969).

95. J. Beiner, Nucl. Phys. B53, 349 (1973).

96. W. R. Gibbs, B. F. Gibson, and G. J. Stephenson, Jr., Phys. Rev C18, 2782 (1978).

97. R. Herman and R. Hofstadter, High-Energy Electron Scattering Tables, (Stanford University Press, Stanford, CA, 1960), pp. 5-13.

98. Compare, for example, electron scattering from gold at 155 MeV, D. R. Yennie et al., Phys. Rev. 95, 500 (1954).

99. B. Zeidman et al., Phys. Rev. Lett. 40, 1539 (1978).

100. M. D. Cooper and R. A. Eisenstein, Phys. Rev. C13, 1334 (1976).

101. M. Sternheim and E. Auerbach, Phys. Rev. Lett. 25, 1500 (1970).

102. P. Bevington, Data Reduction and Error Analysis for the Physical Sciences, Chap. 10 (McGraw-Hill Inc., New York, 1969).

103. J. S. Blair, "Scattering of Strongly Absorbed Particles," in P. D. Kunz et al., eds., Lectures in Theoretical Physics 8C (University of Colorado Press, Boulder, CO, 1966).

104. H. M. Hofmann, Z. Phys. A 289, 273 (1979).

105. J. M. McKinley, Rev. Mod. Phys. 35, 788 (1963).

106. C. W. de Jager et al., Atomic Data and Nuclear Data Tables 14, 480 (1974).

107. L. Ray et al., Phys. Rev. C18, 2641 (1978).

108. J. A. Jansen et al., Nucl. Phys. A188, 337 (1972).

APPENDIX A

THE ANALYZER PROGRAM

```
      SUBROUTINE PROC06
      THIS IS THE EXPERIMENTAL ANALYZER
C
C
C     MODIFICATIONS FOR NEW ALLCOM  27-OCT-77
C
      COMMON/DWD6/ID6,IDW(620)
      COMMON/ALLCOM/ICOM(4096)
      COMMON/CFVALU/NMAX,IST(20),ITERM(500),CF(200)
      COMMON/DRIFTR/DRF(128)
      DIMENSION RCOM(2048),R(300),INT(150),
      1 RDW(250),RCS(10),C(10),A(10),TA(10),
      2 DRFPO(10),DRFREF(10)
C
      BYTE SST,POL
      LOGICAL TSTNOK
      LOGICAL TRUE,FALSE
C
C     COMMON ICOM STORES PARAMETERS OF A PARTICULAR EXPERIMENT
C     AND VALUES USED BY THE ANALYZER FOR CERTAIN CALCULATIONS.
C
      EQUIVALENCE (RCOM(1),ICOM(1)),(R(1),ICOM(3341)),
      1 (INT(1),ICOM(3941))
C
      EQUIVALENCE (I1,INT(1)),(I2,INT(2)),(I3,INT(3)),
      1 (I4,INT(4)),(I5,INT(5)),(I6,INT(6)),(I7,INT(7)),
      2 (I8,INT(8)),(I9,INT(9)),(I10,INT(10)),(I11,INT(11)),
      3 (I12,INT(12)),(NUMHST,INT(36))
C
      EQUIVALENCE (I14,INT(14)),(I15,INT(15)),(I16,INT(16)),
      1 (I17,INT(17)),(I18,INT(18)),(I19,INT(19)),
      2 (I20,INT(20)),(I21,INT(21)),(I22,INT(22)),
      3 (I23,INT(23)),(I24,INT(24)),(I25,INT(25)),
      4 (I26,INT(26)),(I27,INT(27)),(I28,INT(28)),
      5 (I29,INT(29)),(I30,INT(30)),(I31,INT(31))
C
      EQUIVALENCE (I32,INT(32)),(I33,INT(33)),(I34,INT(34))
C
      EQUIVALENCE (I35,INT(35)),(I36,INT(36)),(I37,INT(37)),
      1 (I38,INT(38)),(I39,INT(39)),(I40,INT(40)),
      2 (I41,INT(41)),(I42,INT(42)),(I43,INT(43)),
      3 (I44,INT(44)),(I45,INT(45)),(I46,INT(46)),
      4 (I47,INT(47)),(I48,INT(48)),(I49,INT(49)),
      5 (I50,INT(50)),(I51,INT(51)),(I52,INT(52))
C
      EQUIVALENCE (I53,INT(53)),(I54,INT(54)),(I55,INT(55)),
      1 (I56,INT(56)),(I57,INT(57)),(I58,INT(58)),
      2 (I59,INT(59)),(I60,INT(60)),(I61,INT(61)),
      3 (I62,INT(62)),(I63,INT(63)),(I64,INT(64)),
```

```
       (I65,INT(65)),(I66,INT(66)),(I67,INT(67)),
     5 (I68,INT(68)),(I69,INT(69)),(I70,INT(70))
C
      EQUIVALENCE (I71,INT(71)),(I72,INT(72)),(I73,INT(73)),
     1 (I74,INT(74)),(I75,INT(75)),(I76,INT(76)),
     2 (I77,INT(77)),(I78,INT(78)),(I79,INT(79)),
     3 (I80,INT(80)),(I81,INT(81)),(I82,INT(82)),
     4 (I83,INT(83)),(I84,INT(84)),(I85,INT(85)),
     5 (I86,INT(86)),(I87,INT(87)),(I88,INT(88))
C
      EQUIVALENCE (I89,INT(89)),(I90,INT(90)),(I91,INT(91)),
     1 (I92,INT(92)),(I93,INT(93)),(I94,INT(94)),
     2 (I95,INT(95)),(I96,INT(96)),(I97,INT(97)),
     3 (I98,INT(98)),(I99,INT(99)),(I100,INT(100)),
     4 (I101,INT(101)),(I102,INT(102)),(I103,INT(103)),
     5 (I104,INT(104)),(I105,INT(105)),(I106,INT(106))
C
      EQUIVALENCE (I107,INT(107)),(I108,INT(108)),(I109,INT(109)),
     1 (I110,INT(110)),(I111,INT(111)),
     2 (I114,INT(114)),(I115,INT(115)),
     3 (I120,INT(120)),(I121,INT(121)),(I122,INT(122)),
     4 (I123,INT(123)),(I124,INT(124)),(I125,INT(125)),
     5 (I126,INT(126)),(I128,INT(128))

      EQUIVALENCE (R1,R(1)),(R2,R(2)),(R3,R(3)),(R4,R(4)),
     1 (R5,R(5)),(R6,R(6)),(R7,R(7)),(R8,R(8)),(R9,R(9)),
     2 (R10,R(10)),(R11,R(11)),(R12,R(12)),(R13,R(13)),
     3 (R14,R(14)),(R15,R(15)),(R16,R(16)),(R17,R(17)),
     4 (R18,R(18)),(R19,R(19)),(R20,R(20)),(R21,R(21))
C
C     EQUIVALENCE (R22,R(22)),(R23,R(23)),(R24,R(24)),(R25,R(25))
C
C     EQUIVALENCE (R55,R(55)),(R56,R(56)),(R57,R(57)),
C    1 (R58,R(58)),(R59,R(59)),(R60,R(60)),(R61,R(61))
C
      EQUIVALENCE (R62,R(62)),(R63,R(63)),(R64,R(64)),
     1 (R65,R(65)),(R66,R(66)),(R67,R(67)),(R68,R(68)),
     2 (R69,R(69)),(R70,R(70)),(R71,R(71)),(R72,R(72)),
     3 (R73,R(73)),(R74,R(74)),(R75,R(75)),(R76,R(76)),
     4 (R77,R(77)),(R78,R(78)),(R79,R(79)),(R80,R(80)),
     5 (R81,R(81)),(R82,R(82)),(R83,R(83)),(R84,R(84))
C
      EQUIVALENCE (R85,R(85)),(R86,R(86)),(R87,R(87)),
     1 (R88,R(88)),(R89,R(89)),(R90,R(90)),(R91,R(91)),
     2 (R92,R(92)),(R93,R(93)),(R94,R(94)),(R95,R(95)),
     3 (R96,R(96)),(R97,R(97)),(R98,R(98)),(R99,R(99)),
     4 (R100,R(100))
C
      DIMENSION DISPA(10),RA0(10),RA1(10),RA2(10),RA3(10)
      DIMENSION RC0(10),RC1(10),RC2(10),RC3(10),DISPC(10)
      DIMENSION TA0(10),TA1(10),TA2(10),RCSOFF(10)
C
      EQUIVALENCE (RC0,R(101)),(RC1,R(111)),
     1            (RC2,R(121)),(RC3,R(141)),
     2            (DISPC,R(151))
C
      EQUIVALENCE (RA0,R(161)),(RA1,R(171)),
     1            (RA2,R(181)),(RA3,R(191)),
     2            (DISPA,R(201))
C
      EQUIVALENCE (TA0,R(211)),(TA1,R(221)),
     1            (TA2,R(231)),(RCSOFF,R(241))
C
```

```
      EQUIVALENCE (THETGT,R(45)),(CTHDIF,R(46)),(STHDIF,R(47)),
     1 (TGTXD,R(62)),(TGTX,R(63))
C
      EQUIVALENCE(R251,R(251)),(R252,R(252)),(R253,R(253)),
     1 (R254,R(254)),(R255,R(255)),(R256,R(256)),(R257,R(257)),
     2 (R258,R(258)),(R259,R(259)),(R260,R(260)),
     3 (R261,R(261)),(R262,R(262))
C
      EQUIVALENCE (R270,R(270)),(R271,R(271)),(R272,R(272)),
     1 (R273,R(273)),(R274,R(274)),(R275,R(275)),(R276,R(276)),
     2 (R277,R(277)),(R278,R(278)),(R279,R(279)),(R280,R(280)),
     3 (R281,R(281)),(R282,R(282)),(R283,R(283)),(R284,R(284)),
     3 (R285,R(285)),(R286,R(286)),(R287,R(287)),
     5 (R288,R(288)),(R289,R(289)),(R290,R(290)),(R291,R(291)),
     6 (R292,R(292)),(R293,R(293)),(R294,R(294)),(R295,R(295))
C
      EQUIVALENCE (R296,R(296)),(R297,R(297)),(R298,R(298)),
     1              (R299,R(299)),(R300,R(300))
C
C
C     IDW IS THE COMMON WHICH STORES DATA WORDS, BOTH RAW DATA
C     AND CALCULATED DATA.
C
      EQUIVALENCE (IHDR6,IDW(1)),(IDCRW,IDW(2)),(IDCRG,IDW(3)),
     1 (IS1AA,IDW(4)),(IS2PA,IDW(5)),(IS2NA,IDW(6)),(IS3PA,IDW(7)),
     2 (IS3NA,IDW(8)),(IV4PA,IDW(9)),(IV4NA,IDW(10)),(IJ1PA,IDW(11)),
     3 (IJ1NA,IDW(12)),(IC1PA,IDW(13)),(IC1NA,IDW(14)),(SPR15,IDW(15))
C
      EQUIVALENCE (IS1TT,IDW(16)),(IS2PT,IDW(17)),(IS2NT,IDW(18)),
     1 (IS3PT,IDW(19)),(IS3NT,IDW(20)),(IJ1PT,IDW(21)),(IJ1NT,IDW(22)),
     2 (IV4PT,IDW(23)),(IV4NT,IDW(24)),(IC1PT,IDW(25)),
     3 (IC1NT,IDW(26)),(ITRF1,IDW(27)),(ITRF2,IDW(28)),
     4 (ISP29,IDW(29)),(ISP30,IDW(30))
C
      EQUIVALENCE (ICP,IDW(31)),(ICN,IDW(41))
      EQUIVALENCE (IAP,IDW(51)),(IAN,IDW(61))
C
      EQUIVALENCE (ISP71,IDW(71)),(ISP72,IDW(72)),
     1              (ISP73,IDW(73)),(ISP74,IDW(74)),
     2              (ISP75,IDW(75)),(ISP76,IDW(76)),
     3              (ISP77,IDW(77)),(ISP78,IDW(78)),
     4              (ISP79,IDW(79)),(ISP80,IDW(80))
      EQUIVALENCE (ISP81,IDW(81)),(ISP82,IDW(82)),
     1              (ISP83,IDW(83)),(ISP84,IDW(84)),
     2              (ISP85,IDW(85)),(ISP86,IDW(86)),
     3              (ISP87,IDW(87)),(ISP88,IDW(88)),
     4              (ISP89,IDW(89)),(ISP90,IDW(90)),
     5              (ISP91,IDW(91)),(ISP92,IDW(92)),
     6              (ISP93,IDW(93)),(ISP94,IDW(94))
C
      EQUIVALENCE (ISP95,IDW(95)),(ISP96,IDW(96)),
     1              (ISP97,IDW(97)),(ISP98,IDW(98)),
     2              (ISP99,IDW(99)),(ISP100,IDW(100))
C-----------------------------------------------------
C     RDW ARRAY:
C          THE EQUIVALENCE IS MADE SUCH THAT THE
C     FLOATING TO INTEGER CONVERSIONS WILL PLACE
C     RDW(I) INTO IDW(I).
C
C
      EQUIVALENCE (IDW(101),RDW(1))
C
```

```
      EQUIVALENCE (RCS(1),RDW(101)),(C(1),RDW(111)),(A(1),RDW(121)),
     1  (TA(1),RDW(131)),(DRFPO(1),RDW(141))
C
      EQUIVALENCE (RCPT1,TA(1)),(RCPT2,TA(2)),(RCPT3,TA(3)),
     1            (RCPT4,TA(4)),(RCPT5,TA(5)),(RCPT6,TA(6)),
     2            (RCPT7,TA(7)),(RCPT8,TA(8)),(RCPT9,TA(9)),
     3            (RCP10,TA(10))
C
      EQUIVALENCE (XFRON,RDW(151)),(THFRO,RDW(152)),(YFRON,RDW(153)),
     1 (PHIFR,RDW(154)),(XREAR,RDW(155)),(THRER,RDW(156)),
     2 (YREAR,RDW(157)),(PHIRE,RDW(158)),(SPR159,RDW(159)),
     3 (SPR160,RDW(160))
C
      EQUIVALENCE (DUMM1,RDW(161)),(DELTA,RDW(162)),(DUMM2,RDW(163)),
     1 (XCTGT,RDW(164)),(THTGT,RDW(165)),(YCTGT,RDW(166)),
     2 (PHITG,RDW(167)),(THCHK,RDW(168)),(PHCHK,RDW(169)),
     3 (PATHL,RDW(170))
C
      DIMENSION DIST1(4),DIST2(4),DIST3(4),DIST4(4)
C
      EQUIVALENCE (DIST1(1),RDW(171)),(DIST2(1),RDW(175)),
     1 (DIST3(1),RDW(179)),(DIST4(1),RDW(183)),(SPR187,RDW(187))
C
      EQUIVALENCE (S1DELE,RDW(188)),(S2DELE,RDW(189)),
     1 (S3DELE,RDW(190))
C
      EQUIVALENCE (DE523,RDW(191)),(PBEAM,RDW(192)),(EBEAM,RDW(193)),
     1 (PSPCT,RDW(194)),(ESPCT,RDW(195)),(QVALU,RDW(196)),
     2 (THSPC,RDW(197)),(DLOSS,RDW(198)),(FUN,RDW(199)),
     3 (QOFPD,RDW(200)),(POFPD,RDW(201))
C
      EQUIVALENCE (TS1R,RDW(202)),(DTOF,RDW(203)),(XDEF,RDW(204)),
     1 (XS1,RDW(205)),
     2            (XROTG,RDW(206)),(YROTG,RDW(207))
C
      EQUIVALENCE (RCP5C,RDW(231)),(RCP6C,RDW(232)),(RCP7C,RDW(233)),
     1            (RCP8C,RDW(234)),(RCP9C,RDW(235)),(RC10C,RDW(236)),
     2            (RCP56,RDW(237)),(RCP78,RDW(238)),(RC910,RDW(239))
C
      EQUIVALENCE (DRFREF(1),RDW(241))
C
      EQUIVALENCE (XQAD,RDW(226)),(THTQAD,RDW(227)),
     1            (YQAD,RDW(228)),(PHIQAD,RDW(229))
C
C
C ------------------------------------------------------------------
C
      EQUIVALENCE (ITMS2,IDW(251)),(ITMS3,IDW(252)),(ITREF,IDW(253)),
     1            (ITS1R,IDW(254)),(ITV4P,IDW(255)),(ITV4N,IDW(256)),
     2            (ITMC1,IDW(257)),(ITJ1P,IDW(258)),(ITJ1N,IDW(259)),
     3            (ISP60,IDW(260))
C
      EQUIVALENCE (IBOX,IDW(261)),(IELP,IDW(262)),(IGAT,IDW(263))
C
      EQUIVALENCE (ISP264,IDW(264)),
     1            (ISP265,IDW(265)),(ISP266,IDW(266)),
     2            (ISP267,IDW(267)),(ISP268,IDW(268)),
     3            (ISP269,IDW(269)),(ISP270,IDW(270)),
     4            (ISP271,IDW(271)),(ISP272,IDW(272))
C
      EQUIVALENCE (ISP273,IDW(273)),(ISP274,IDW(274)),
```

```
     1          (ISP275,IDW(275)),(ISP276,IDW(276)),
     2          (ISP277,IDW(277)),(ISP278,IDW(278)),
     3          (ISP279,IDW(279)),(ISP280,IDW(280))
C
C
      DIMENSION IDRFTM(10)
      EQUIVALENCE (IDRFTM(1),IDW(281))
C
C
C
C     EXIT IMMEDIATLY
C
      IF (I123 .EQ. -12345) RETURN
C
C     TRIGGER EVENT 18 DURING REPLAY
C
      IF (I114 .EQ. -12345) CALL PROC18
      I114=0
C
C     PRINT VALUES OF COMMON BLOCK IF I115=-12345
C
      IF (I115 .NE. -12345) GO TO 66
      I115=0
      CALL ASSIGN (5,'LP0:',4)
      WRITE (5,1000) NMAX,IST,ITERM
      WRITE (5,1050) CF
      WRITE (5,1050) DRF
 1000 FORMAT (1X,10I7)
 1050 FORMAT (1X,10E12.3)
      CALL CLOSE(5)
   66 CONTINUE
C
C     CLEAR ALL CALCULATED QUANTITIES
C
      CALL VALSET(IDW(101),520,0)
C
C     COUNTER DATA
C
      ITMS2 = IS2PT + IS2NT
      ITMS3 = IS3PT + IS3NT
      ITREF = (ITMS2 + ITMS3)/2 + I101
      ITS1R = 2*IS1TT - ITREF + I102
      TS1R = FLOAT(ITS1R)*.01
      ITV4P = 2*IV4PT - ITREF + I103
      ITV4N = 2*IV4NT - ITREF + I104
      ITMC1 = IC1PT + IC1NT - ITREF + I105
      ITJ1P = 2*IJ1PT - ITREF + I106
      ITJ1N = 2*IJ1NT - ITREF + I107
C
      S1DELE=FLOAT(IS1AA)/100.
      S2DELE = FLOAT(IS2PA)*FLOAT(IS2NA)
      S3DELE = FLOAT(IS3PA)*FLOAT(IS3NA)
      DES23 = S2DELE*S3DELE
      DES23 = DES23**.25
      DES23=DES23/100.
      S2DELE = SQRT(S2DELE)/100.
      S3DELE = SQRT(S3DELE)/100.
```

```
      CALL INTGRZ (RDW(188),IDW(188),4)
C
C     SKIP REST OF CALCULATIONS IF PROTON.
      THE TEST SUBROUTINE IS USED TO ELIMINATE PROTONS BY SETTING LIMITS
      ON THE ENERGY LOSS IN THE SCINTILLATORS.
C
C
      CALL ALLTST(1)
      IF (TSTNOK(4) .AND. I128.NE.-12345) GO TO 650
C
      DRFREF(5)=ITREF*R245
      DRFREF(6)=ITREF*R246
      DRFREF(9)=ITREF*R247
      DRFREF(10)=ITREF*R248
C
C     IF INT(120) = -12345 TURN OFF CHMBRS
C
      IF(I120.NE.-12345) CALL CHMBRS
      CALL INTGRZ (RDW(101),IDW(101),10)
C
      IF (I124.NE.-12345) CALL ALLTST(2)
C
C     FOR EXAMPLE, R254, EQUIVALENT TO ICOM(3848),IS THE Z
C     POSITION OF CHAMBER 2.
C
      X24=R254-R252
      X14=R254-R251
      X13=R253-R251
      IF(ABS(X13).LE.10.) X13=10.
      IF(ABS(X24).LE.10.) X24=10.
      IF(ABS(X14).LE.10.) X14=10.
      THFRO = 1000.*(C(4)-C(2))/X24
      PHIFR = 1000.*(C(3)-C(1))/X13
      IF(ABS(THFRO).GT.250.) THFRO=250.
      IF(ABS(PHIFR).GT.100.) PHIFR=100.
      XFRON = C(4)
C     C(4) IS THE X POSITION, GIVEN BY CATHODE DELAY CIRCUITRY,
C     IN CHAMBER 4.
C
      YFRON = C(3)+PHIFR*(R254-R253)*.001
      X=(R259+R260-R255-R256)*.5
      IF(ABS(X).LT.1.)X=1.
C
      IF (I125.NE.-12345) CALL XDRFT
C
      YY1 = (C(5) + C(6))*.5
      YY2 =C(10)
      XX1=RCP56
      XX2=RCP10
      THRER = 1000.*(XX2-XX1)/X
      PHIRE = 1000.*(YY2-YY1)/X
      XREAR = XX1
      YREAR = YY1
      IF(ABS(THRER).GT.500.)THRER=500.
      IF(ABS(PHIRE).GT.100.)PHIRE=100.
C
C     DETERMINE THOSE VALUES WHICH DEPEND ON FITTED COEF-
C     FICIENTS OF LINEAR EQUATIONS.
C
C     CALCULATE POLYNOMIALS
C
```

```
C         IF INT(121) = -12345 TURN OFF POLYNOMIALS
C
          IF (INT(121) .NE. -12345) CALL MULTIS
          DTOF=TS1R-PATHL
          DELTA=DELTA-TGTXD
          PHITG=PHITG + R261
C
C
C
          ZP=1.-(THTGT*THTGT + PHTGT*PHTGT)*.5E-6
          ZROT = -YTGT*STHDIF/(ZP*CTHDIF + PHTGT*STHDIF*1.E-3)
          XROTG = XCTGT + THTGT*ZROT*1.E-3
          YROTG = YCTGT + PHTGT*ZROT*1.E-3
C
C         SIMPLE DELTA LOSS CALCULATION
C
          DLOSS = XROTG/10. - DELTA
C
          IF(I110.LE.0) I110 = 161
          IF(I111.LE.0) I111 = 164
C
C         CALKIN PERFORMS RELATIVISTIC KINEMATIC CALCULATIONS.
C
C         IF I125 = -12345 TURN OFF CALKIN
C
          IF (I125.NE.-12345) CALL CALKIN (I110,I111)
C
C         CALCULATE FUN TERMS
C
          IF (I126 .NE. -12345) CALL FUNNY
C
C         CHANGE UNITS OF ANGLES BEFORE CONVERSION TO INTEGERS
C                 AFTER CHANGE, 1CHANNEL=0.1MILLIRADIAN
C
          THFRO=THFRO*0.1
          PHIFR=PHIFR*0.1
          THRER=THRER*0.1
          PHIRE=PHIRE*0.1
          THTGT=THTGT*0.1
          PHITG=PHITG*0.1
          THCHK=THCHK*0.1
          PHCHK=PHCHK*0.1
          THSPC=THSPC*0.1
C
C         CONVERT REALS TO INTEGERS
C
C         IF INT(122) = -12345 TURN OFF FLOAT TO INTEGER CONVERSION
C
          IF (INT(122).NE.-12345) CALL INTGRZ(RDW(101),IDW(101),150)
C
C         COMMENT OUT INDIRECT GATES,BOXES,ELLIPSES
C
```

Appendix B. Elastic pion-carbon cross sections at 162 MeV were used to normalize pion scattering from beryllium, silicon, nickel, and lead.

Listed below is the differential cross section for elastic pion scattering on ^{12}C. This cross section provided the normalization for those scattering yields measured during this experiment.

π^+

ϕ_S	$d\sigma/d\Omega$	Δ_T $(d\sigma/d\Omega)$
10.50	467.1	39.71
12.50	406.1	34.97
14.50	365.1	29.79
16.50	329.2	27.63
17.50	292.2	23.04
19.50	256.4	19.59
21.50	214.1	16.89
24.20	157.9	10.08
26.60	125.2	8.462
29.00	93.36	6.417
30.20	70.05	4.537
32.60	55.88	3.651
36.20	33.61	2.334
37.40	24.77	1.644
38.60	19.54	1.303
39.80	15.21	1.0557
41.00	10.96	0.7692
43.40	5.425	0.3816
45.80	2.302	0.1769
48.20	0.7566	0.07024
50.56	0.1956	0.02745
53.00	0.1689	0.02360
54.20	0.2832	0.02811
56.60	0.5601	0.04950
59.99	0.8773	0.06707
61.40	1.171	0.08437
63.80	1.264	0.08937
66.17	1.330	0.09238
67.40	1.355	0.1156
68.60	1.277	0.08915

Appendix B continued

π^+

ϕ_S	$d\sigma/d\Omega$	Δ_T $(d\sigma/d\Omega)$
71.00	1.160	0.08026
73.40	1.05235	0.07291
75.80	0.7959	0.05730
78.20	0.5825	0.04352
80.60	0.3561	0.02867
83.00	0.2278	0.01995
85.40	0.1358	0.01348
87.77	0.06642	0.009250
90.20	0.04632	0.006960
92.60	0.03727	0.006300
95.00	0.04541	0.006780
97.40	0.08100	0.01237
99.80	0.09190	0.01311
102.20	0.1552	0.02058
104.60	0.1656	0.01662
107.00	0.2335	0.02097
109.40	0.2238	0.02065
111.80	0.2159	0.02013
114.20	0.2298	0.02118
116.60	0.2230	0.02006
119.00	0.2040	0.01834
120.20	0.2137	0.01854

Appendix B continued

π^-

ϕ_S	$d\sigma/d\Omega$	Δ_T $(d\sigma/d\Omega)$
12.50	445.1	105.5
14.50	413.6	97.93
16.50	334.1	81.33
18.50	298.4	70.47
20.50	236.5	55.88
23.00	191.3	12.90
25.40	146.7	9.904
27.80	113.4	7.653
30.20	79.22	5.361
32.60	56.96	3.856
35.00	37.83	2.591
37.40	23.28	1.650
39.80	13.92	0.9961
41.00	9.897	0.6720
43.40	4.679	0.3760
45.80	2.388	0.2121
48.20	0.7916	0.08732
50.60	0.2693	0.04250
53.00	0.3123	0.04274
55.40	0.6183	0.06282
57.40	0.8574	0.07667
60.20	1.09468	0.08807
62.60	1.2779	0.1016
65.00	1.4140	0.1065
66.20	1.5165	0.1215
68.60	1.4129	0.1131
71.00	1.1290	0.09192
73.40	1.04195	0.08509
75.80	0.7538	0.06801
78.30	0.4756	0.05955
80.60	0.3371	0.04360
83.00	0.1865	0.02378
85.50	0.1530	0.02672
89.50	0.05959	0.01267
93.50	0.04310	0.01448
99.50	0.08171	0.01990
105.50	0.1680	0.02863
111.45	0.2168	0.03532
117.40	0.2024	0.03928
118.40	0.1490	0.02818

Appendix C. Listed on the following pages are the positive and negative c.m. cross sections for this experiment. The first compilation shows the unmodified data in the order c.m. cross section, cross section error, and c.m. angle. The next compilation lists the data modified for angular resolution and contaminant electromagnetic scattering.

```
    21624121..21.120424
153.60001    7.09200   30.20000
130.30000    5.79200   31.40000
107.99000    4.46800   32.50000
 77.69000    3.64500   33.90000
 49.54000    2.41000   35.00000
 24.56000    1.43400   36.30000
 15.33000    0.77580   37.50000
  8.13200    0.65450   38.70000
  5.46300    0.32240   39.90000
  6.59690    0.36440   41.10000
  5.22700    0.34580   39.90000
  6.46100    0.42540   41.10000
  9.56300    0.51570   42.30000
 13.21000    0.56400   43.50000
 15.76000    0.92180   44.70000
 19.44000    1.93500   45.90000
 15.90000    1.24400   44.70000
 19.44000    1.33900   45.90000
 19.35000    0.90130   47.10000
 18.42000    0.85290   48.30000
 17.50000    0.92200   49.50000
 14.39000    0.77030   50.70000
 10.70000    0.54180   52.30000
  7.65700    0.40560   53.50000
  5.34100    0.33640   54.30000
  2.54200    0.20210   55.50000
  1.29300    0.11470   55.70000
  0.66350    0.07564   57.90000
  0.50610    0.07533   59.10000
  0.91100    0.09515   60.30000
  1.59200    0.13510   61.50000
  1.31600    0.14430   62.70000
  2.16900    0.21840   63.90000
  2.48200    0.23440   65.10000
  0.00000    0.00000   66.30000
  0.00000    0.00000   67.50000
  2.71900    0.22180   66.30000
  2.27400    0.18330   67.50000
  3.03300    0.19550   66.30000
  2.74800    0.17990   67.50000
  2.21000    0.16360   68.70000
  1.34400    0.14200   69.90000
  1.40400    0.11030   71.10000
  0.99310    0.09733   72.30000
  0.51270    0.10390   73.50000
  0.23780    0.07197   74.70000
  0.52420    0.09591   73.50000
  0.27500    0.05510   74.70000
  0.14100    0.02875   75.90000
  0.04347    0.01871   77.10000
  0.03541    0.01424   78.30000
  0.12470    0.02544   79.50000
  0.23680    0.03764   80.70000
```

```
    0.29320    0.03904   91.90000
    0.40635    0.04354   43.10000
    0.35570    0.03431   44.30000
    0.42480    0.04324   45.50000
    0.34140    0.03425   45.70000
    0.31430    0.04304   47.90000
    0.29460    0.03910   49.10000
    0.14210    0.03204   90.30000
    0.12490    0.02914   91.50000
    0.04839    0.01545   92.70000
    0.05705    0.02155   93.90000
    0.01715    0.01145   95.10000
    0.01005    0.00504   95.30000
    0.02197    0.00590   97.50000
    0.04955    0.01544   98.70000
    0.04932    0.02373   99.90000
    0.13000    0.03151  101.10000
    0.04793    0.02540  104.70000
    0.22730    0.03440  105.90000
    0.13310    0.03043  102.30000
    0.15910    0.03261  103.50000
    0.17240    0.03425  107.10000
    0.20280    0.03039  108.30000
    0.15300    0.03395  109.50000
    0.17840    0.03554  110.70000
  155.39999    3.56400   30.20000
  130.30000    7.90200   31.40000
  149.50000   10.36000   27.80000
  191.20000   10.22000   29.00000
  161.50001    8.56400   25.40000
  173.10001    8.94200   25.60000
   95.52000    5.56100   23.00000
  125.10000    5.55700   24.20000
  155.50001   23.94000   20.60000
  115.30000   17.72000   21.30000
     29823(21-,21-)20823
  111.90000    5.46300   30.20000
   71.44000    4.75800   31.40000
  237.70000   12.90000   27.80000
  183.50001   10.31000   29.00000
  307.39999   15.75000   25.40000
  278.50001   15.11000   25.60000
  240.10001   15.00000   23.00000
  310.39999   15.34000   24.20000
  139.70000    7.79000   20.60000
  195.39999    9.57000   21.80000
  210.10001   12.53000   18.20000
  125.90000    8.49500   19.40000
  393.59998   53.46000   15.80000
  421.20001   27.75000   17.00000
   31.37000    2.31300   32.60000
   10.34000    1.10400   33.90000
    3.26400    0.42840   35.00000
    5.20500    0.62500   35.30000
   15.49000    1.46500   37.50000
   25.50000    1.48200   38.70000
```

```
 41.91000    2.47400   41.10000
 35.11000    2.50500   42.30000
 28.34000    1.91500   44.70000
 21.29000    1.43700   45.90000
  7.55600    0.57220   48.30000
  3.17000    0.17410   49.50000
  1.32200    0.24140   50.70000
  0.71580    0.17080   51.90000
  1.77000    0.37550   53.10000
  2.30200    0.49530   54.30000
  5.43400    0.70430   55.50000
  5.43600    0.63510   55.70000
  5.27600    0.54180   59.10000
  5.31500    0.49050   60.30000
  4.75100    0.47290   62.70000
  2.53200    0.30750   63.90000
  1.05500    0.16390   65.30000
  0.30510    0.09463   67.50000
  0.12150    0.06095   68.70000
  0.15910    0.08138   69.90000
  0.47410    0.10140   72.30000
  0.74350    0.11030   73.50000
  1.14300    0.15590   75.90000
  1.22100    0.15810   77.10000
  0.30730    0.11590   79.50000
  0.52680    0.09030   80.70000
  0.24350    0.05013   83.10000
  0.06437    0.02515   84.30000
  0.03824    0.01913   85.70000
  0.05432    0.12553   87.90000
  0.05545    0.03703   90.30000
  0.13100    0.04940   91.50000
  0.17800    0.04507   93.30000
  0.14700    0.04224   94.50000
  0.15250    0.03751   95.70000
  0.03500    0.02537   96.90000
   5341(21..21+)534NI
  4.36700    0.32470   30.40000
  3.07200    0.23190   31.60000
  5.54400    0.34030   32.80000
  8.51300    0.45320   34.00000
 14.44000    0.71910   35.20000
 17.74000    0.83160   36.40000
 22.55000    1.06500   37.60000
 23.74000    1.08900   38.80000
 25.21000    1.16900   40.00000
 25.89000    1.17500   41.20000
 23.79000    1.10300   42.40000
 23.18000    1.05500   43.60000
 21.70000    0.99450   44.80000
 18.79000    0.83520   46.00000
 15.37000    0.72880   47.20000
 11.59000    0.55230   48.40000
  8.95100    0.42240   49.60000
  6.59100    0.32400   50.80000
  5.37500    0.29090   52.10000
```

```
  3.07100    0.17900   53.30000
  1.30700    0.16270   54.50000
  0.35520    0.12500   56.70000
  0.34200    0.05130   56.90000
  0.07571    0.03259   58.10000
  0.05900    0.01644   59.30000
  0.17080    0.02568   60.50000
  0.51790    0.05584   61.70000
  0.51160    0.07422   62.90000
  0.94600    0.06432   64.10000
  1.11300    0.07269   65.30000
  1.52700    0.14180   66.50000
  1.50900    0.12580   67.70000
  1.79200    0.13970   68.90000
  1.55200    0.12360   70.10000
  1.54500    0.10470   71.30000
  1.40400    0.09253   72.50000
  0.82030    0.07303   76.10000
  0.62760    0.06149   77.30000
  0.46970    0.05294   78.50000
  0.33620    0.04157   79.70000
  0.19840    0.02575   80.90000
  0.12110    0.01767   82.10000
  0.05680    0.01541   83.30000
  0.01052    0.01051   84.50000
  0.00000    0.00000   85.70000
  0.02044    0.00790   86.90000
  0.03004    0.01162   88.10000
  0.05597    0.01024   89.30000
  0.06922    0.01727   90.50000
  0.11960    0.02015   91.70000
  0.14740    0.02934   92.90000
  0.13180    0.02545   94.10000
  0.14630    0.02545   95.30000
  0.21200    0.02793   96.50000
  0.19390    0.02217   97.70000
  0.14450    0.01945   98.90000
  0.14580    0.02574  100.10000
  0.12720    0.02043  101.30000
  0.04489    0.01734  102.50000
  0.12150    0.01744  103.70000
  0.09836    0.01527  104.90000
  0.09169    0.01745  106.10000
  0.05242    0.01275  107.30000
  0.04006    0.00924  108.50000
  3.91600    0.30530   30.40000
  3.04600    0.26210   31.60000
 23.12000    1.40900   27.90000
  9.46100    0.78170   29.20000
 77.31000    4.23000   25.50000
 46.57000    2.77800   26.70000
175.59001    9.49700   23.10000
125.39000    7.13500   24.30000
429.20001   43.40000   20.70000
310.10001   35.27000   21.90000
```

```
     5341(21-+21-)5841
  3.11400     0.43780    30.40000
  5.44100     0.50290    31.60000
 10.38600     1.01500    27.90000
  4.94200     0.51480    29.20000
 54.45000     1.16190    25.50000
 25.49000     1.49400    25.70000
155.10001     7.46200    23.10000
 94.04000     5.37100    24.30000
365.39999    17.27000    20.70000
230.20000    12.16000    21.90000
575.20001    35.85000    18.30000
502.39999    27.59000    19.50000
1391.00000   57.84000    15.90000
442.59998    45.14000    17.10000
 12.55000     1.03400    32.80000
 15.93000     1.16300    34.00000
 27.96000     1.77000    35.20000
 25.72000     1.58500    36.40000
 32.56000     2.02500    37.60000
 35.52000     2.12200    38.80000
 31.86000     1.94700    41.20000
 27.31000     1.71400    42.40000
 21.70000     1.30400    44.80000
 17.24000     1.07400    45.00000
  9.23100     0.62100    49.40000
  5.73600     0.44090    47.50000
  4.36400     0.40520    50.80000
  2.59800     0.27380    52.10000
  1.43000     0.13500    53.30000
  0.56200     0.09433    54.50000
  0.14950     0.04121    55.70000
  0.11999     0.03524    56.90000
  0.75600     0.09784    59.30000
  1.16800     0.12200    60.50000
  1.72400     0.17070    62.90000
  2.26200     0.19360    64.10000
  2.03300     0.24720    66.50000
  2.16600     0.24090    67.70000
  2.01600     0.17040    69.90000
  1.79400     0.15850    70.10000
  1.34300     0.14820    72.50000
  0.96870     0.11570    73.70000
  0.51290     0.05645    75.10000
  0.31100     0.04219    77.30000
  0.20940     0.31770    79.00000
  0.39350     0.22520    80.00000
  0.04481     0.01301    83.30000
  0.02740     0.01180    84.50000
  0.09750     0.01935    85.90000
  0.14960     0.02402    88.10000
  0.17630     0.02955    90.50000
  0.19930     0.02513    91.70000
  0.14380     0.03319    93.50000
  0.14800     0.02307    94.70000
     2351(21++21+)2851
 45.87000     2.21700    30.50000
```

```
31.40000     1.48300   31.70000
21.36000     1.03400   33.00000
11.50000     0.59050   34.20000
 7.30000     0.37520   35.40000
 3.43500     0.19340   35.60000
 1.46390     0.10380   37.80000
 0.45800     0.04764   39.00000
 0.54630     0.05441   40.20000
 1.15300     0.07558   41.40000
 2.56500     0.14240   42.50000
 3.49100     0.18030   43.80000
 4.55500     0.23710   45.10000
 5.46300     0.26310   45.30000
 6.35600     0.30570   47.50000
 6.96300     0.32440   48.70000
 7.46800     0.36200   49.90000
 7.41900     0.35080   51.10000
 7.75800     0.39150   52.30000
 6.71900     0.33360   53.50000
 6.72000     0.38560   54.70000
 5.74000     0.32760   55.90000
 3.97200     0.19310   59.60000
 3.36100     0.17070   60.80000
 2.79500     0.14460   62.00000
 2.18300     0.11470   63.20000
 1.79500     0.11120   64.40000
 1.30800     0.08943   65.60000
 0.89250     0.05250   66.80000
 0.59250     0.04173   68.00000
 0.44890     0.03841   69.20000
 0.23300     0.02707   70.40000
 0.14430     0.01919   71.60000
 0.06275     0.01245   72.80000
 0.03633     0.00741   74.00000
 0.04975     0.00954   75.20000
 0.06939     0.00350   76.40000
 0.11800     0.00993   77.60000
 0.13510     0.02005   78.80000
 0.21180     0.02502   80.10000
 0.25010     0.02249   81.30000
 0.26170     0.02260   82.50000
 0.26520     0.03041   83.70000
 0.29140     0.02987   84.90000
 0.26440     0.03068   86.10000
 0.27130     0.02575   87.30000
 0.30870     0.02370   88.50000
 0.27650     0.02524   89.70000
 0.14530     0.02205   90.90000
 0.18010     0.02508   92.10000
 0.16540     0.02092   93.30000
 0.12880     0.01757   94.50000
 0.10820     0.01344   95.70000
 0.06639     0.01109   96.90000
 0.02724     0.00915  100.50000
 0.03260     0.00775  101.70000
 0.07446     0.01395   99.10000
```

```
    0.05150    0.00475   99.30000
    0.03113    0.00467  102.80000
    0.03603    0.00567  104.00000
    0.03926    0.00519  105.20000
    0.03303    0.00524  105.40000
    0.03976    0.00570  107.60000
    0.02615    0.00504  108.80000
   47.29000    2.25500   30.50000
   26.71000    1.37300   31.70000
   44.55000    4.55500   28.10000
   54.30000    3.35200   27.30000
  145.37999    7.52300   25.70000
  111.20000    5.48500   25.90000
  225.29000   11.59300   23.30000
  149.49999   10.03300   24.50000
  357.10001   41.48000   20.80000
  303.00000   34.30000   22.00000
     285I(2I-+2I-)285I
   41.33000    2.54500   30.50000
   26.39000    1.77300   31.70000
   44.30000    4.46300   28.10000
   55.22000    3.17500   27.30000
  143.29000    7.15300   25.70000
  105.00000    5.45200   25.90000
  234.00000   11.54000   23.30000
  175.30000    3.90500   24.50000
  357.10001   17.47000   20.80000
  267.99999   13.54000   22.00000
  448.20001   25.16000   13.40000
  347.39999   21.72000   13.50000
   15.55000    1.37400   33.00000
   10.29000    1.02000   34.20000
    4.59700    0.43240   35.40000
    1.57700    0.25550   35.60000
    1.03200    0.17230   37.80000
    0.31050    0.15090   39.00000
    2.54500    0.26290   41.40000
    3.94200    0.24430   42.60000
    6.25500    0.43950   45.10000
    7.59000    0.50170   45.30000
    9.22500    0.55470   49.70000
    9.05100    0.53910   49.90000
    8.22000    0.54500   51.10000
    8.32500    0.52260   52.30000
    9.12800    0.59520   53.50000
    5.94400    0.50550   54.70000
    7.05800    0.44370   55.90000
    5.48800    0.35920   57.20000
    3.59000    0.29140   59.60000
    3.21200    0.25370   60.80000
    2.11300    0.18510   63.20000
    1.25900    0.12750   64.40000
    0.71770    0.08049   65.80000
    0.38510    0.04984   68.00000
    0.33550    0.04533   69.20000
    0.15460    0.02423   70.40000
```

```
 0.07211    0.01721   72.80000
 0.10620    0.01940   74.00000
 0.15820    0.02344   75.40000
 0.14820    0.02494   77.60000
 0.28090    0.03517   80.10000
 0.33970    0.03705   81.30000
 0.30920    0.03434   83.70000
 0.28370    0.03245   84.90000
 0.32900    0.03205   87.30000
 0.26680    0.02717   88.50000
 0.19630    0.02440   90.40000
 0.16800    0.02104   92.10000
 0.16100    0.02026   93.40000
 0.09546    0.01502   95.10000
   99F(P1•.P1•)99F
 0.11460    0.01544  111.30000
 0.10560    0.01368  112.50000
 0.09508    0.01374  104.90000
 0.11280    0.01419  110.10000
 0.10790    0.01515  105.50000
 0.09472    0.01374  107.70000
 0.09482    0.01524  104.20000
 0.09221    0.01230  105.40000
 0.09593    0.01541  101.80000
 0.08367    0.01241  103.00000
 0.09549    0.01564   99.20000
 0.09581    0.01345   99.40000
 0.08385    0.01517   94.60000
 0.09555    0.01465   95.80000
 0.13130    0.01784   91.00000
 0.13200    0.01585   92.20000
 0.18770    0.02454   87.40000
 0.15690    0.02034   89.50000
 0.23460    0.03144   83.60000
 0.21460    0.02964   85.00000
 0.30250    0.03184   80.20000
 0.27570    0.02582   81.40000
 0.41920    0.03710   75.50000
 0.38140    0.03354   77.80000
 0.39920    0.03754   72.90000
 0.45920    0.03789   74.10000
 0.53290    0.04325   69.30000
 0.42790    0.03759   70.50000
 0.44610    0.04430   65.60000
 0.41220    0.04094   65.80000
 0.46100    0.05505   62.00000
 0.47580    0.05215   63.20000
 0.50010    0.07778   59.30000
 0.40260    0.05783   59.50000
 0.34560    0.09952   54.60000
 0.54470    0.07539   55.80000
 2.00500    0.16240   50.90000
 1.24800    0.11530   52.20000
 4.18300    0.25360   47.30000
 3.14600    0.20100   48.50000
 9.17400    0.47510   43.60000
```

```
   7.19600     0.37370    44.80000
  11.11000     0.56920    41.60000
   8.50200     0.44790    42.80000
  20.93000     1.02500    39.60000
  15.46000     0.77540    39.90000
  30.58000     1.46500    35.20000
  24.70000     1.20000    37.40000
  40.98000     1.97500    33.70000
  33.33000     1.64500    34.90000
  43.46000     2.05500    33.70000
  32.53000     1.57200    34.90000
  55.55000     2.56100    31.20000
  45.31000     2.21500    32.50000
  75.76000     3.98100    29.70000
  58.30000     3.13800    30.00000
 117.30000     5.54500    23.80000
 102.10000     4.92900    25.00000
 153.30000    17.40000    21.30000
 135.30000    15.49000    22.60000
    93F(PI-.PI-)93F
  51.24000     3.46100    31.20000
  45.38000     2.77000    32.50000
  37.42000     4.51700    29.70000
  59.06000     3.68300    30.00000
 108.90000     5.44200    25.30000
  91.10000     4.59200    27.50000
 139.39999     5.95000    23.80000
 122.70000     5.14100    25.00000
 159.70000     8.46100    21.30000
 151.80000     7.54700    22.60000
  44.90000     2.50700    33.70000
  35.31000     2.08900    34.90000
  29.73000     1.88500    35.20000
  24.77000     1.51900    37.40000
  19.76000     1.30500    38.60000
  14.81000     1.04100    39.90000
  10.55000     0.90820    42.30000
   6.81200     0.55590    43.60000
   4.38000     0.45940    45.00000
   3.90700     0.34830    47.30000
   1.85100     0.18530    49.70000
   1.41700     0.15560    50.90000
   1.08400     0.13710    52.20000
   0.80520     0.10420    53.40000
   0.82590     0.12350    54.60000
   0.80460     0.10560    55.80000
   0.46810     0.06144    57.10000
   0.59840     0.06844    58.30000
   0.55560     0.08123    60.70000
   0.58030     0.07025    62.00000
   0.57120     0.07519    64.40000
   0.52210     0.07070    65.60000
   0.72600     0.08574    68.00000
   0.73690     0.07433    69.30000
   0.57850     0.07407    70.50000
   0.54030     0.07081    71.70000
```

0.55330	0.08012	74.10000
0.59010	0.07554	75.30000
0.47500	0.05572	77.80000
0.46840	0.05324	79.00000
0.29240	0.03439	81.40000
0.26640	0.03552	82.60000
0.20430	0.02592	85.00000
0.23720	0.02396	85.20000
0.15420	0.02252	88.60000
0.16100	0.01901	89.80000
0.11270	0.01810	92.20000
0.13210	0.01734	93.40000
0.08029	0.01421	95.20000
0.10200	0.01539	96.40000

```
FOLLOWING IS A COMPILATION OF THE MODIFIED DATA IN THE ORDER C.M. ANGLE,
C.M. CROSS SECTION, AND CROSS SECTION EROR.
208PB(PI+,PI+)208PB
 20.60000 156.60001  23.98000
 21.80000 98.610000  16.92000
 23.00000   79.2000   5.09400
 24.20000 117.10000   6.32700
 25.40000 161.60001   8.66400
 26.60000 173.10001   8.94200
 27.80000 196.00000  10.36000
 29.00000 198.80000  10.22000
    30.20     163.6     7.092
 30.20000 165.39999   8.56400
 31.40000 130.80000   5.70200
 31.40000 130.80000   7.00200
 32.60000 107.00000   4.96800
 33.90000  77.49000   3.68600
    35.00     46.57     2.190
    36.30     26.28     1.323
    37.50     13.46     .6760
    38.70     6.180     .3668
    39.90     3.844     .2582
    39.90     3.685     .3086
    41.10     5.690     .3279
    41.10     5.492     .3836
 42.30000     8.872    .51630
 43.50000  13.21000    .64400
 44.70000  15.30000   1.24400
 44.70000  16.26000    .92180
 45.90000  19.44000   1.03600
 45.90000  19.44000   1.33900
 47.10000    19.850    .98130
 48.30000    19.190    .86290
 49.50000  17.50000    .92200
 50.70000  14.38000    .77030
 52.30000  10.70000    .54180
 53.50000   7.65700    .40560
    54.30     5.074     .3229
    55.50     2.299     .1880
    56.70     .9624     .0973
    57.90     .4173    .05521
    59.10     .4182     .0588
    60.30     .7197     .0809
 61.50000     1.427    .13510
 62.70000   1.81600    .14430
 63.90000   2.16900    .21880
 65.10000   2.48200    .23480
 66.30000     3.151    .19550
 66.30000     2.825    .22180
 67.50000   2.74800    .17990
 67.50000   2.27400    .18330
 68.70000   2.21000    .16360
 69.90000   1.84400    .14200
 71.10000   1.40400    .11030
 72.30000    .99310    .08733
 73.50000    .62420    .09691
 73.50000    .51270    .10990
    74.70     .2282     .0698
    74.70     .2640     .0544
    75.90     .1230     .0273
```

```
     77.10     .03307      .0172
     78.30     .02727      .0125
     79.50      .0935      .0224
     80.70      .1870      .0358
  81.90000       .274     .03908
  83.10000     .40432     .04354
  84.30000     .35570     .03031
  85.50000       .446     .04829
  86.70000     .39140     .03025
  87.90000     .31430     .04309
  89.10000     .29440     .03810
  90.30000     .14210     .03209
  91.50000     .12490     .02819
     92.70     .04644     .01596
     93.90      .0496     .02047
     95.10     .01269      .0105
     96.30    .006320     .00440
     97.50     .01553     .00774
     98.70     .03922     .01467
  99.90000     .09730     .02873
 101.10000     .13000     .03151
 104.70000     .08763     .02540
 105.90000     .22730     .03480
 102.30000     .13310     .03083
 103.50000     .15810     .03241
 107.10000     .17240     .03425
 108.30000     .20280     .03038
 109.50000     .15300     .03396
 110.70000     .17880     .03554
208PR(PI-,PI-)208PB
  15.80002 993.59998   53.46000
  17.00000 421.20001   27.75000
  18.20000     163.7      9.770
  19.40000     95.70      6.500
  20.60000     128.8       7.36
  21.80000 186.89999    9.57000
  23.00000 290.10001   15.00000
  24.20000    322.80   15.34000
  25.40000    319.30   16.78000
  26.60000 278.60001   15.11000
  27.80000 237.73000   12.90000
  29.00000 183.60001   10.31000
     30.20     109.7      6.726
     31.40     65.01      4.330
     32.60     26.22      1.900
     33.90     8.210      .8300
     35.00     2.288      .3001
     36.30     5.026      .5060
  37.50000   14.4100      1.360
  38.70000  25.50000    1.88200
  41.10000     42.75      3.833
  42.30000  35.11000    2.60500
  44.70000  28.39000    1.91500
  45.90000  21.29000    1.49700
     48.30     7.254      .6700
     49.50     2.758      .3298
     50.70     .9518      .1741
     51.90     .3579      .0854
     53.10     1.310      .2780
  54.30000     1.842       .324
```

```
     77.10     .03307      .0172
     78.30     .02227      .0125
     79.50      .0935      .0224
     80.70      .1870      .0358
  81.90000       .274     .03908
  83.10000     .00430     .04350
  84.30000     .35570     .03031
  85.50000       .446     .04829
  86.70000     .34140     .03825
  87.90000     .31430     .04309
  89.10000     .29440     .03810
  90.30000     .14210     .03209
  91.50000     .12490     .02819
     92.70     .04644     .01596
     93.90      .0496     .02047
     95.10     .01269      .0105
     96.30    .006320     .00440
     97.50     .01553     .00774
     98.70     .03922     .01467
  99.90000     .09730     .02873
 101.10000     .13000     .03151
 104.70000     .08763     .02540
 105.90000     .22730     .03480
 102.30000     .13310     .03083
 103.50000     .15810     .03241
 107.10000     .17240     .03425
 108.30000     .20280     .03038
 109.50000     .15300     .03396
 110.70000     .17880     .03550
208PB(PI-,PI-)208PB
  15.80000 993.59998   53.46000
  17.00000 421.20001   27.75000
  18.20000     163.7      9.770
  19.40000     95.70      6.500
  20.60000     128.8       7.36
  21.80000 186.89999    9.57000
  23.00000 290.10001   15.00000
  24.20000    322.80   15.34000
  25.40000    319.30   16.78000
  26.60000 278.60001   15.11000
  27.80000 237.73000   12.90000
  29.00000 183.60001   10.31000
     30.20     109.7      6.726
     31.40     65.01      4.330
     32.60     26.22      1.900
     33.90     8.210      .8300
     35.00     2.288      .3001
     36.30     5.026      .5600
  37.50000   14.4100      1.360
  38.70000  25.50000    1.88200
  41.10000     42.75      3.033
  42.30000  35.11000    2.60500
  44.70000  28.39000    1.91500
  45.90000  21.29000    1.49700
     48.30     7.254      .6700
     49.50     2.758      .3298
     50.70     .9518      .1741
     51.90     .3579      .0854
     53.10     1.310      .2780
  54.30000     1.842       .324
```

```
      77.10     .03307      .0172
      78.30     .02227      .0125
      79.50      .0935      .0224
      80.70      .1870      .0358
   81.90000       .274     .03908
   83.10000     .00430     .04350
   84.30000     .35570     .03031
   85.50000       .446     .04829
   86.70000     .34140     .03825
   87.90000     .31430     .04309
   89.10000     .29440     .03810
   90.30000     .14210     .03209
   91.50000     .12490     .02819
      92.70     .04644     .01596
      93.90      .0496     .02047
      95.10     .01269      .0105
      96.30    .006320     .00440
      97.50     .01553     .00770
      98.70     .03922     .01467
   99.90000     .09730     .02873
  101.10000     .13000     .03151
  104.70000     .08763     .02540
  105.90000     .22730     .03480
  102.30000     .13310     .03083
  103.50000     .15810     .03241
  107.10000     .17240     .03425
  108.30000     .20280     .03038
  109.50000     .15300     .03396
  110.70000     .17800     .03550
  208PB(PI+,PI-)208PB
   15.80000 993.59998  53.46000
   17.00000 421.20001  27.75000
   18.20000     163.7     9.770
   19.40000     95.70     6.500
   20.60000     128.8      7.36
   21.80000 186.89999   9.57000
   23.00000 290.10001  15.00000
   24.20000    322.80  15.34000
   25.40000    319.30  16.78000
   26.60000 278.60001  15.11000
   27.80000 237.70000  12.90000
   29.00000 183.60001  10.31000
      30.20     109.7     6.726
      31.40     65.01     4.330
      32.60     26.22     1.900
      33.90     8.210     .8300
      35.00     2.280     .3001
      36.30     5.026     .5060
   37.50000   14.4100     1.360
   38.70000  25.50000   1.88200
   41.10000     42.75     3.033
   42.30000  35.11000   2.60500
   44.70000  28.39000   1.91500
   45.90000  21.29000   1.49700
      48.30     7.254     .6700
      49.50     2.758     .3298
      50.70     .9518     .1741
      51.90     .3579     .0854
      53.10     1.310     .2780
   54.30000     1.842      .324
```

```
55.50000      5.325      .70430
56.70000    5.43600      .63510
59.10000      6.527      .54180
60.30000    6.01500      .49050
62.70000    4.76100      .47290
63.90000      2.553      .30750
   66.30      0.919       .1426
   67.50      .2288       .0710
   68.70      .0778       .0390
   69.90      .1361       .0585
72.30000      .4502      .10140
73.50000     .74350      .11030
75.90000    1.14300      .15500
77.10000      1.269      .15810
79.50000     .80790      .11990
80.70000       .511      .09030
   83.10      .2552       .0452
   84.30      .0583       .0220
   86.70      .0252      .01266
   87.90     .04629       .0199
90.30000     .05430      .03703
91.50000     .13100      .04940
93.30000     .17800      .04507
94.50000     .19700      .09228
95.70000     .16250      .03751
96.90000     .08500      .02637
SANI(PI+,PI+)SANI
    20.7      429.2       48.48
    21.9      310.1       35.27
    23.1      175.6       9.497
    24.3      125.3       7.136
    25.5      77.81       4.280
    26.7      46.67       2.778
    27.9      23.12       1.409
    29.2      7.404      0.7817
    30.4      2.506      0.3063
    30.4      2.795      0.3247
    31.6      1.889      0.2621
    31.6      1.905      0.2318
    32.8      4.247      0.3403
    34.0      8.513      0.4532
    35.2      14.44      0.7181
    36.4      17.74      0.8316
    37.6      22.55       1.065
    38.8      23.74       1.089
    40.0      25.21       1.169
    41.2      25.89       1.175
    42.4      23.79       1.103
    43.6      23.18       1.055
    44.8      21.70      0.9945
    46.0      18.09      0.8362
    47.2      15.87      0.7288
    48.4      11.69      0.5523
    49.6      8.951      0.4224
    50.8      6.691      0.3240
    52.1      5.375      0.2809
    53.3      3.071      0.1780
    54.5      1.807      0.1627
    55.7     0.8552      0.1260
    56.9     0.2568       .0385
```

```
       58.1    0,04845      ,0209
       59,3    0.03660      ,0092
       60.5     0.1300      .0205
       61,7     0.5179    0,06880
       62.9     0.6116    0,07422
       64,1      .9460    0,06832
       65,3      1.113    0.07269
       66.5      1.527     0.1410
       67.7      1.509     0.1268
       68.9      1.792     0.1397
       70.1      1.652     0.1236
       71.3      1.545     0.1047
       72.5      1.404    0,09253
       76.1     0.8203    0,07303
       77.3     0.6276    0,06199
       78.5     0.4697    0,05289
       79.7     0.3362    0,04157
       80.9     0.1984    0,02575
       82,1     0.1211    0,01767
       83.3    0.06680    0,01541
       84.5    0.01052    0,01053
       86.9    0.02094    0,00760
       88.1    0.03004    0,01162
       89.3    0.05597    0,01024
       90.5    0.06822    0,01727
       91.7     0.1106    0,02015
       92.9     0.1478    0,02934
       94.1     0.1318    0,02548
       95.3     0.1863    0,02848
       96.5     0.2120    0,02783
       97.7     0.1938    0,02217
       98.9     0.1845    0,01945
      100.1     0.1468    0,02674
      101.3     0.1272    0,02043
      102,5    0.09889    0,01734
      103.7     0.1215    0,01740
      104.9    0.09836    0,01527
      106.1    0.09169    0,01745
      107.3    0.05242    0,01275
      108.5    0.04006    0.00920
SANI(PI-,PI-)SANI
  15.900001091.00000   57,84000
  17.10000 842.59998   46,14000
  18.30000 676.20001   35,85000
  19.50000 502.89999   27,59000
  20.70000 345.89999   17,27000
  21.90000 230.20000   12,16000
  23.10000 158.10001    7,94200
  24.30000  98.08000    5.37100
      25.5     52.12       3.02
      26.7     24.74      1.743
      27.9     9.992      0.924
     29.20     4.285     0.4462
      30.4     2.697       ,379
      31.6     5.082       .470
  32.80000  12.55300    1,03400
  34.00000  16.03000    1,16300
  35.20000  27.26000    1,77000
  36.40000  26.72000    1,68600
  37.60000  32.66000    2.02600
```

```
 38.80000   35.62000    2.12200
 41.20000   31.86000    1.94700
 42.40000   27.91000    1.71900
 44.80000   21.70000    1.30400
 46.00000   17.24000    1.07400
 48.40000    9.23100     .62180
 49.60000    5.73600     .44090
 50.80000    4.36400     .40520
     52.1      2.485       0.27
     53.3      1.301      0.131
     54.5     0.4777     0.0759
     55.7     0.1121     0.0309
     56.9     0.0995      0.027
 59.30000     .75600     .09784
 60.50000    1.16800     .12200
 62.90000    1.72900     .17070
 64.10000    2.24200     .18360
 66.50000    2.09300     .24720
 67.70000    2.16600     .24090
 68.90000    2.01600     .17040
 70.10000    1.75800     .15850
 72.50000    1.34300     .14820
 73.70000     .96870     .11670
 76.10000     .51290     .05646
 77.30000     .31100     .04219
 79.00000     .20940     .31770
 83.30000     .04481     .01801
     84.5    0.02329       0.01
     86.9     0.0745     0.0165
     88.1     0.1466     0.0235
 90.50000     .17630     .02955
 91.70000     .18930     .02613
 93.50000     .14380     .03319
 94.70000     .14800     .02907
2PSI(PI+,PI+)2PSI
 20.80000 367.10001   41.48000
 22.00000 303.00000   34.30000
 23.30000 226.20000   11.89000
 24.50000 189.89999   10.03000
 25.70000 146.39999    7.62800
 26.90000 111.20000    5.98500
 28.10000  88.56000    4.65500
 29.30000  59.30000    3.36200
 30.50000  48.87000    2.21700
     31.7      30.62      1.451
     33.0      21.35      1.005
     34.2      11.14     0.5669
     35.4      6.594     0.3534
     36.6      3.092     0.1789
     37.8      1.229     0.0872
     39.0     0.3774     0.0393
     40.2     0.5429     0.0457
     41.4      1.061      0.069
     42.6      2.501     0.1388
 43.90000    3.49100     .18030
 45.10000    4.65500     .23710
 46.30000    5.46300     .26310
 47.50000    6.36600     .30670
 48.70000    6.94300     .32440
 49.90000    7.46800     .36200
```

```
  51.10000    7,41900    ,35080
  52.30000    7.95800    ,39150
  53.50000    6.71900    ,33360
  54.70000    6.92000    ,38660
  55.90000    5.74000    ,32760
  59.60000    3,97200    ,19810
  60.80000    3.36100    ,17070
  62.00000    2.79500    ,14460
  63.20000    2.18300    ,11470
  64,40000    1.79500    ,11120
  65.60000    1.30800    ,08988
  66.80000     .89250    ,05250
  68.00000     .58250    ,04173
  69.20000     .44880    .03891
      70,4      0.221    0.0257
      71.6     0.1349   0,01790
      72.8     0.0565   0,01120
      74.0    0,03197   0,00652
      75.2    0.04603   0.00882
      76.4    0,06696    0.0082
  77.60000     .11800    ,00993
  78.80000     .13510    ,02005
  80.10000     .21180    ,02502
  81.30000     .25010    ,02249
  82.50000     .26170    ,02260
  83.70000     .25520    ,03041
  84.90000     .28140    ,02887
  86.10000     .26440    ,03068
  87.30000     .27130    ,02676
  88.50000     .30070    ,02870
  89.70000     ,27650    ,02624
  90.90000     .14530    ,02205
  92.10000     .18010    ,02508
  93.30000     .16540    ,02092
  94.50000     .12880    ,01757
  95.70000     .10820    ,01344
  96.90000     .06639    ,01109
  98.10000     .07446    ,01386
  99,30000     .05150    ,00976
 100.50000     .02724    ,00915
 101.70000     .03260    ,00778
 102.80000     .01113    ,00447
 104.00000     .01503    ,00567
 105,20000     .00926    ,00618
 106.40000     .01303    ,00524
 107.60000     .01974    ,00570
 108.80000     .02615    .00604
2ASI(PI-,PI-)2ASI
  18.40000 488.20001  26,06000
  19.60000 397.39999  21,72000
  20.80000 357.10001  17,47000
  22,00000 267.89999  13,60000
  23.30000 234.00000  11,54000
  24.50000 175.30000   8,90600
  25.70000 143.20000   7,15800
  26.90000 105.00000   5,45200
  28.10000  84.90000   4,46300
  29.30000  56.22000   3,17600
  30.50000  41.83000   2,54600
  31.70000  24.99000   1.77800
```

```
  33.00000   16.56000    1.37400
  34.20000   9.74            .974
  35.40000    4.27           .403
  36.60000   1.46            .223
  37.80000   .824            .138
  39.00000   .700            .130
  41.40000    2.54500     .26290
  42.60000    3.94200     .29430
  45.10000    6.25500     .43950
  46.30000    7.69000     .50170
  48.70000    8.22500     .55470
  49.90000    8.05100     .53910
  51.10000    8.22300     .54800
  52.30000    8.32500     .57260
  53.50000    8.12800     .58520
  54.70000    6.84800     .50560
  55.90000    7.05800     .44370
  57.20000    5.48800     .35920
  59.60000    3.69000     .29140
  60.80000    3.21200     .25370
  63.20000    2.11300     .18610
  64.40000    1.26900     .12750
  66.80000     .71770     .08048
  68.00000  .374            .0480
  69.2000  .323             .0436
  70.40000    .147          .0231
  72.80000  .268            .0162
  74.00000  .102            .0181
  76.40000     .15820     .02944
  77.60000     .19820     .02998
  80.13000     .28090     .03817
  81.30000     .33870     .03706
  83.70000     .30820     .03439
  84.90000     .28370     .03235
  87.30000     .32940     .03206
  88.50000     .26480     .02717
  90.90000     .19690     .02490
  92.10000     .14800     .02103
  93.90000     .14100     .02026
  95.10000     .09546     .01502
 9PE(PI+,PI+)98E
  21.30000 153.80000   17.40000
  22.60000 136.80000   15.49000
  23.80000 117.30000    5.64500
  25.00000 102.10000    4.92900
  28.70000  75.76000    3.98100
  30.00000  58.30000    3.13800
  31.20000  56.66000    2.66100
  32.50000  46.81000    2.21600
  33.70000  43.46000    2.05500
  33.70000  40.98300    1.97600
  34.90000  33.83000    1.64500
  34.90000  32.53000    1.57200
  36.20000  30.58000    1.46600
  37.40000  24.70000    1.20000
  38.60000  22.93000    1.02500
  39.90000  15.46000     .77540
  41.60000  11.11000     .56920
  42.80000   8.60200     .44790
  43.60000   9.17800     .47810
```

```
   44.80000    7.19600     .37870
   47.30000    4.18300     .25360
   48.50000    3.19600     .20100
   50.90000    2.00500     .16240
   52.20000    1.29800     .11630
   54.60000     .94560     .09952
   55.80000     .64470     .07539
   58.30000     .60010     .07778
   59.50000     .40260     .05783
   62.00000     .46100     .05505
   63.20000     .47580     .05215
   65.60000     .44610     .04430
   66.80000     .41220     .04094
   69.30000     .53280     .04826
   70.50000     .42700     .03759
   72.90000     .39920     .03754
   74.10000     .45920     .03789
   76.50000     .41920     .03710
   77.80000     .38140     .03354
   80.20000     .30260     .03184
   81.40000     .27570     .02682
   83.80000     .23960     .03144
   85.00000     .21940     .02964
   87.40000     .18770     .02464
   88.60000     .15690     .02034
   91.00000     .13190     .01789
   92.20000     .13200     .01685
   94.60000     .08386     .01517
   95.80000     .09555     .01445
   98.20000     .09589     .01644
   99.40000     .09581     .01345
  101.80000     .09593     .01541
  103.00000     .08367     .01241
  104.20000     .09882     .01524
  105.40000     .09221     .01230
  106.50000     .10790     .01515
  107.70000     .09872     .01374
  108.90000     .09608     .01374
  110.10000     .11280     .01410
  111.30000     .11460     .01548
  112.50000     .10560     .01368
98E(PI-,PI-)98E
   21.30000  169.70000    8.46100
   22.60000  151.80000    7.54700
   23.80000  139.39999    6.96000
   25.00000  122.70000    6.14100
   26.30000  108.90000    5.44200
   27.50000   91.10000    4.59200
   28.70000   87.42000    4.51700
   30.00000   69.06000    3.68300
   31.20000   61.28000    3.46100
   32.50000   48.38000    2.77000
   33.70000   44.00000    2.50700
   34.90000   36.31000    2.08900
   36.20000   29.73000    1.88600
   37.40000   24.77000    1.61900
   38.60000   19.76000    1.30600
   39.90000   14.81000    1.04100
   42.30000   10.66000     .90820
   43.60000    6.81200     .65590
```

```
46.00000     4.88000     .45960
47.30000     3.30700     .34830
49.70000     1.85100     .18530
50.90000     1.41700     .15660
52.20000     1.08400     .13710
53.40000      .80520     .10420
54.60000      .92590     .12350
55.80000      .80460     .10560
57.10000      .46810     .06140
58.30000      .59840     .06840
60.70000      .56560     .08123
62.00000      .58030     .07026
64.40000      .67120     .07519
65.60000      .62210     .07070
68.00000      .72600     .08574
69.30000      .73690     .07433
70.50000      .57850     .07407
71.70000      .64030     .07081
74.10000      .65330     .08712
75.30000      .59010     .07554
77.80000      .47500     .05672
79.00000      .46840     .05320
81.40000      .29240     .03838
82.60000      .26640     .03652
85.00000      .20430     .02682
86.20000      .23720     .02896
88.60000      .16420     .02252
89.80000      .16100     .01901
92.20000      .11270     .01810
93.40000      .13210     .01734
95.20000      .08029     .01421
96.40000      .10200     .01639
```

Appendix D. The real part of the forward-scattering amplitude and the total cross section based on the optical-model fit to scattering data are shown. The forward-scattering amplitude is calculated from the components of the Coulomb scattering matrix, S_ℓ^c, and the S-matrix components, S_ℓ, due to both the Coulomb and nuclear interactions:

$$f(o) = \frac{A}{A-1}\,\frac{1}{2ki}\sum_{\ell=0}^{\ell_{max}} (2\ell-1)(S_\ell - S_\ell^c).$$

Using f(o), the optical theorem provides total cross sections:

$$\sigma_T = \frac{4\pi}{k}\, I_m f(o).$$

	Re[f(0)]	σ_T(mb)
$\pi^+, {}^9$Be	-0.8214	570.8
$\pi^-, {}^3$Be	-0.1669	689.5
$\pi^+, {}^{28}$Si	-3.765	1144.0
$\pi^-, {}^{28}$Si	4.145	1179.0
$\pi^+, {}^{58}$Ni	-11.72	1352.0
$\pi^-, {}^{58}$Ni	13.25	1467.0
$\pi^+, {}^{208}$Pb	-17.34	-2506.0
$\pi^-, {}^{208}$Pb	18.21	-3644.0

ACKNOWLEDGMENTS

It is a pleasure to thank George Burleson, my advisor, for the unremitting patience, forbearance, and support that he has offered during this project. I am happy to have had the valuable help of W. R. Gibbs and G. J. Stephenson, Jr. Their knowledge, advice, and friendship are gifts that I have undeservedly accepted. My special thanks go to Lilly Cordova for typing this thesis.

☆U.S. Government Printing Office: 1979 – 677-013/98